1-1-2012

Modeling and Uncertainty Analysis of CCHP systems

Joshua Aaron Smith

Modeling and uncertainty analysis of CCHP systems

By

Joshua Aaron Smith

A Dissertation
Submitted to the Faculty of
Mississippi State University
in Partial Fulfillment of the Requirements
for the Degree of Doctor of Philosophy
in Mechanical Engineering
in the Department of Mechanical Engineering

Mississippi State, Mississippi

December 2012

Modeling and uncertainty analysis of CCHP systems

By

Joshua Aaron Smith

Approved:

Rogelio Luck Professor of Mechanical Engineering (Major Professor)	Sergio D. Felicelli Professor of Mechanical Engineering (Committee Member)
Pedro J. Mago Associate Professor of Mechanical Engineering (Committee Member)	W. Glenn Steele Jr. Committee Participant of Mechanical Engineering (Committee Member)
Kalyan K. Srinivasan Associate Professor of Mechanical Engineering (Graduate Coordinator)	Sarah A. Rajala Dean of the College of Engineering

Name: Joshua Aaron Smith

Date of Degree: December 15, 2012

Institution: Mississippi State University

Major Field: Mechanical Engineering

Major Professor: Dr. Rogelio Luck

Title of Study: Modeling and uncertainty analysis of CCHP systems

Pages in Study: 119

Candidate for Degree of Doctor of Philosophy

Combined Cooling Heating and Power (CCHP) systems have been recognized as a viable alternative to conventional electrical and thermal energy generation in buildings because of their high efficiency, low environmental impact, and power grid independence. Many researchers have presented models for comparing CCHP systems to conventional systems and for optimizing CCHP systems. However, many of the errors and uncertainties that affect these modeling efforts have not been adequately addressed in the literature. This dissertation will focus on the following key issues related to errors and uncertainty in CCHP system modeling: (a) detailed uncertainty analysis of a CCHP system model with novel characterization of weather patterns, fuel prices and component efficiencies; (b) sensitivity analysis of a method for estimating the hourly energy demands of a building using Department of Energy (DOE) reference building models in combination with monthly utility bills; (c) development of a practical technique for selecting the optimal Power Generation Unit (PGU) for a given building that is robust with respect to fuel cost and weather uncertainty; (d) development of a systematic

method for integrated calibration and parameter estimation of thermal system models. The results from the detailed uncertainty analysis show that CCHP operational strategies can effectively be assessed using steady state models with typical year weather data. The results of the sensitivity analysis reveal that the DOE reference buildings can be adjusted using monthly utility bills to represent the hourly energy demands of actual buildings. The optimal PGU sizing study illustrates that the PGU can be selected for a given building in consideration of weather and fuel cost uncertainty. The results of the integrated parameter estimation study reveal that using the integrated approach can reduce the effect of measurement error on the accuracy of predictive thermal system models.

Key Words: CHP, CCHP, Uncertainty Analysis, Parameter Estimation, Optimal Sizing, Optimal Operation

ACKNOWLEDGEMENTS

The choice to pursue a doctoral degree has drastically changed my life for the better. I would like to thank my advisor Dr. Rogelio Luck for inspiring me to pursue graduate school and for his dedication to providing inspiration and encouragement to me throughout my graduate education. I am also grateful to Dr. Pedro Mago, Dr. Sergio Felicelli, and Dr. Glenn Steele for their continual support in my graduate education and professional development. Many hours of my time were spent working on problems in class or research with Dr. Kyung Tae Yun and Robert Thomas, fellow graduate students. I would like to thank them for their contribution to my work and their encouragement. I am especially grateful to my wife for her love and support. She has been behind me through the entire process, even though it meant many sacrifices for her. I am so thankful that she shared my vision for this graduate degree, which I never would have completed without her support. I am thankful to my parents for raising me and always seeking the best for me. My whole life I have walked in full assurance of their love and acceptance of me, and this security has been vital to my success. Above all, I would like to thank God, on whom I depend for every breath and from whom I have abundantly received.

TABLE OF CONTENTS

LIST OF TABLES

LIST OF FIGURES

NOMENCLATURE

b	Intercept for the engine fuel/power linear relationship
B	Baseline
Bench	Hourly energy load for the benchmark model
c	Model coefficients
C	Cooling
C_c	Coolant heat capacity rate (W/°K)
C_e	Cost of electricity
C_f	Cost of natural gas
c_p	Specific heat (kJ/kgK)
C_w	Heat capacity rate of water in recovery loop (W/°K)
Calc	Hourly energy load calculated by the methodology
CC	Capital cost
CDE	Carbon Dioxide Emissions
$Cost_{ref}$	Cost of conventional system operation without CHP
$Cost_{CHP}$	Cost of a CHP operation
COP_{ch}	Coefficient of performance
E	Error
E_2	Electricity produced when Savings equals zero for case 1
E_3	Electricity produced when Savings equals zero for case 2

E_{ftl}	Electricity produced when following the thermal load
E_{load}	Electric Load of building
E_m	Electricity registered at the meter
E_{PGU}	Electricity generated by PGU
E_{PGU_nom}	Nominal (rated) engine power output
E_{PGU_min}	Minimum engine power output
ECB	Energy consumption baseline
ECC	Energy consumption for cooling
ECF_{CDE}	Electricity conversion factor for carbon dioxide emissions
ECF_{PEC}	Electricity conversion factor for PEC
ECV	Energy consumption variable
f	Fraction
F_m	Natural Gas registered at the meter
F_b	Fuel consumed by the boiler
F_{PGU}	Fuel consumed by the PGU
F_{ref}	Fuel energy consumed in the conventional system
FCF_{CDE}	Natural gas conversion factor for carbon dioxide emissions
FCF_{PEC}	Natural gas conversion factor for PEC
HX	Heat Exchanger
PEC	Primary Energy Consumption
PGU	Power Generation Unit
m	Slope for the engine fuel/power linear relationship
N_{OY}	Number of expected operation years

Q_b	Heat generated by boiler
Q_c	Cooling Load for the building
Q_h	Heating Load for the building
Q_{REC}	Recovered thermal energy from the engine
Q_{REC_min}	Recovered heat from engine at minimum power output
Q_{REC_nom}	Recovered heat from the engine at nominal power output
Q_{REQ}	Required thermal energy from engine or boiler
Q_{stor}	Heat energy in storage tank
R_{CHP}	Parameter comprised of m, η_{QNET}, and η_{boiler}
R_{Cost}	Cost ratio of electricy cost to fuel cost
R_{CostU}	Upper bound on cost ratio
R_{CostL}	Lower bound on cost ratio
s	Engine performance factor
Savings	Operational savings from using a CHP system
Sim	Hourly energy load for the test building model
T	Temperature (°C)
V	Variable
$\dot{V}_{B\_F}$	Volumetric flow rate of boiler fuel (m^3/s)
$\dot{V}_{cool}$	Volumetric flow rate of coolant (m^3/s)
$\dot{V}_{E\_F}$	Volumetric flow rate of engine fuel (m^3/s)
$\dot{V}_{HC\_A}$	Volumetric flow rate of air through heating coil (m^3/s)
$\dot{V}_{N\_W}$	Volumetric flow rate of water in location N (m^3/s)

YS	Yearly operational savings
YS_{MY_AVG}	Yearly operational savings, multiple year average
YS_{T_AVG}	Yearly operational savings, total average
η_b	Boiler efficiency
η_{hc}	Heating coil efficiency
η_{hrs}	Efficiency of a heat recovery system
η_{rec}	Recovery system efficiency
η_{ref}	Heating system efficiency for a conventional system
η_{QNET}	Fraction of heat energy recovered from fuel energy to PGU
ξ	Factor for PGU losses before heat recovery system
ε	Heat exchanger effectiveness
ρ	Density (kg/m^3)
Φ	Operation mode step function
$\Phi_{1e}, \Phi_{2e}, \Phi_{3e}, \Phi_{4e}$	Step functions for FEL operation mode changes
$\Phi_{1t}, \Phi_{2t}, \Phi_{3t}, \Phi_{4t}$	Step functions for FTL operation mode changes

Subscripts

e	Electricity
f	Fuel
coef	Coefficient
B	Boiler
HC	Heating Coil
pgu	Power Generation Unit

M	Main water loop
cool	Coolant loop
1-7	When subscripts of T, these indicate locations in Figure 6.1
amb	Ambient
HC_WI	Heating Coil Water Inlet
HC_AI	Heating Coil Air Inlet
HC_AO	Heating Coil Air Outlet
A	Air
B_WI	Boiler Water Inlet

CHAPTER I

INTRODUCTION

Improving energy efficiency and reducing environmental impact of building energy systems are critical issues in the United States (U.S.). Figure 1.1 illustrates the energy consumption in the U.S. by end use sector for the year of 2010. This figure reveals that building energy systems account for 42% of the total energy consumption in the U.S. A large portion of the energy consumed in the building sector in 2010 was in the form of electricity. Electricity consumption constituted 52% of the energy consumption for commercial buildings and 42% for residential buildings [Energy Information Administration (EIA), 2012]. Another important note about building energy usage is that a large portion of the energy consumed is used to meet the building thermal demand (i.e. air heating and cooling, water heating). In 2010 energy used for meeting the building thermal load made up 36% and 69% of the total energy consumed in commercial and residential buildings, respectively [EIA, 2012]. These statistics show a large potential for impact in the design and operation of the energy systems used to meet the building thermal and electrical load.

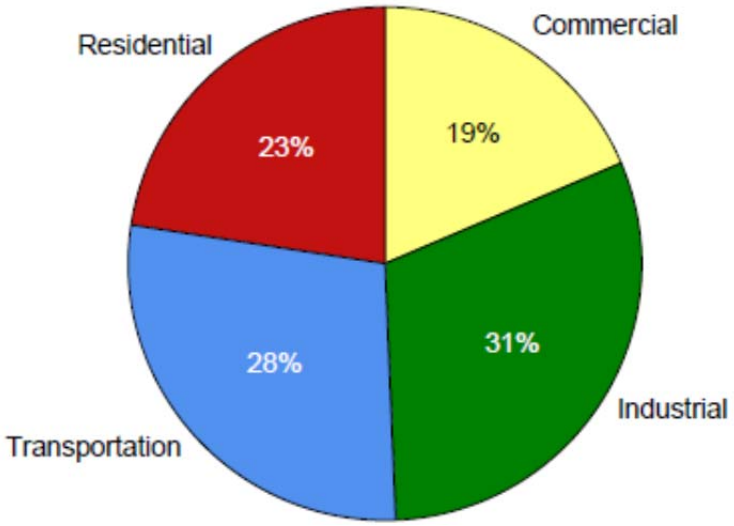

Figure 1.1 End-Use Sector Shares of Total Consumption [EIA, 2011]

Electricity consumed by the building sector is typically provided by traditional power plants located a long distance from the end use. In traditional power plants there are large losses in the generation and transmission processes. In 2010, approximately 63% of the energy consumed in generating electricity was converted into waste heat [EIA, 2011]. Additionally, 7% of the electricity generated was lost in the process of transmission to the end user.

1.1 Overview of CCHP Systems

The low efficiencies of traditional power plants have naturally led to the investigation of Combined Cooling Heating and Power (CCHP) systems. The term CCHP describes all electrical power generation systems that utilize recoverable waste heat for space heating, cooling, and domestic hot water purposes. A schematic of the energy flows for a topping-cycle CCHP system is given in Figure 1.2. In a topping-cycle CCHP system, the electric load of the building ($El_{building}$) is met by a combination of electricity

generated on-site (El_{PGU}) and electricity purchased by the grid (El_{grid}). In some cases, excess electricity (El_{excess}) produced by the on-site power generation unit (PGU) can be sold back to the grid. Additionally, the combustion process in the PGU produces recoverable heat (Q_{rcv}) in the form of heated engine coolant and high temperature exhaust. This heat energy can be supplemented by thermal energy from a boiler (Q_{boiler}) to meet the cooling load (Q_{cool}) or heating load (Q_{heat}) of the building. The use of the recoverable thermal energy for space heating, space cooling, and domestic hot water purposes is the driving factor behind the increased overall energy usage from conventional power generation systems. With this added benefit, CCHP systems can have combined efficiencies of 75 to 90% [International Energy Agency (IEA), 2008].

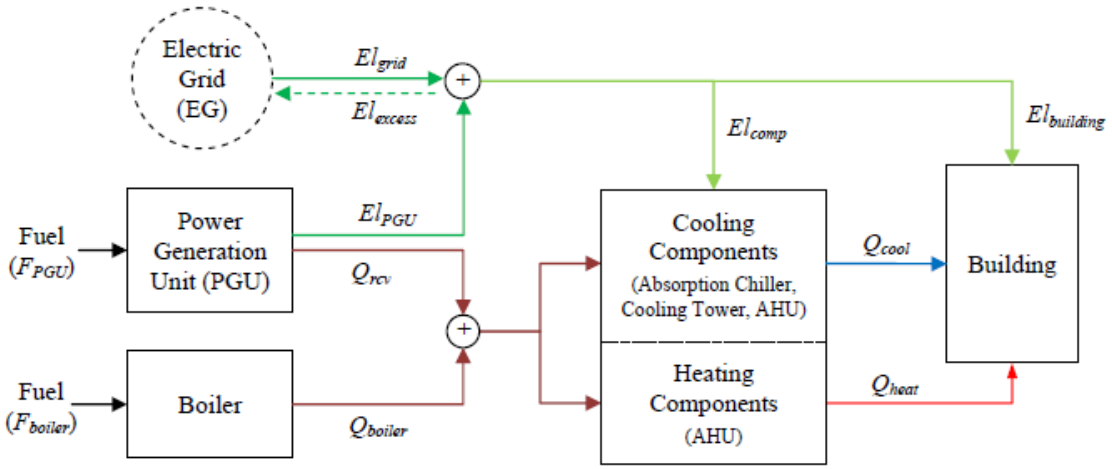

Figure 1.2 Schematic of CCHP system [Cho, 2009a]

1.2 Obstacles for CCHP Systems

There are many obstacles to overcome in the area of design, analysis and optimization of CCHP systems. The first problem arises when using CCHP system models to determine performance metrics such as the energy consumption, the cost of

operation, the system efficiencies (electrical, thermal, and total), and in some cases the emissions generated. In such modeling efforts, the uncertainty in the results of the model must be considered before the results can be used to make any conclusions. A quantitative uncertainty analysis uses currently available information to provide insight into the appropriate level of confidence in model simulation predictions. For problems where data are limited and where simplifying assumptions have been used, uncertainty analysis can be employed to help identify the strength of the conclusions that can be made about the model predictions [Frey, 1992]. Additionally, an uncertainty analysis can lead to the identification of the key sources of uncertainty, which merit further research, as well as the sources of uncertainty that are not important with respect to a given result. This identification of the key sources of uncertainty can help target data gathering efforts for improving the model.

An integral part of uncertainty analysis is the definition of the input uncertainties. However, many of the inputs for CCHP models are difficult to characterize. For example, the factors contributing to variation in weather conditions are complex and numerous. Additionally, weather patterns can vary significantly from year to year. Other key input parameters whose uncertainties are difficult to characterize are the PGU performance, the cost of electricity purchased from the grid, and the cost of natural gas.

A second obstacle in designing CCHP systems is the difficulty in obtaining the hourly building energy consumption. For proper design and operation of CCHP systems, a good estimate of the hourly thermal and electric load of the building is required. However, building utility bills give only the total monthly energy consumption for the

facility. Even with building modeling software such as EnergyPlus, simulating the hourly building energy requires extensive knowledge of the building configuration and loads.

In addition to uncertainty analysis and building load estimation, there is a need for real-time, accurate, predictive modeling of CCHP system operation. When thermal and electrical storage are available, predictive modeling is essential for determining the optimal balance of energy consumption between the conventional system and a topping-cycle CCHP system. However, predicting the states of thermal systems several time steps ahead can be difficult to model accurately. This inaccuracy results from the combination of errors in each component model with each future time step prediction.

One final obstacle to effective implementation of CCHP systems is the need for a practical method for optimal sizing of the components in CCHP systems. Over sizing components can lead to wasted capital cost and can cause the components to operate in low efficiency ranges. Under sizing components reduces the benefit from CCHP systems. For the sizing method to be effective sizing, it must address the extensive variation in weather conditions and fuel prices. Additionally, the sizing method must have a practical way to include commercially available components.

1.3 Objective of Dissertation

The objective of this dissertation is to provide solutions to the modeling challenges addressed in Section 1.2 in the areas of uncertainty analysis, building load estimation, optimal component sizing and predictive modeling of CCHP systems. The following research efforts are contributions in these areas:

- Chapter II presents a literature review to establish the current level of technical development in these areas.

- Chapter III presents an uncertainty analysis of a CCHP system model with practical consideration of uncertainty in weather, fuel and component efficiencies.
- Chapter IV illustrates a sensitivity analysis of a simple method for estimating hourly energy consumption using DOE reference building models and monthly utility bills.
- Chapter V describes a method for optimally sizing of CCHP system components that is robust to weather and fuel cost uncertainty.
- Chapter VI demonstrates an integrated parameter estimation method for accurate, predictive modeling of thermal systems.

CHAPTER II

LITERATURE REVIEW

A review of the literature in the area of CCHP system modeling will be presented in this chapter. Modeling of CCHP systems is an active area of research. Many researchers have presented modeling efforts to evaluate the performance of CCHP systems. Sections 2.1-2.4 summarize the state of four different areas of research related to CCHP modeling: Uncertainty Analysis, building load estimation, optimal sizing and predictive modeling.

2.1 Uncertainty Analysis

Many studies have used CCHP models to compare their performance under different operation strategies [Moran et al., 2008; Longo et al., 2005; Sun and Guo et al., 2006; Malico et al., 2009]. However, comparisons based on the results of computer simulations need to take into account the uncertainty in the results. A quantitative uncertainty analysis uses currently available information to provide insight into the appropriate level of confidence in model simulation predictions. For problems where data are limited and where simplifying assumptions have been used, uncertainty analysis can be employed to help identify the strength of the conclusions that can be made about the model predictions [Frey, 1992]. There are two general methods used to propagate input uncertainty through the model to determine output uncertainty. The first method is the

Monte Carlo Method (MCM). In this method, the probability distribution of the input variables are randomly sampled and used to run a large number of simulations. From these simulations, the probability distributions of the output variables are generated [Coleman and Steele, 2009]. The MCM has been used by many to determine uncertainty in the results of building simulations. For example, Wang et al. [2012] used the MCM to study the effect of variation in weather and building operations on the annual energy consumption. They found that a large degree of uncertainty was introduced by variations in building operations practice. Dominguez-Munoz et al. [2010] used the MCM to find the uncertainty in the peak load estimation of a simple resistance-capacitance (RC) building model. They studied the effect of twenty uncertain operation gains and building envelope parameters. A second method for uncertainty propagation is the Taylor Series Method (TSM). In this approach a Taylor series approximation of the relationship between inputs and outputs is used to propagate the uncertainty values [Coleman and Steele, 2009]. For accuracy the TSM requires that the model must behave linearly around the nominal operation point and the probability distributions must be Gaussian. However, when applicable, the TSM can greatly reduce the computational difficulty of the uncertainty propagation procedure. The TSM method is standard in many areas of uncertainty analysis, but has seen limited attention in the simulation of building energy systems.

An integral part of uncertainty analysis is the definition of the input uncertainties. The uncertainty of the thermal load in a building, for example, is expected to be an important factor contributing to the overall uncertainty, and previous studies have not given a full and adequate characterization of the factors that contribute to the thermal

load uncertainty. The variation in the weather conditions is the main source of uncertainty in the thermal load. MacDonald and Strachan [2001] accounted for uncertainties in the weather conditions by using a fixed uncertainty range for basic weather parameters (e.g. temperature, radiation, wind speed, etc.). Corrado and Mechri [2009] used a similar approach except only monthly averages of a few weather parameters (e.g. Temperature, solar radiation, and wind speed) were used. However, since the amount of variation in weather conditions that can be expected is not constant throughout the year, this method does not adequately characterize the uncertainty in the thermal load. Additionally, these studies greatly over simplify the problem, since many relevant weather parameters are ignored and the interactions between the various weather parameters are not considered.

Other key input parameters whose uncertainty is difficult to characterize are the PGU performance, the cost of electricity purchased from the grid, and the cost of natural gas. For example, the uncertainty in the performance of PGU's can be difficult to characterize because of their nonlinear efficiency curves. Additionally, the uncertainty in the prices for natural gas and electricity can be difficult to model. Houwing et. al [2008] have presented uncertainties in energy prices that result from implementation of CHP systems. They consider uncertainty in factors such as energy provider policy and government policy (e.g. taxes and tariffs). However, these factors are hard to characterize a priori and require extensive knowledge of the policies that apply to specific areas. This approach is difficult to implement in the modeling process and the assumptions required are extensive.

2.2 Building Load Simulation

Hourly values of the building thermal and electrical loads are essential for many studies on CCHP and other building energy systems. Knowledge of the building energy consumption profile facilitates the implementation of several types of efforts to reduce building operational costs [Neto and Fiorelli, 2007; Gamou, 2002]. For instance, hourly energy consumption data can be used to compare the costs of using conventional heating and cooling equipment with the cost of using technologies such as CCHP systems, ground-coupled heat exchangers, solar thermal, and solar photovoltaic technologies. Additionally, the hourly building consumption data is useful for optimal sizing and operation of CCHP system equipment.

Unfortunately, building energy profiles on an hourly basis are not usually available for existing buildings. The dynamic interactions between the weather conditions and building configuration require the use of highly sophisticated computer models to accurately simulate the hourly building loads. Drawbacks in using computer simulations include the considerable amount of detailed input data and time required from even experienced users [Zhu, 2006; Catalina et al., 2008]. Therefore, several methodologies have been developed that can be used to estimate energy consumption without the need for detailed simulation. Some of these methodologies are based on a combination of statistics and simulations [Yik et al., 2001; Pedrini et al., 2002; Gugliermetti et al., 2004]. On-line building energy predictions based on neural networks and genetic algorithms [Yokoyama et al., 2009; Yang et al., 2005; Canyurta et al. 2005] can also be used in some applications. Even the most detailed building simulations will not reproduce the energy consumption profile exactly because of uncertainty in the weather, usage pattern and

because of the extensive number of building parameters. Because of these limitations tools for estimating energy consumption have an accepted degree of uncertainty [Catalina et al., 2008; Gamou et. al, 2002; Deru et al., 2006].

Fumo et al. [2010] have presented a methodology that estimates the hourly building energy consumption based on the building utility bills and existing simulation results of Department of Energy (DOE) reference[1] EnergyPlus models [Torcellini et al., 2008]. A main assumption used in the development of Fumo's work was that buildings of roughly similar sizes and usage patterns, i.e., offices, hospitals, schools, supermarkets, etc., have similar distributions of electrical and fuel energies that are well characterized by the reference models. The building utility bill is used to shift the reference building profiles to account for differences in building parameters and weather conditions.

2.3 Optimal Sizing of CHP Systems

Many researchers have published studies concerning the problem of determining the optimal PGU size for a given building using mixed integer linear programming or nonlinear programming approaches [Ren et al., 2008; Beihong and Weiding, 2006; Azit and Nor, 2009; Li et al., 2008]. Others have developed heuristic approaches for selecting the PGU size based on the load duration curve. For example, Bruno et al. [2007] uses the "biggest rectangle method" in which the PGU with a thermal output that fills the largest area of the thermal load duration curve is selected. It has been shown by many, that such rule of thumb graphical techniques often do not yield optimal PGUs [Voorspools and D'haeseleer, 2006; Piacentino and Cardona, 2008].

[1] DOE reference building models were previously called benchmark building models.

Because optimal operation modes are based on the heating demand, an optimal sizing technique must include an approximation of the range of future weather conditions that are expected during the term of operation of the PGU. Many of the studies in the literature have used a single year of historical weather data or less to simulate the hourly heating and electric loads for a given building [Beihong and Weiding, 2006; Azit and Nor, 2009; Li et al., 2008]. For example, Li et al. [2008] bases optimal decisions on three representative days. They separate a single year of historical, hourly heating demands into three seasons, and use this data to define a probability distribution for each hour of the representative days. However, weather conditions can vary significantly from one year to the next, so a single year of weather data may not accurately approximate the hourly heating demand probability distribution for the several years in which the PGU is expected to operate. An optimal sizing method that accounts for several years of historical weather data would give more robust results, since several years of historical data can more accurately predict the range of variation that can be expected in the term of operation of the PGU. This approach has probably been avoided in recent works because of the extensive calculations that are required in mixed integer approaches.

Variation in the cost of electricity and fuel can also have a significant effect on the optimal sizing problem. For example, Yun et al. [2012] reveals that the ratio of the electricity cost to the fuel cost determines the operation modes that yield savings for a given PGU. Some studies on optimal sizing have presented the sensitivity of their solution with respect to fuel and electricity price [Ren et al., 2008; Azit and Nor, 2009]. However, these sensitivities are not incorporated into the decision making process. There

is a need, therefore, for a reasonable approach to making a decision in the midst of uncertainty in the future cost of electricity and fuel.

Another limitation of many of the works in the literature is that they are only loosely based on commercially available PGUs, and, therefore, the simulation results are not as useful for design. For example, many studies define the equipment performance characteristics as either constants [Li, 2008] or as analytic functions of capacity [Ren et al., 2008; Beihong and Weiding, 2006]. These functions oversimplify the relationship between capacity and performance characteristics, and this simplification can lead to false conclusions. When the optimal sizing problem is cast in terms of fictitious performance characteristics the solution can be a PGU that is not commercially available, which is not practical for design decisions. The work by Azit et al. [2009] uses performance curves derived directly from real engines and implements a discrete optimal sizing scheme. This approach is essential to ensuring realistic solutions to the optimal sizing problem.

2.4 Predictive Modeling of Thermal Systems

Predictive or feed-forward operational control schemes have been shown to greatly improve the efficiency of building energy systems. For example, some researchers have developed algorithms that use thermal storage systems to shift the thermal building load to off-peak hours and, therefore, reduce the demand energy charges for the building. This load shifting is accomplished by producing extra energy during off-peak hours and storing that thermal energy for use during on-peak hours [Yao et al. 2004; Zhou et al. 2008]. Braun et al. [2001] demonstrated the advantages in operation cost of using pre-cooling to shift the cooling load to off-peak time. Another way that feed-

forward control schemes can improve building energy efficiency is demonstrated in topping-cycle combined heating and power (CHP) systems. In these systems the optimal balance between load met by the electric and gas distribution grids and the CHP system must be found for a variety of electric and thermal loading conditions. Based on the variable efficiencies of the system components at different load conditions the operation mode must be selected for each loading condition and for a given fuel to electricity cost ratio. Cho et al. [2010] and Yun et al. [2011] presented optimal CHP system operation algorithms that were based on prediction of building load and CHP performance using non-experimentally based TRNSYS models. They found that significant savings could be achieved using this predictive control approach versus using a control scheme based on estimates of current load values only.

Predictive modeling of building energy systems is essential for implementing optimal feed-forward HVAC and CHP control strategies. While purely theoretical models have their place for general studies, experimentally based models are needed to make detailed conclusions for design and control purposes. Once a model is validated using experimental data, the effects of all assumptions and inaccuracies can be clearly determined and the challenges for optimal operation and control can be plainly understood.

A variety of approaches have been used to develop thermal system models for building energy systems. These approaches can be categorized as three basic types: physical models, black-box models, and grey-box models. Physical models of building energy systems use modeling equations derived directly from known physical laws such as energy conservation. EnergyPlus is an example of a standard building energy system

model that allows the user to put in very detailed information about the building and energy systems. This type of model is effective for general studies, but when trying to model a specific building, this technique can be very time consuming because of the need to find all of the information and physical parameters for the system. Black-box models, on the other hand, rely heavily on experimental data in order to develop models. In other words, a model is developed through parameter estimation techniques to generate models that match experimental data with less focus on matching known physical laws. Researchers have developed a variety of black-box models for predicting building loads and internal conditions such as artificial neural networks [Kawashima et al., 1996], recursive least squares [Chen, 2002; Chen and Athienitis, 2003], Box Jenkins [Mustafaraj et al., 2010], and auto-regressive techniques [Mustafaraj et al., 2010]. The drawback of black-box models is that the model training data may not be rich enough to develop an accurate model for all expected operating conditions [Zhou et al., 2008]. In other words, the model may not work well in some conditions that are not included in the training data set. Grey-box models present an effective compromise between physical and black-box models. Grey-box models are based on energy conservation, but the physical parameters are determined using parameter estimation techniques. This approach reduces the effort required to determine the parameters of the system, and does not require as rich of a training data set for accurate models. For example, Balan et al. [2011] presented a grey-box model for temperature inside a house that only perturbed a set of guess values for the physical parameters using a search method to minimize the error between the model and the experimental data. Wang and Xu [2006] presented a grey-box model of a

multilayered wall and used a genetic algorithm to find the thermal capacitance and resistances for a lumped capacitance model.

One common link among the many different techniques for parameter estimation used for black-box and grey-box models is that they all include similar information in the cost function (i.e. the error minimization function). The parameters for a given component in the system are typically selected to minimize a cost function that is some form of the error between the measured output and the predicted output (e.g. square of the residual error) for that component. For example, Anderson et al. [2007] presented a grey-box model for an HVAC system that can be used in predictive control. In this model a least-squares polynomial fit was used to estimate the parameters for each component in the model separately. In other words, the parameters were selected to minimize the error between the prediction of one component and the measured output of that component without considering the other measurements and predictions in the thermal system. Nassif et al. [2008] presented a grey-box dynamic model of an HVAC system and zone temperature. A genetic algorithm was used to estimate the parameters for the model. For each component, parameter estimation was performed and the parameters were selected to minimize the square of the error between the predicted values of each component and the measured values for each component.

When a model is used to predict the states of a multi-component thermal system several time steps ahead, parameter estimation using the standard cost function approach can produce models that yield excessive drift due to the propagation of measurement and modeling errors. Small errors in a given measurement or component model propagate through the entire system and their effects are compounded as the prediction time

increases. The effects of these errors can be significantly reduced by taking advantage of the functional relationship between the variables in the system. When variables of interest in a system are functionally related, experimental measurements of these variables must be correlated. Accounting for this correlation during parameter estimation helps minimize the effect of the measurement and modeling errors in the predictions of the model. This can be accomplished by estimating the parameters for each component in the thermal system model simultaneously.

CHAPTER III

UNCERTAINTY ANALYSIS OF BUILDING SIMULATIONS

As mentioned in Chapter II, CCHP system models have been used by many researchers to compare the performance of CCHP systems against conventional systems. However, decisions based on the results of computer simulations need to take into account the uncertainty of these results to get insight into the level of confidence in the predictions. This chapter presents an analysis of a CCHP system model under different operating strategies with input and model data uncertainty. Unfortunately, the uncertainties that underlie the variation in input parameters such as the thermal load, natural gas prices and electricity prices are not readily available. Additionally, engine performance uncertainty can be difficult to characterize because of the nonlinearity of engine efficiency curves. Therefore, a significant contribution of the work presented in this chapter is the definition of practical and novel approaches to estimating the uncertainty in these and other input parameters. A case study using a small office building located in Atlanta, GA is described to illustrate the importance of the use of uncertainty and sensitivity analysis in CCHP system performance predictions. The results of the case study show how the primary energy consumption, operational cost, and carbon dioxide emissions are affected by the uncertainty associated with the model input parameters.

3.1 Analysis

As in Mago et al. [2009] the performance of the CCHP system studied in this chapter was evaluated according to three factors: primary energy consumption, cost, and carbon dioxide emissions. Following the example of previous studies [Mago et al., 2009; Cho et al., 2009b], two different operational strategies are employed and analyzed: following the electric load (FEL) and following the thermal load (FTL). To study and evaluate the performance of CCHP systems operating under these strategies, thermodynamic models of the different components have been developed. A schematic of the CCHP system analyzed in this chapter is shown in Figure 3.1. The building model, energy loads, and basic modeling equations that were used to model the system are defined in Section 3.1.1. The fuel and electricity requirements for the electric and thermal load following strategies are presented in Sections 3.1.2 and 3.1.3, respectively. The ultimate goal in these sections is to define the fuel and grid electricity requirements so that the three performance factors listed above can be used to evaluate the two operation strategies.

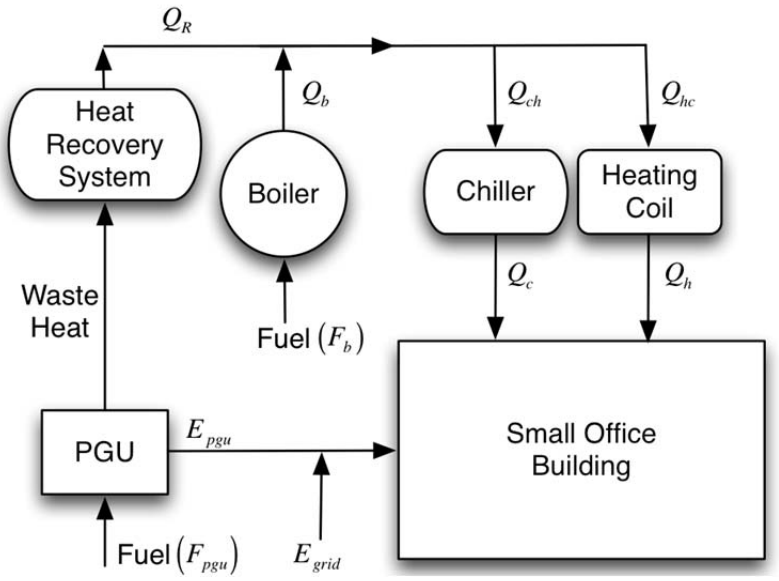

Figure 3.1 Schematic of a CCHP system

3.1.1 Building Model, Energy Loads, and Basic CCHP System Model Equations

The U.S. Department of Energy has developed several commercial building reference models. These building models provide standard values of parameters such as floor area, occupancy schedule, equipment and lighting schedules and thermostat schedule for different building types and locations. The main benefit of the standardized reference models is that they form a common point of comparison between research projects [Torcellini et al., 2008]. The current study focuses on a new small office reference building with a 511 m^2 floor area that is located in Atlanta, GA. The reference building was simulated using the software, EnergyPlus, to obtain hourly site energy load data.

Typical Meteorological Year (TMY3) data from the National Renewable Energy Laboratory (NREL) is widely used to simulate building electric and thermal loads. Therefore, TMY3 data for the city of Atlanta was used in an EnergyPlus simulation to

find the hourly energy loads for the reference building described above. The electric load generated by EnergyPlus represents all of the non-thermal electricity needs of the building (lights, appliances, etc.) and will be denoted as E_{load}. The cooling and heating loads generated from the EnergyPlus simulation are denoted as Q_c and Q_h, respectively. When the efficiencies of the chiller and heating coil are considered, the thermal load of the building translates into the following heat energy requirement

$$Q_{REQ} = \frac{Q_C}{COP_{ch}} + \frac{Q_h}{\eta_{hc}} \tag{3.1}$$

where COP_{ch} and η_{hc} represent the chiller coefficient of performance and the heating coil efficiency, respectively. The first term of Equation (3.1) represents the heat required by the chiller to meet the cooling load and the second term of Equation (3.1) represents the heat required by the heating coil to meet the heating load.

The engine selected for the power generation unit (PGU) for this model has a nominal power output of 15 kW, which will be represented as E_{PGU_nom}. Cho et al. [2009b] have shown that the relationship between power output of an internal combustion engine PGU and the rate of input fuel energy can be modeled using a straight line. Likewise, for the PGU selected for this case study, the data supplied by the manufacturer revealed a straight line relationship between the power output of and the rate of fuel input as illustrated in Figure 3.2. Based on this straight line relationship the power output of the PGU is defined in the model as

$$E_{PGU} = m \cdot F_{PGU} + b \tag{3.2}$$

where m and b are the slope and intercept of the line describing the relationship between power output and the rate of fuel energy input.

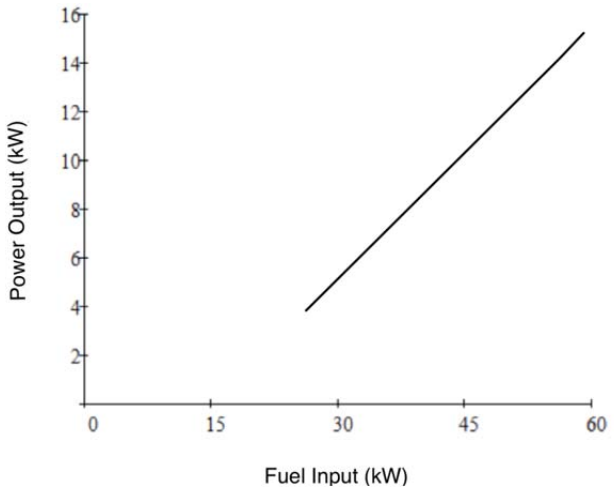

Figure 3.2 Engine Power Output Vs. Fuel Input (using data from engine manufacturer)

The recovered waste heat from the prime mover can be estimated as

(3.3)

where Q_{REC} is the recovered thermal energy and η_{rec} is the heat recovery system efficiency.

When the boiler is required for meeting the building thermal demand, the boiler fuel energy consumption is computed as

— (3.4)

where η_b is the boiler thermal efficiency and Q_b is the useful heat generated by the boiler.

3.1.2 CCHP system model following the electric load (FEL).

For the FEL operation strategy the electric load of the building drives the PGU operation. The PGU is limited to operate between a power output range of 3.75 kW (i.e. quarter load) to 15 kW (i.e. nominal or rated load), and these limits will be denoted as E_{PGU_min} and E_{PGU_nom}. When the electric load of the building is less than E_{PGU_min}, the

electric load is met entirely by the grid. When the electric load of the building is greater than or equal to E_{PGU_min} and less than or equal to E_{PGU_nom}, the PGU provides for the electric load of the building. Thirdly, when the electric load is greater than E_{PGU_nom}, the PGU provides E_{PGU_nom} and the rest of the electric load is met by the grid. These three cases are defined as

- Case 1: If $E_{load} < E_{PGU\_min}$, then $E_m < E_{load}$ and $E_{PGU} = 0$
- Case 2: If $E_{PGU\_min} \leq E_{load} \leq E_{PGU\_nom}$, then $E_m = 0$ and $E_{PGU} = E_{load}$
- Case 3: If $E_{load} > E_{PGU\_nom}$, then $E_m = E_{load} - E_{PGU\_nom}$ and $E_{PGU} = E_{PGU\_nom}$

The total electricity registered at the meter for the FEL operation strategy is defined as

$$E_m = E_{load} \cdot (1 - \phi_{1e}) + (E_{load} - E_{PGU\_nom}) \cdot \phi_{2e} \tag{3.5}$$

where Φ_{1e} and Φ_{2e} represent unit step functions which act as triggers for the case logic transition points and are defined as follows

$$\phi_{1e} = \phi(E_{load} - E_{PGU\_min}) \tag{3.6}$$

$$\phi_{2e} = \phi(E_{load} - E_{PGU\_nom}) \tag{3.7}$$

where $\Phi(\cdot)$ is the Heaviside step function, which takes a value of one if the argument is greater than zero and takes a value of zero otherwise.

The fuel input to the system depends on the PGU and boiler operation. The fuel to the PGU is defined according to the three cases described above. If the recovered

thermal energy is not large enough to handle the thermal load (cooling or heating) additional heat has to be provided by the auxiliary boiler. It follows that the fuel requirement of the system can be described using the following five cases

- Case 1: If $E_{load} \leq E_{PGU\_min}$, then $F_{PGU} = 0$ and $F_b = \frac{Q_{REQ}}{\eta_B}$
- Case 2: If $E_{PGU\_min} \leq E_{load} \leq E_{PGU\_nom}$ and $Q_{REC} \geq Q_{REQ}$, then $F_{PGU} = \frac{E_{load} - b}{m}$ and $F_b = 0$
- Case 3: If $E_{PGU\_min} \leq E_{load} \leq E_{PGU\_nom}$ and $Q_{REC} < Q_{REQ}$, then $F_{PGU} = \frac{E_{load} - b}{m}$ and $F_b = \frac{Q_{REQ} - Q_{REC}}{\eta_b}$
- Case 4: If $E_{load} > E_{PGU\_nom}$ and $Q_{REC} \geq Q_{REQ}$, then $F_{PGU} = \frac{E_{PGU\_nom} - b}{m}$ and $F_b = 0$
- Case 5: If $E_{load} > E_{PGU\_nom}$ and $Q_{REC} < Q_{REQ}$, then $F_{PGU} = \frac{E_{PGU\_nom} - b}{m}$ and $F_b = \frac{Q_{REQ} - Q_{REC}}{\eta_b}$

These five cases can be combined to obtain the total fuel energy consumption registered at the meter for the FEL operation strategy as follows

$$F_m = \begin{matrix} \frac{Q_{REQ}}{\eta_b} \cdot (1 - \phi_{1e}) + \left[\frac{E_{load} - b}{m} + \left(\frac{Q_{REQ} - Q_{REC}}{\eta_b}\right) \cdot \phi_{3e}\right] \cdot (\phi_{1e} - \phi_{2e}) \\ + \left[\frac{E_{PGU\_nom} - b}{m} + \left(\frac{Q_{REQ} - Q_{REC}}{\eta_b}\right) \cdot \phi_{4e}\right] \cdot \phi_{2e} \end{matrix} \quad (3.8)$$

where Φ_{3e} and Φ_{4e} represent step functions which act as additional triggers for the case logic transition points. Φ_{3e} takes a value of one when case three occurs and a value of zero when case two occurs. Φ_{4e} takes a value of one when case 5 occurs and a value of zero when case four occurs. These step functions are defined as follows

$$\phi_{3e} = \phi\left(Q_{REQ} - Q_{REC_{23}}\right) = \phi\left(Q_{REQ} - \left(\frac{E_{load} - b}{m} + E_{load}\right) \cdot \eta_{rec}\right) \quad (3.9)$$

$$\phi_{4e} = \phi\left(Q_{REQ} - Q_{REC_{45}}\right) = \phi\left(Q_{REQ} - \left(\frac{E_{PGU\_nom} - b}{m} + E_{PGU\_nom}\right) \cdot \eta_{rec}\right) \quad (3.10)$$

3.1.3 CCHP system model following the thermal load (FTL)

For the FTL operation strategy the thermal load of the building drives the PGU operation. Again, the PGU is limited to operate between a power output range of 3.75 kW (E_{PGU_min}) to 15 kW (E_{PGU_nom}). When the thermal energy required to meet the building load, Q_{REQ}, corresponds to a power output less than E_{PGU_min}, then the engine is not operated and the boiler is used to meet the thermal load. When Q_{REQ} corresponds to a power output greater than or equal to E_{PGU_min} and less than or equal to E_{PGU_nom}, then the PGU is used to satisfy the thermal load. Thirdly, when Q_{REQ} corresponds to a power output greater than E_{PGU_nom}, then the PGU provides the thermal energy available for recovery at E_{PGU_nom} and the rest of the thermal load is met by the boiler. By combining Equations (3.2) and (3.3) we can find the recovered heat from the PGU in terms of power output as

$$Q_{REC} = \eta_{rec} \cdot \left(\frac{E_{PGU} - b}{m} - E_{PGU}\right) \quad (3.11)$$

The transition points for the three cases presented above can be found by substituting the values of E_{PGU_min} and E_{PGU_nom} into Equation (3.11). The resulting transition points are 16.73 kW (Q_{REC_min}) and 32.38 kW (Q_{REC_nom}). Therefore, the thermal load is met by the system as defined by the following cases

- Case 1: If $Q_{REQ} < Q_{REC\_min}$, then $F_{PGU} = 0$ and $F_B = \frac{Q_{REQ}}{\eta_b}$
- Case 2: If $Q_{REC\_min} < Q_{REQ} < Q_{REC\_nom}$, then $F_{PGU} = \frac{\frac{Q_{REQ}}{\eta_b}+b}{1-m}$ and $F_B = 0$
- Case 3: If $Q_{REQ} > Q_{REC\_nom}$, then $F_{PGU} = \frac{E_{PGU\_nom}+b}{m}$ and $F_B = \frac{Q_{REQ}-Q_{REC\_nom}}{\eta_b}$

These three cases can be combined to obtain the total fuel registered at the meter for the FTL operation strategy as

$$F_m = \frac{Q_{REQ}}{\eta_b}(\phi_{1t} - \phi_{2t}) + \left[\frac{\frac{Q_{REQ}}{\eta_{rec}}+b}{1-m}\right](\phi_{2t} - \phi_{3t}) + \left[\frac{E_{PGU_{nom}}-b}{m} + \left(\frac{Q_{REQ}-Q_{REC\_nom}}{\eta_b}\right)\right]\phi_{3t} \quad (3.12)$$

where Φ_{1t}, Φ_{2t}, and Φ_{3t} represent step functions which act as triggers for the case logic transition points and are defined as follows

$$\phi_{1t} = \phi(Q_{REQ} - 0) \quad (3.13)$$

$$\phi_{2t} = \phi(Q_{REQ} - Q_{REC\_min}) \quad (3.14)$$

$$\phi_{3t} = \phi(Q_{REQ} - Q_{REC\_nom}) \quad (3.15)$$

Electricity will only be imported from the grid if the electric load is greater than that provided by the engine. Therefore, the total electricity registered at the meter for the FTL operation strategy is defined as

$$E_m = (E_{load} - E_{PGU}) \cdot \phi_{4t} \quad (3.16)$$

where Φ_{4t} represents a step function which acts as a trigger for the case logic transition points and is defined as follows

$$\phi_{4t} = \phi(E_{load} - E_{PGU}) \tag{3.17}$$

Equation (3.16) can be expanded by writing E_{PGU} in terms of E_{PGU_nom} and Q_{REQ} as

$$E_m = \left[E_{load} - \left(\begin{matrix}\frac{m}{1-m}\left[\frac{Q_{REQ}}{\eta_{rec}} + b\right](\phi_{2t} - \phi_{3t}) \\ +b + \left[E_{PGU\_nom}\right]\phi_{3t}\end{matrix}\right)\phi_{2t}\right]\phi_{4t} \tag{3.18}$$

The export of the excess electricity generated onsite to the power grid can represent a primary energy saving and cost reduction that could be taken into consideration when comparing this system with the conventional system. However, this option is not available in many locations, so any excess electricity that is produced is assumed to be burned away through a bank of resistors.

3.1.4 Primary Energy Consumption, Carbon Dioxide Emissions and Cost for all the operation modes

The first standard metric for assessing the thermal energy efficiency from the use of CCHP systems is primary energy consumption (PEC). PEC is defined by the energy information administration (EIA) as the amount of site energy consumption, plus losses that occur in the generation, transmission, and distribution of energy. Therefore, the building PEC is determined as

$$PEC = (E_m \cdot ECF_{PEC} - F_m \cdot FCF_{PEC}) \tag{3.19}$$

where ECF_{PEC} and FCF_{PEC} are the site-to-primary energy conversion factors for electricity and natural gas, respectively. The site-to-primary energy conversion factors

used in the model are 3.336 for electricity and 1.047 for natural gas [Environmental Protection Agency, 2008].

The amount of Carbon Dioxide Emissions (CDE) per year can be determined using the emission conversion factors for electricity and natural gas as follows

$$\mathrm{CDE} = (\mathrm{E_m} \cdot \mathrm{ECF_{CDE}} - \mathrm{F_m} \cdot \mathrm{FCF_{CDE}}) \tag{3.20}$$

where $\mathrm{ECF_{CDE}}$ and $\mathrm{FCF_{CDE}}$ are the emission conversion factors for electricity and natural gas, respectively. The emission conversion factors used in the model are 0.000601 ton $\mathrm{year^{-1}kWh^{-1}}$ for electricity and 0.0002 ton $\mathrm{year^{-1}kWh^{-1}}$ for natural gas [Environmental Protection Agency, 2008].

The Cost of operation for each mode can be determined using the cost of electricity and natural gas as follows

$$\mathrm{Cost} = (\mathrm{E_m} \cdot \mathrm{C_e} - \mathrm{F_m} \cdot \mathrm{C_f}) \tag{3.21}$$

The average yearly prices of electricity in Georgia from 1991 to 2007 were obtained from the Energy Information Administration (EIA) [2007], and these prices were used to calculate the expected cost of electricity in 2010 used in the model. The price of electricity used in the model is 0.082 $/kWh and is found by adding three times the average yearly price shift to the price of electricity in 2007. Similarly, the monthly prices of natural gas for a representative company in Georgia from 2001 to 2009 were obtained from the Georgia Public Service Commission [2009]. The expected cost of natural gas in 2010 used in the model is found by adding the average yearly price shift for each month to the monthly natural gas prices of 2009; the results for 2010 are as follows: 4.9¢/kWh

in January, 4.7¢/kWh in February, with a steady monthly increase to 8.7¢/kWh in July, followed by a steady decrease to 4.6¢/kWh in December.

3.2 Model Uncertainty

To evaluate the performance of the CCHP model presented in Section 3.1, a complete uncertainty analysis was completed. To conduct an appropriate uncertainty analysis, all the model parameters and their associated uncertainties must first be identified. For each input variable, the uncertainties were calculated using a combination of manufacturer's specifications, engineering judgment and experience, analytical models, and previous data.

The uncertainty in the performance factors was determined by propagating the input uncertainties through the model equations using the Taylor Series Method (TSM). Since the model presented in Section 3.1 is linear, the TSM should provide the same results as the Monte Carlo uncertainty propagation method (assuming all input distributions are Gaussian) but with much lower CPU time. Uncertainty propagation using the TSM is defined as [Coleman and Steele, 2009]

$$u_s{}^2 = \begin{array}{l} \sum_{i=1}^{J} \theta_i{}^2 b_i{}^2 + 2\sum_{i=1}^{J-1}\sum_{k=i+1}^{J} \theta_i \theta_k b_{ik} \\ + \sum_{i=1}^{J} \theta_i{}^2 s_i{}^2 + 2\sum_{i=1}^{J-1}\sum_{k=i+1}^{J} \theta_i \theta_k s_{ik} \end{array} \tag{3.22}$$

where u_s represents the combined standard uncertainty for the variable predicted by the model (i.e. *S)*. The θ_i terms represent the partial derivatives of the model equation with respect to input variable, i. The variables, b_i and s_i represent the estimates of the systematic and random error standard deviations. Finally, the terms b_{ik} and s_{ik} represent estimates of the covariance between errors in input variables for systematic and random

error sources, respectively. For the model discussed in this chapter, correlation in the systematic error sources is not considered. Also, the systematic and random error terms can be combined to simplify Equation (3.22) as follows

$$u_s{}^2 = \sum_{i=1}^{J} \theta_i{}^2 u_i{}^2 + 2 \sum_{i=1}^{J-1} \sum_{k=i+1}^{J} \theta_i \theta_k s_{ik} \tag{3.23}$$

where u_i represents the combination of the systematic and random error standard deviations. The uncertainty at a 95% confidence can then be obtained by multiplying the combined standard uncertainty by a coverage factor, K, as

$$\mathrm{U_s} = \mathrm{K} u_s \tag{3.24}$$

In the case of a small sample of the input parameters, the t distribution is used to represents the 95% confidence interval (assuming a normal distribution) and the coverage factor is determined based on the number of degrees of freedom in the sample. Otherwise, a value of two is used for the coverage factor in most engineering applications [Coleman and Steele, 2009].

In addition to the simulation uncertainty calculated using Equation (3.23), the Uncertainty Percentage Contribution (*UPC)* for each variable can be obtained by using the definition that follows

$$\mathrm{UPC_i} = \frac{\theta_i{}^2 \mathrm{U_i}{}^2}{U_s{}^2} \tag{3.25}$$

UPC_i reprecents the percentage of the uncertainty in the result that was contributed by the uncertainty in input i. For this model the uncertainty in the input parameters is propagated through the use of Equation (3.23) to find the uncertainty in the performance parameters discussed in Section 3.1.4 (PEC, CDE, and Cost,). For reasons specified below the

uncertainty will be calculated on a monthly basis and then combined to find the yearly total.

3.3 Input Parameter Uncertainty

This section presents the input parameter uncertainties for the thermal load, PGU power output, component efficiencies, fuel and electricity cost, primary energy conversion factors, and emissions conversion factors.

3.3.1 Thermal Load Uncertainty

The fuel and grid electricity requirement equations (i.e. Equations (3.5), (3.8), (3.12) and (3.16)) contain several factors that are dependent on the thermal load of the building including Q_c, Q_h, Φ_{3e}, Φ_{4e}, Φ_{1t}, Φ_{2t}, Φ_{3t}, Φ_{4t} and combinations (i.e. products) of these terms. These terms and their combinations will be referred to as thermal load factors. Many of the thermal factors are correlated since one factor may be a function of another factor (e.g. Φ_{1t} is a function of Q_c and Q_h). To find how the uncertainty in these factors affects the uncertainty in the performance metrics, the covariance matrix for the factors must be calculated. Different combinations of the thermal load occur in the two operation strategies (FEL and FTL). Therefore, separate covariance matrices must be calculated for the two strategies. In the remainder of this section, a method for creating the covariance matrix will be illustrated for the FEL strategy, i.e. Equations (3.5) and (3.8). Equations (3.5) and (3.8) can be expanded in terms of the thermal and electrical loads as

$$E_{m_i} = \left(E_{load_i}\right)\left(1-\Phi_{1e_i}\right)+\left(E_{load_i}-\mathrm{E}_{\mathrm{PGU\_nom}}\right)\Phi_{2e_i} \tag{3.26}$$

$$
\begin{aligned}
F_{m_i} = & \left[\left(\frac{Q_{c_i}}{COP_{ch}} + \frac{Q_{h_i}}{\eta_{hc}}\right)\frac{1}{\eta_B}\right]\left(1 - \Phi_{1e_i}\right) \\
& + \left[\frac{E_{load_i} - b}{m} + \left(\frac{Q_{c_i}}{COP_{ch}} + \frac{Q_{h_i}}{\eta_{hc}} - \left(\frac{E_{load_i} - b}{m} - E_{load_i}\right)\eta_{rec}\right)\frac{1}{\eta_B}\Phi_{3e_i}\right]\left(\Phi_{1e} - \Phi_{2e_i}\right) \\
& + \left[\frac{\mathrm{E_{PGU\_nom}} - b}{m} + \left(\frac{Q_{c_i}}{COP_{ch}} + \frac{Q_{h_i}}{\eta_{hc}} - \left(\frac{\mathrm{E_{PGU\_nom}} - b}{m} - \mathrm{E_{PGU\_nom}}\right)\eta_{rec}\right)\frac{1}{\eta_B}\Phi_{4e_i}\right]\Phi_{2e_i}
\end{aligned}
\qquad (3.27)
$$

where the i subscript indicates an hourly value.

The only variable terms in Equations (3.26) and (3.27) are the thermal load factors (i.e. the thermal loads and the thermal mode step functions) and the electric load factors (i.e. the electrical load and the electrical mode step functions). The covariance between these variables could be calculated for every hour in the year. However, no accuracy is lost if the covariance matrices are calculated monthly. To understand this fact, consider the equations for the performance metrics (i.e. Equations (3.19), (3.20), and (3.21)). Each of these equations contains factors multiplied by the fuel and electricity consumption. The conversion factors used in Equations (3.19) and (3.20) to obtain PEC and CDE are constants. In Equation (3.21) the cost of natural gas varies monthly and the cost of electricity for this analysis varies yearly. Therefore, calculating the uncertainty of the performance metrics on an hourly basis will give the same result as calculating the uncertainty on a monthly basis. If the uncertainty in the fuel was calculated on an hourly basis, then when propagating the uncertainty, the hourly uncertainty would be multiplied by the same constant for the entire month. Therefore, to minimize computation effort, the covariance matrices for the thermal load and electrical load factors were calculated on a monthly basis. Summing Equations (3.26) and (3.27) for each month and rearranging gives the following equations in terms of distinct thermal load electrical load factors as

$$E_{m_j} = \left\lfloor E5_j + E1_j + E4_j - \mathrm{E}_{\mathrm{PGU\_nom}} E3_j \right\rfloor \tag{3.28}$$

$$\begin{aligned} F_{m_j} = & \left(\frac{T1_j + T3_j + T7_j - T10_j - T14_j}{COP_{ch}\eta_B} + \frac{T2_j + T4_j + T8_j - T11_j - T15_j}{\eta_{hc}\eta_B} \right) \\ & + C1\left(T5_j - T13_j\right) + C2\left(T6_j - T12_j\right) + C3\left(T9_j\right) \\ & + \left(\frac{E1_j - b\left(E2_j\right) + \mathrm{E}_{\mathrm{PGU\_nom}}\left(E3_j\right) - E4_j}{m} \right) \end{aligned} \tag{3.29}$$

where, the T variables are products of the thermal load, the E variables are products of the electric load.

As described above in Section 3.1.1, TMY3 data for the city of Atlanta was used in an EnergyPlus simulation to find the hourly energy loads for the reference building. The TMY3 weather data was created from an analysis of forty-five years (1961 to 2005) of weather data. A team of analysts at the National Renewable Energy Laboratory (NREL) surveyed the forty-five sets of weather conditions for each month and selected the data set that was most typical for that month. In this study, the weather variability expected from year to year was assessed using the most recent fifteen consecutive years of weather data (1991-2005) from the forty-five year set. Each of the fifteen years of weather data were used in a simulation for the same building using Energy Plus to find hourly heating and cooling loads.

The covariance matrix for each month is obtained by considering the year-to-year variation of the monthly values. Each year will produce twelve sets of 15 thermal load factors as defined above. The covariance matrix between the 15 thermal load factors is then calculated for each month. The covariance matrix for the thermal load factors for the j-th month was calculated as

$$Cov_j = \frac{1}{N-1}\sum_{k=1}^{15}\left[T_{k,j}{T_{k,j}}^T\right] \tag{3.30}$$

where N is the total number of years (15 for this case study), the subscript, k, represents the year of weather data used, and T is a vector defined as

$$T_{k,j} = \left[T1_{k,j} - \mu_{T1} \quad T2_{k,j} - \mu_{T2} \quad \cdots \quad T14_{k,j} - \mu_{T14} \quad T15_{k,j} - \mu_{T15}\right]^T$$

where each term in the vector T represents a random variable defined as one thermal load factor minus its mean value, μ. Each random term will have a distribution of 15 terms, one for each of the 15 years of weather data.

This covariance matrix can then be used in Equation (3.23) to find the uncertainty in the fuel and electricity requirements for the FEL operation strategy. The diagonal terms of this matrix represent the square of the standard deviations denoted as s_i in Equation (3.22). The off-diagonal terms give the covariance between thermal load factors, which are denoted as s_{ik} in Equation (3.22).

These uncertainties in the fuel and electricity requirements are then used to find the uncertainty in the each of the performance metrics for the FEL strategy. Additionally, the process for finding the uncertainty in the thermal load factors for the FTL operational strategy is similar to that described above.

As with the heating and cooling loads, the electric load for the building was found by simulating a small reference office building in EnergyPlus. The uncertainty associated with the electric load generated by EnergyPlus was set as zero since the load is expected to be fairly constant from year to year, and no adequate way to model the variation has been determined.

3.3.2 Engine Power Output Uncertainty

The uncertainty used for the power output of the PGU was designed to vary with the operating point. In the authors' experience, the PGU performance will be more predictable when operating at rated conditions (E_{PGU_nom}) and will become more uncertain as the operation mode departs from rated conditions. For simplicity, the uncertainty range for the power output was introduced using a single variable, i.e., the slope, as shown in Figure 3.3 (exaggerated for visualization). As Figure 3.3 illustrates, the uncertainty bands intersect the Power output/Fuel input line at 26.25 kW and branch out from this point. The choice of 26.25 kW was merely a consequence of the specification of the uncertainty range as described below. These lines represent the uncertainty in the slope and intercept of the straight line relationship between the power output and power input.

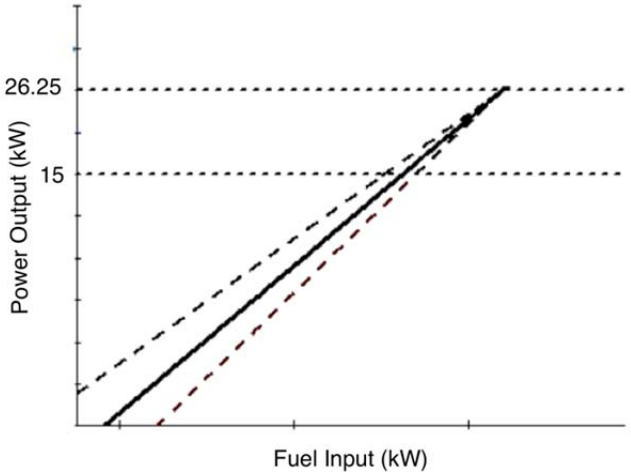

Figure 3.3 Engine power output uncertainty range (exaggerated for visualization)

The uncertainty range shown in Figure 3.3 was implemented by using a single parameter to modify both the slope and the intercept with a fixed intersection point at 26.25 kW. The random uncertainty factor was chosen such that the uncertainty range was +/- 0.6 kW at a power output of 3.75 kW i.e., quarter load and +/- 0.3 kW at E_{PGU_nom} (15 kW). No systematic uncertainty was considered for the engine curve. The new equation relating the power output and fuel input with the added uncertainty factor is given as

$$E_{PGU} = (m + c_m s)F_{PGU} + (b + c_b s) \tag{3.31}$$

where c_m and c_b are constants and s is the uncertainty factor. The constants c_m and c_b are chosen such that the slope and intercept of the line vary according to the selected range when s is equal to 0.6. For nominal operation the s factor is zero and Equation (3.31) becomes equivalent to Equation (3.2). However, the s factor is given an uncertainty of +/- 0.6. Figure 3.4 illustrates zoomed in views of the power output uncertainty graph. As illustrated in Figure 3.4 the uncertainty ranges from 14.7 kW to 15.3 kW at rated conditions and from 3.15 kW to 4.35 kW at an operating point of 3.75 kW.

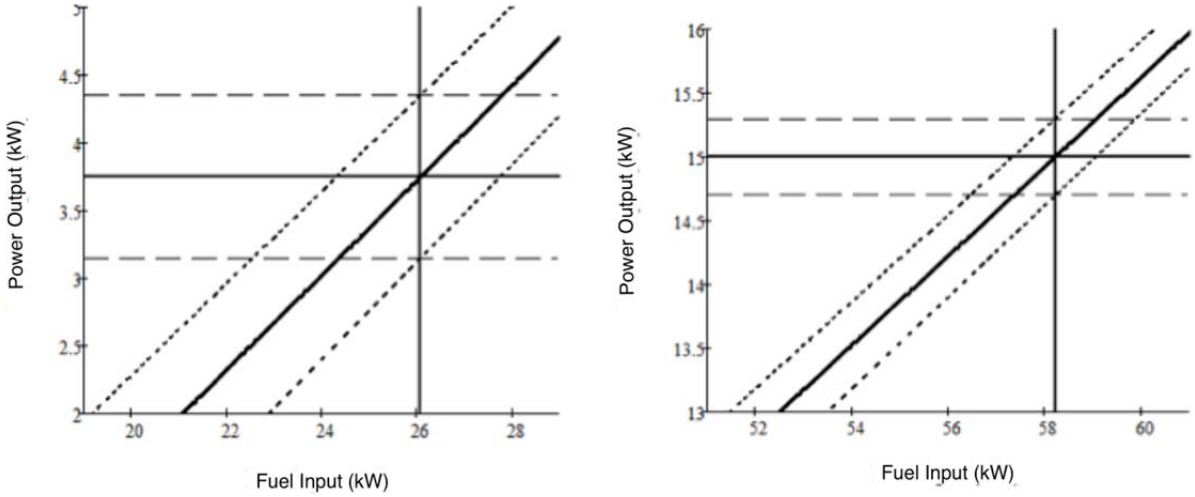

Figure 3.4 Zoomed in views of the power output uncertainty graphs

3.3.3 Conversion factor uncertainty

The primary energy conversion factors for electricity and natural gas are based on a national average stipulated by the Environmental Protection Agency (EPA). The EPA uses the same conversion factors for all areas of the United States so that fair comparisons can be made for building energy standards [EPA, 2008]. Because the EPA stipulates these conversion factors, no uncertainty was specified for these factors.

Similarly, the EPA stipulates the carbon dioxide emissions conversion factors for electricity and natural gas. These factors are based on the fuel mix used by the energy providers and can be expected to be relatively constant. Therefore, no uncertainty was specified for these factors.

The natural gas cost was estimated based on a representative Atlanta provider. Monthly price data from several Georgia power companies was collected from the Georgia Public Service Commission [2009]. The prices for each company followed a similar trend. Therefore, a single representative company was selected to define the

monthly cost and variation. The monthly natural gas prices were analyzed for the years from 2001 to 2009. As expected, the general trend was an increase in prices from one year to the next. Therefore, a factor was defined to quantify the expected shift upward in the prices each year. For each month, the average shift over the nine-year period was taken as the shift to be expected for the tenth year. Therefore, for each month the cost was defined as the cost in 2009 plus the average shift for that month. Additionally, the uncertainty of the shift factor was defined using the small sample t-distribution as a model. The random uncertainty in the shift factor was defined as the sample standard deviation of the distribution for each month multiplied by the t-distribution factor. No systematic uncertainty was defined for the shift factor.

A similar process was used for the calculation of electricity cost and electricity cost uncertainty. Monthly price data for the electricity was not available. However, average yearly prices for the state of Georgia were obtained from the EIA website [2007]. The yearly prices were analyzed from 1990 to 2007. By a similar process as that used for natural gas, the average shift was used to estimate the cost of subsequent years, and the t-distribution factor was multiplied by the sample standard deviation to find the 95% confidence random uncertainty. Additionally, there is a systematic uncertainty in the cost of electricity since the monthly prices analyzed were averages for the state of Georgia. Therefore, the systematic uncertainty was estimated as 5% of the hourly electric load.

3.3.4 Efficiency uncertainty

The random and systematic uncertainty values for the chiller COP, the heating coil efficiency, and the heat recovery efficiency were selected to be +/- 0.5% and +/- 5% on the basis of engineering judgment, manufacturer data, and experience with the

equipment. Table 3.1 illustrates the random and systematic uncertainty values that were used for the inputs for this simulation.

Table 3.2 Random and Systematic Uncertainty in Input Parameters

Parameter	Random Uncertainty	Systematic Uncertainty
Thermal Load Factors	Covariance matrix, C	
Electric Load Factors	0	0
COP_{ch}	0.00325	0.05
n_{hc}	0.00375	0.05
n_{rec}	0.00375	0.05
n_B	0.00425	0.05
b	0	0
m	0	0
s	0.02	0.6
ECF_{PEC}	0	0
FCF_{PEC}	0	0
C_e (\$ kWh^{-1})	0.00535	5%
C_f (\$ kWh^{-1})	Variable	5%
ECF_{CDE} (ton $year^{-1}kWh^{-1}$)	0	0
FCF_{CDE} (ton $year^{-1}kWh^{-1}$)	0	0

3.4 Results

The uncertainties in the inputs were propagated using the standard uncertainty method as described in Section 3 for each month of the year-long simulation. The uncertainty was summed for the whole year for the performance factors of interest: Primary Energy Consumption, Operational Cost, and Carbon Dioxide Emissions. The total uncertainties and parameter values for the yearly simulation of the CCHP system FEL are given in Table 3.2. Additionally, the UPCs for each output of interest are composed in pie charts as illustrated in Figure 3.5.

Table 3.3 Output uncertainty for FEL model

Parameter	Total	Uncertainty	Percentage
Cost ($/year)	16,137	+/- 2,136	+/- 13.24%
PEC (kWh)	293,429	+/- 8,471	+/- 2.89%
CDE (ton/year)	55.53	+/- 1.62	+/- 2.91%

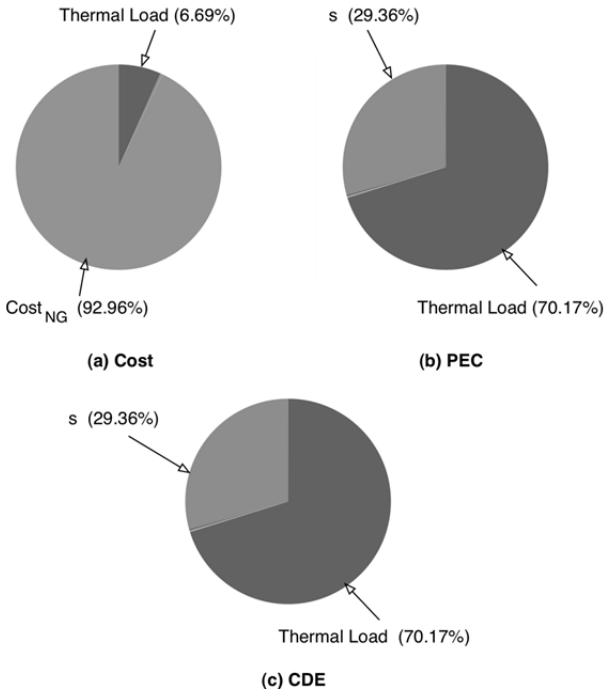

Figure 3.5 UPC Chart for the (a) Cost, (b) PEC, and (c) CDE for CHP system FEL

Figure 3.5(a) illustrates that the uncertainty in the cost of natural gas dominates the uncertainty in the operational cost. The partial derivative with respect to the fuel cost and the uncertainty in fuel cost are comparatively high, so this combination results in a much higher output uncertainty for the total yearly cost. Additionally, this conclusion is supported by the extensive use of the PGU in this strategy. For example, the PGU operates for approximately half of the hours of the simulation for this strategy. Figure

3.5(b) illustrates that the uncertainty in the yearly PEC is dominated the by the thermal load factors. This is expected since the uncertainty in the weather conditions is quite high. The s factor in the PGU power output versus fuel input relationship (see Equation (3.31)) also has a significant effect on the PEC uncertainty. It is important to mention here that there is no input uncertainty from the conversion factors for PEC. If there was uncertainty in the conversion factor, then a similar trend as in Figure 3.5(a) would occur where the primary energy conversion factor would have a significant effect on the total uncertainty. Figure 3.5(c) illustrates that the behavior of the CDE uncertainty is equivalent to that for the PEC.

The total uncertainties and parameter values for the yearly simulation of the CCHP system in the FTL operation mode are given in Table 3.3. Additionally, the UPCs for each performance metric are given in pie charts as illustrated in Figure 3.6. In the FTL operation strategy the PGU operates for only 20 % of the simulation time. Therefore, the results show that the "s" variable in the PGU model does not have as much of an effect on the output uncertainties in this operation strategy. Additionally, the uncertainty factors related to the thermal load and electricity cost have a much more significant effect on the output uncertainties.

Table 3.4 Output uncertainty for FTL model

Parameter	**Total**	**Uncertainty**	**Percentage**
Cost ($/year)	11,128	+/- 1,245	+/- 11.19%
PEC (kWh)	277,083	+/- 4,916	+/- 1.77%
CDE (ton/year)	50.9	+/- 0.96	+/- 1.89%

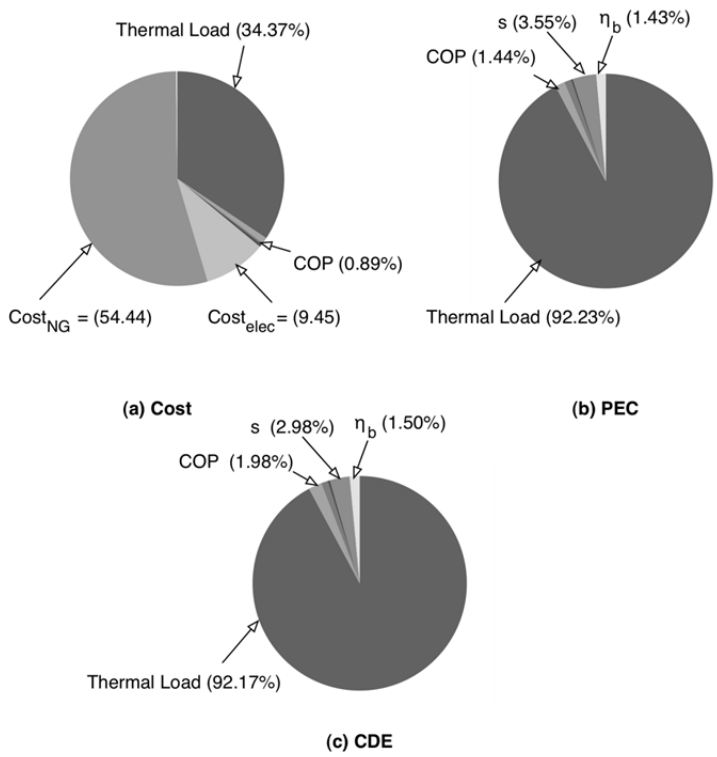

Figure 3.6 UPC Chart for the Cost, PEC, and CDE for CHP system FTL

Figure 3.6(a) illustrates that the uncertainty in the yearly operational cost is dominated by the uncertainty in the thermal load, cost of fuel, and cost of electricity. The uncertainty in the cost of fuel dominates for the same reason as in the FEL strategy. The uncertainty in the cost of electricity is much lower than that for the cost of fuel, but it is significant in this case because the electric grid is used nearly the entire simulation while the PGE operates for only 20% of simulation. The uncertainty in the thermal load has more of an effect in this case because the overall uncertainty is much lower. Figures 6(b) and 6(c) illustrate that the uncertainty in the thermal load dominates the uncertainty in the PEC and CDE. Again these figures differ from the trend in Figure 3.6(a) because no uncertainty was specified for the CDE and PEC conversion factors. An interesting fact

illustrated by Figure 3.6 is that the uncertainty in the thermal load plays a significant role in all three of the performance factors.

Figure 3.7 illustrates a comparison of each performance parameter for the different operational strategies. It can be observed that operating the CCHP system FTL shows better performance than operating the system FEL. The operational cost, PEC, and CDE for the FTL strategy are approximately 68%, 94%, and 92% of that for the FEL strategy. Additionally, Figure 3.7 indicates that there is no cross over between the uncertainty ranges for the two strategies. In other words, the maximum cost, PEC, and CDE for the FTL strategy are less than the minimum values for the FEL strategy.

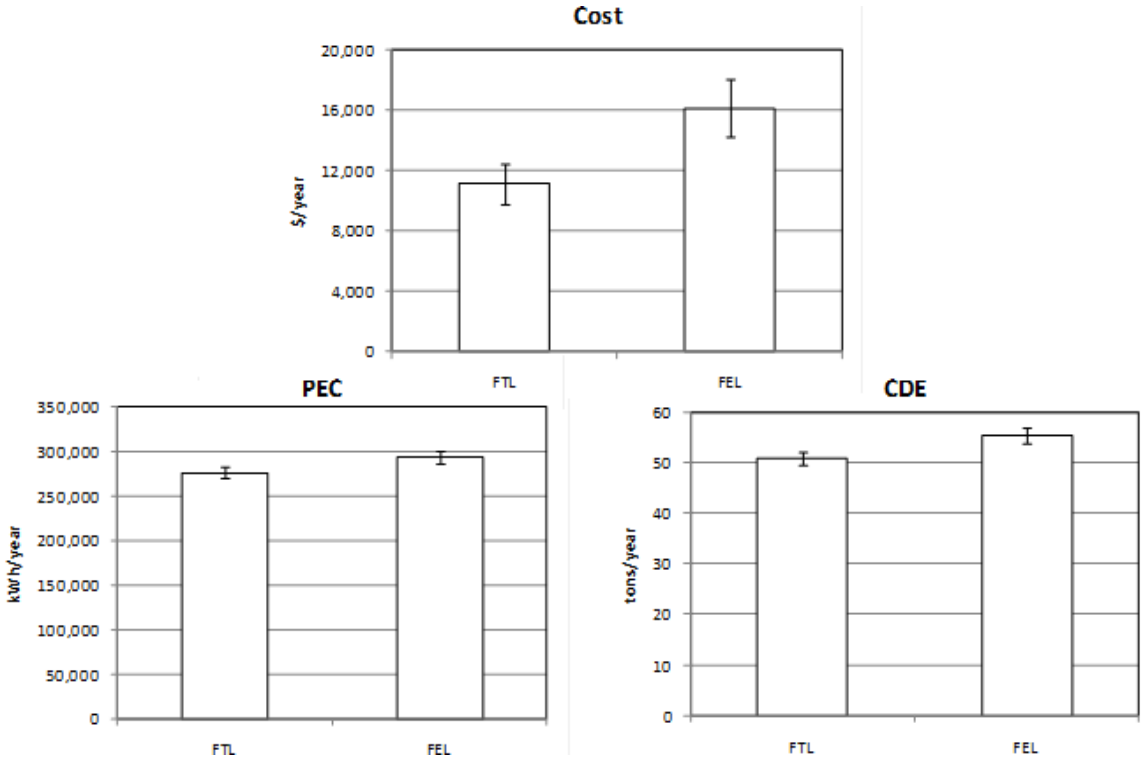

Figure 3.7 Comparison of Cost, PEC, and CDE for FTL and FEL

3.5 Discussion of Results

Tables 3.2 and 3.3 indicate that the total uncertainties in the PEC and CDE are minimal for both operational strategies (FEL and FTL) in comparison to the uncertainty in the operational cost. This sharp difference occurs because the uncertainties in natural gas and electricity prices are high while there is no uncertainty specified for the PEC and CDE conversion factors. Additionally, Figure 3.7 shows that the magnitudes of the performance uncertainties are small enough that this model can make legitimate comparisons between the FEL and FTL operation strategies.

The UPC's presented in Figures 3.6 and 3.7 provide insight into how the model can be improved. The UPCs for each performance factor in the FTL strategy, shown Figure 3.6, reveals that the uncertainty is primarily driven by external factors (weather, energy prices, etc.) as opposed to model parameters. Therefore, for any significant improvement in the uncertainty, the model must be adjusted to address the variation in weather and energy prices. Similarly, the uncertainty in the cost of natural gas dominates the uncertainty in the cost of operation for the FEL strategy. This is because the PGU is operated much more extensively in this case. However, since no uncertainty is specified for the PEC and CDE input conversion factors, this trend does not follow in the uncertainty in the PEC and CDE for the FEL strategy. The uncertainty in the thermal loads dominates these cases. Additionally, the uncertainty in the s factor used to characterize the PGU performance plays a larger role in these cases. However, since the total uncertainties in these two cases are minimal, not much will be gained by improving the PGU model.

CHAPTER IV

ROBUST BUILDING LOAD PREDICTION

The evaluation of building energy consumption under typical meteorological conditions requires building energy profiles on an hourly basis. Computer simulations can be used to obtain this information, but generating simulations requires a significant amount of experience, time, and effort to enter detailed building parameters. This chapter considers a simple methodology for using existing EnergyPlus reference building energy profiles to estimate the energy profiles of buildings with similar characteristics to a given reference model as presented in Fumo et al. [2010]. The method utilizes the building monthly energy bills to scale a given reference building energy profile to approximate the real building energy profile. Further, this study examines the robustness of the methodology considered with respect to the parameter discrepancies between a given building and the corresponding EnergyPlus reference model used to estimate its profile. Test buildings are defined by perturbing several combinations of the parameters defined in the reference building model. The test buildings examined are similar to the EnergyPlus, medium sized office, reference building in Baltimore, MD, and a total of 72 distinct test building configurations are examined. The analysis reveals that the methodology can significantly reduce the errors introduced by discrepancies from the EnergyPlus reference model.

4.1 EnergyPlus and DOE Reference Models

The methodology proposed by Fumo et al. [2010] is based on existing simulations of DOE reference buildings. In cooperation with Pacific Northwest National Laboratory, Lawrence Berkeley National Laboratory, and National Renewable Energy Laboratory, DOE's Building Technologies Program has developed commercial building reference models for new constructions [Torcellini et al., 2008]. The reference models were developed to provide a consistent baseline for comparing energy technologies. The reference models were constructed to best represent the results of sector-wide survey of building characteristics, locations, and weighting factors. A total of 16 commercial building types exist for each of 16 different locations representing all U.S. climate zones. Since reference models are designed to describe the energy performance of buildings with similar characteristics in a given U.S. climate zone, these reference models are used in this study as a source of data to generate normalized energy profiles. These normalized energy profiles are then used to estimate hourly energy consumption for similar buildings using the building utility bill as a scaling factor.

The software EnergyPlus is used to obtain the hourly energy profile for the reference models. This software combines the best capabilities and features from BLAST and DOE-2 along with new capabilities. Additionally, EnergyPlus is widely used in the building energy analysis community around the world. Stadler et al. [2006] used EnergyPlus as source of site end-energy loads for the analysis of distributed generation (DG) technology. Similarly, Mago et al. [2009] used it for the analysis of combined cooling, heating, and power (CCHP) systems. Although references give a general representation of the range of U.S. climate zones with 16 locations, EnergyPlus weather

data is available for more than 1042 locations in the USA, 71 locations in Canada, and more than 1000 locations in other countries throughout the world. When data is not available in the format required by EnergyPlus, weather data conversion tools can be used. The weather data used in this study is the Typical Meteorological Year (TMY3) data from the National Renewable Energy Laboratory (NREL). TMY3 is widely used to simulate building electric and thermal loads.

4.2 Methodology Summary

Fumo et al. [2010] introduced the definition of "*EnergyPlus normalized energy consumption coefficients"* (E+NECC) which is a set of normalized energy consumption profiles obtained from DOE reference models. The E+NECC for a given reference building can be used to estimate the energy consumption of buildings with similar characteristics as the reference model. Generally, analysis of energy consumption requires information of the base load and the total consumption. Therefore, in this study five sets of "*normalized energy consumption coefficients*" are obtained. Each set represents the normalized hourly energy consumption profile. Using the meters output variables from EnergyPlus simulations, the energy consumption sets are obtained as

- Baseline electricity (B_e): Building: Electricity + ExteriorLights: Electricity
- Variable electricity (V_e): Electricity: Facility – (Building: Electricity + ExteriorLights: Electricity)
- Baseline fuel (B_f): Gas: Facility – Heating: Gas
- Variable fuel (V_f): Heating: Gas
- Cooling electricity (C_e): Cooling: Electricity

Once the hourly energy consumption is obtained for a given reference model, each value is divided by the corresponding monthly energy consumption to obtain the normalized energy consumption coefficient for that hour of that particular day of the month. Mathematically the coefficients can be expressed as

$$\left(B_{e,coef}\right)_i = \left[\frac{(B_e)_i}{\sum(B_e)_i}\right]_m \tag{4.1}$$

$$\left(V_{e,coef}\right)_i = \left[\frac{(V_e)_i}{\sum(V_e)_i}\right]_m \tag{4.2}$$

$$\left(B_{f,coef}\right)_i = \left[\frac{(B_f)_i}{\sum(B_f)_i}\right]_m \tag{4.3}$$

$$\left(V_{f,coef}\right)_i = \left[\frac{(V_f)_i}{\sum(V_f)_i}\right]_m \tag{4.4}$$

$$\left(C_{e,coef}\right)_i = \left[\frac{(C_e)_i}{\sum(C_e)_i}\right]_m \tag{4.5}$$

where *i indicates the* hour, and *m* indicates the month.

The methodology also defines "*baseline fraction contribution factors*" for the baseline, electricity and fuel, for the monthly energy consumption. These factors give the percentage of the total monthly consumption that is baseline energy. Mathematically, these baseline fraction contribution factors are defined as

- Baseline Electricity $\left(f_{B_e}\right)$:

$$\left(f_{B_e}\right)_m = \left[\frac{B_e}{B_e+V_e}\right]_m \tag{4.6}$$

- Baseline Fuel $\left(f_{B_f}\right)$:

$$\left(f_{B_f}\right)_m = \left[\frac{B_f}{B_f+V_f}\right]_m \tag{4.7}$$

In order to apply the cooling electricity coefficients, an additional set of fraction factors is required to define the contribution of the cooling electricity to the monthly variable electricity. Mathematically, the cooling fraction factors are defined as

$$\left(f_{C_e}\right)_m = \left[\frac{C_e}{V_e}\right]_m \tag{4.8}$$

The five sets of hourly energy consumption coefficients ($B_{e,coef}$, $\mathrm{V_{e,coef}}$, $B_{f,coef}$, $V_{f,coef}$, $\mathrm{C_{e,coef}}$) and the three sets of fraction factors (f_{B_e}, f_{B_f}, f_{C_e}) constitute the E+NECC.

To obtain the estimated energy consumption from energy utility bills using the E+NECC, the following equations must be used.

- Energy consumption for baseline electricity (ECB_e):

$$(ECB_e)_i = E_m \cdot \left(f_{B_e}\right)_m \cdot \left[\left(B_{e,coef}\right)_i\right]_m \tag{4.9}$$

where E_m is the monthly electricity consumption from the utility bills.

- Energy consumption for variable electricity (ECV_e):

$$(ECV_e)_i = E_m \cdot \left[1 - \left(f_{B_e}\right)_m\right] \cdot \left[\left(V_{e,coef}\right)_i\right]_m \tag{4.10}$$

- Energy consumption for baseline fuel $\left(ECB_f\right)$:

$$\left(ECB_f\right)_i = F_m \cdot \left(f_{B_f}\right)_m \cdot \left[\left(B_{f,coef}\right)_i\right]_m \tag{4.11}$$

where F_m is the monthly fuel consumption from the utility bills.

- Energy consumption for variable fuel $\left(ECV_f\right)$:

$$\left(ECV_f\right)_i = F_m \cdot \left[1 - \left(f_{B_f}\right)_m\right] \cdot \left[\left(V_{f,coef}\right)_i\right]_m \tag{4.12}$$

- Energy consumption for cooling (ECC_e):

$$(ECC_e)_i = E_m \cdot \left[1 - \left(f_{B_e}\right)_m\right] \cdot \left(f_{C_e}\right)_m \cdot \left[\left(C_{e,coef}\right)_i\right]_m \quad (4.13)$$

In this analysis, the utility bill for a given month is based on the exact number of days of that month. However, the monthly bills usually do not follow this strict pattern. Therefore, when the coefficient methodology is implemented in software, it should be adjusted to account for the number of days billed in each monthly utility bill.

4.3 Analysis of Error in Methodology

This section gives an analysis of the error introduced in using the coefficient methodology to determine the energy profiles of buildings similar to the reference building described in Section 4.1. Several test buildings are defined by making a range of small changes to several of the design parameters in the reference building model. The parameters perturbed include: floor area, building orientation, and usage-density. Usage-density is composed of the following parameters that are expected to vary as a group: occupancy density, equipment usage-density, and lighting usage-density. A representative group of combinations of changes to floor area, orientation, and usage-density were tested to illustrate the limits of applicability of the coefficient methodology. These design parameters were selected as representative of the most significant perturbations from the reference building.

4.3.1 Building Simulated

This study focuses on a medium sized office reference building with a 4980 m^2 floor area that is located in Baltimore, MD. The building is approximately 50m by 33m

and has three stories with five zones on each floor. Typical Meteorological Year (TMY3) data for the city of Baltimore was used in an EnergyPlus simulation to find the hourly energy loads for all the building configurations tested in this study. The most significant building schedules are for the thermostat, lighting, occupancy, equipment and elevator. Table 4.1 illustrates the reference building thermostat set points for cooling and heating in the summer and winter seasons. Figure 4.1 shows the schedule distribution for the lighting, occupancy, equipment and elevator.

Table 4.1 Thermostat Set Points

Cooling Set Point		
	Summer	Winter
10 pm - 6 am	30 C (86 F)	30 C (86 F)
6 am - 10 pm	24 C (75 F)	30 C (86 F)
Heating Set Point		
	Summer	Winter
7 pm - 5 am	15.6 C (60 F)	15.6 C (60 F)
5 am - 7 pm	15.6 C (60 F)	21 C (70 F)

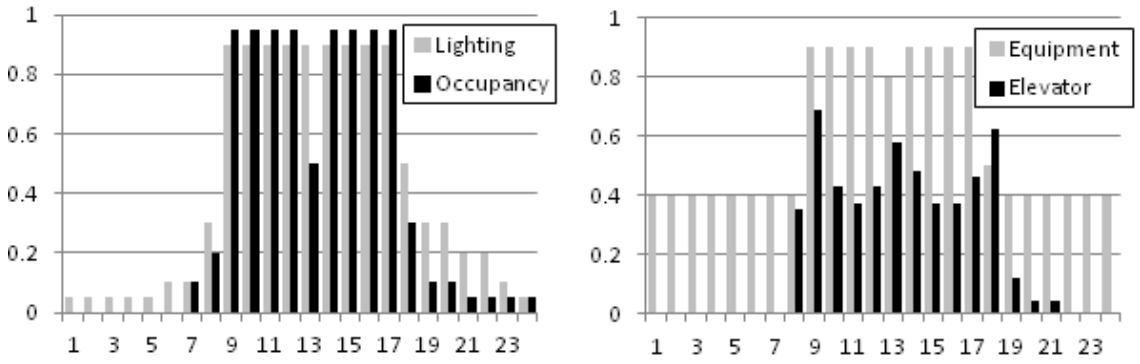

Figure 4.1 Building activity schedules

4.3.2 Normalized error metric

This section defines the normalized error metric that is used in this study to characterize the error in using the coefficient methodology. To study the error in using the methodology for a given test building the energy profiles are simulated using EnergyPlus. The monthly energy sums of electricity and fuel obtained in these simulations are then used to calculate the energy consumption profiles using the coefficient methodology described in section 4.2. The error in the coefficient method for a given hour is defined as the difference between the load simulated by EnergyPlus and that calculated using the coefficient methodology. This error is then normalized by the root mean square of the simulated energy loads of the corresponding month. The normalized hourly error is defined as

$$E_i = \frac{Sim_i - Calc_i}{\sqrt{\frac{1}{N} * \left(\sum_{j=1}^{N} Sim_j{}^2 \right)}} \tag{4.14}$$

where Sim_i represents the hourly energy load simulated by EnergyPlus, $Calc_i$ represents the hourly energy load calculated by the coefficient methodology, and N represents the number of hours in the corresponding month.

Figure 4.2 shows some representative histograms of the normalized errors for the case when the building is perturbed from the reference by: -5% usage-density, +10% floor area and 60 degrees rotation. These plots for variable electricity, variable gas, and cooling electricity (i.e. Figures 4.2a, 4.2b, and 4.2c) reveal a symmetric distribution. The vertical lines on each chart illustrate the limits which contain 95 % of the normalized

errors that occur in the year. These 95 % error limits will be used as a basis for summarizing the error in using the method for each real building configuration tested.

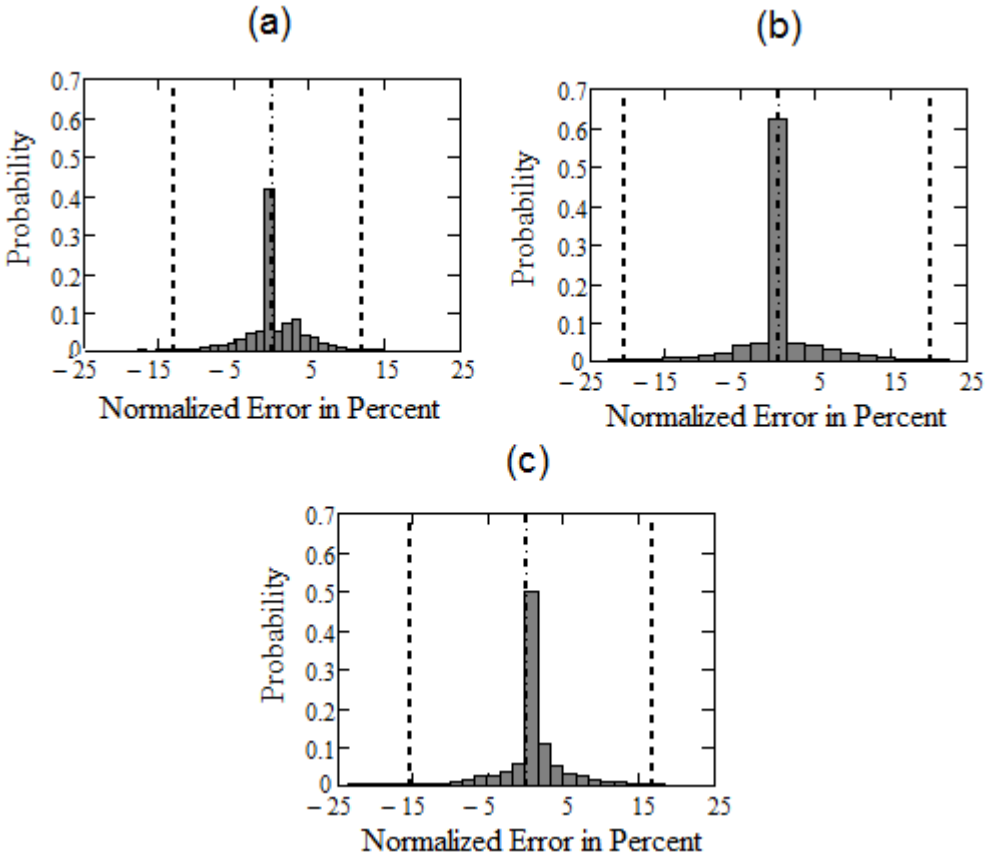

Figure 4.2 Histograms of energy loads at 60 degree orientation, -5% usage-density, and +10% floor area: (a) Variable Electricity, (b) Variable Gas, (c) Cooling

The normalized errors in the baseline electricity were minimal in comparison to the errors for the thermally driven energy loads. However, in some cases the error limits for baseline gas were very large. Further analysis of the baseline gas profile revealed that the error was mainly due to a phase difference between the simulated profile and the profile calculated using the coefficient method. When the monthly baseline fuel fraction is known, the energy load levels, however, where the same. An example of this type of

error is shown in Figure 4.3. To verify that the error was mainly due to a phase shift the average error for each hour in the day was studied. For a representative configuration, Figure 4.4a reveals the baseline gas average error for each hour of the day. The Figure illustrates a reversal of the error polarity at almost every time step. This behavior is characteristic of phase shift error. A moderate, three-point moving average filter can be used to reduce this effect. Figure 4.4b reveals how this error becomes negligible when the errors are averaged based on 3 hour intervals. The authors determined this phase error to be irrelevant to the task of assessing energy technologies for an entire year simulation. The same filter did not reduce the error in some cases when the monthly fuel fraction was not known. However, it seems that the monthly fuel fractions could easily be corrected since the baseline gas is based mainly on hot water usage. For example, the minimum loads in Figure 4.3 indicate parasitic loads when no hot water is being produced. This value should be easily obtained for the real building and could be used to correct the load fractions. Therefore, error in both baseline energy types are determined to be negligible and only the error in the thermally driven loads will be presented in the remainder of the discussion.

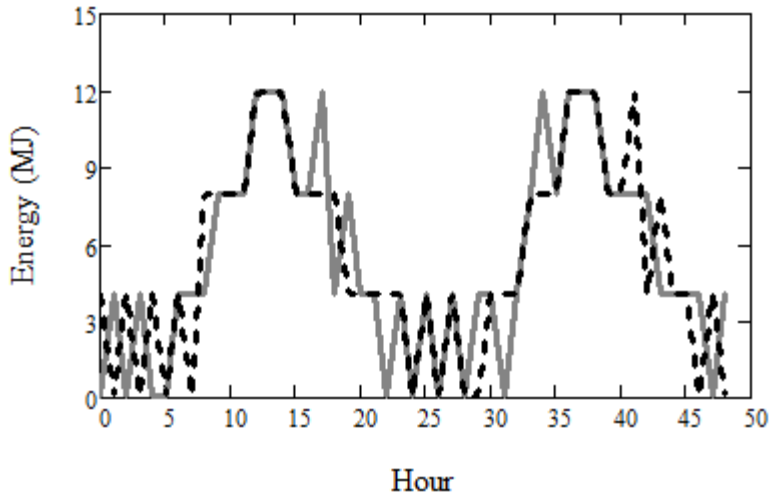

Figure 4.3 Example 48 hours of Baseline Gas energy loads

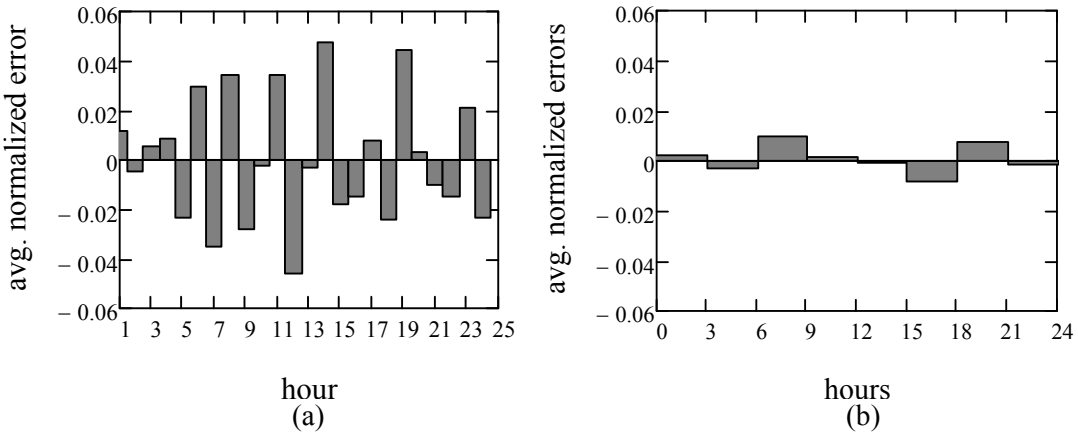

Figure 4.4 Graphs of average normalized error for each hour (Baseline Gas)

4.4 Results

As discussed above, the following reference model parameters were perturbed: floor area, building orientation, and usage density. The error limits were analyzed with the building orientation perturbed by 0 degrees, 30 degrees, 60 degrees, and 90 degrees.

At each of these orientations the building floor area was perturbed by +/-2%, +/-5% and +/- 10%. Also, at each orientation and floor area and the usage density were perturbed by 0% and +/- 5%. A total of 72 configurations were tested in this investigation. These configurations were categorized into four groups according to orientation for ease of analysis and display of results. For example, Figure 4.5 reveals the error limits for cooling and variable electricity for buildings oriented at 60 degrees rotation and for all of the floor area and usage density perturbations described above. Figure 4.6 reveals the error limits for variable gas for buildings oriented at 60 degrees rotation and for all of the floor area and usage density perturbations described above. The error limit results at 60 degrees rotation yielded the largest error limits for all of the configurations tested. The error limits for the configurations tested at 90 degree rotation were almost identical to those found for the 60 degree rotation group. Also, the error limits for the 30 degree rotation group yielded very similar trends to that found in the 60 degree and 90 degree rotation groups, but the magnitudes were reduced. The error limits for the 0 degree rotation group showed a different trend, but the magnitudes were smaller than that found in the other groups.

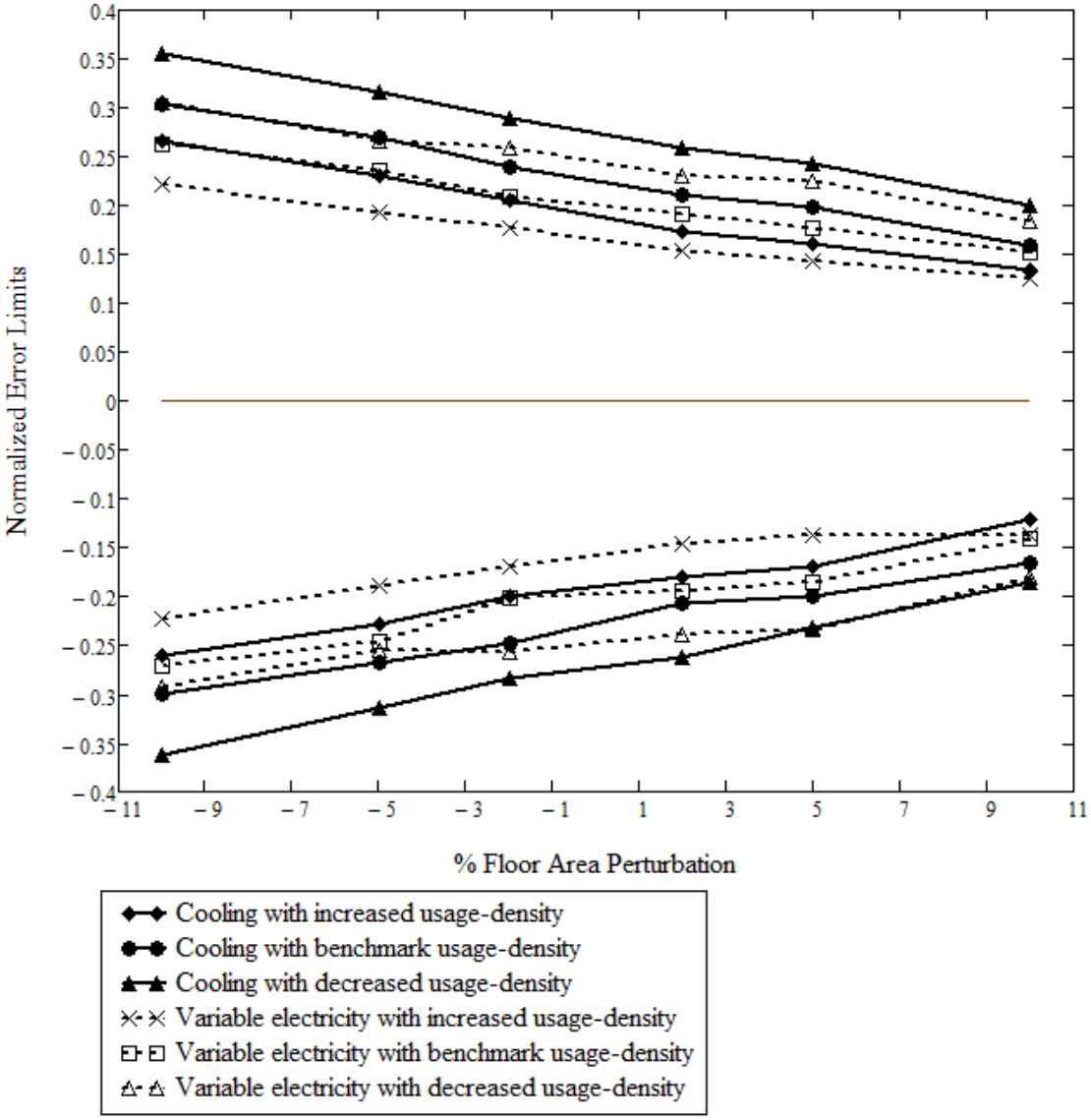

Figure 4.5 Cooling and Variable Electricity Error Limits for 60 Degree Rotation

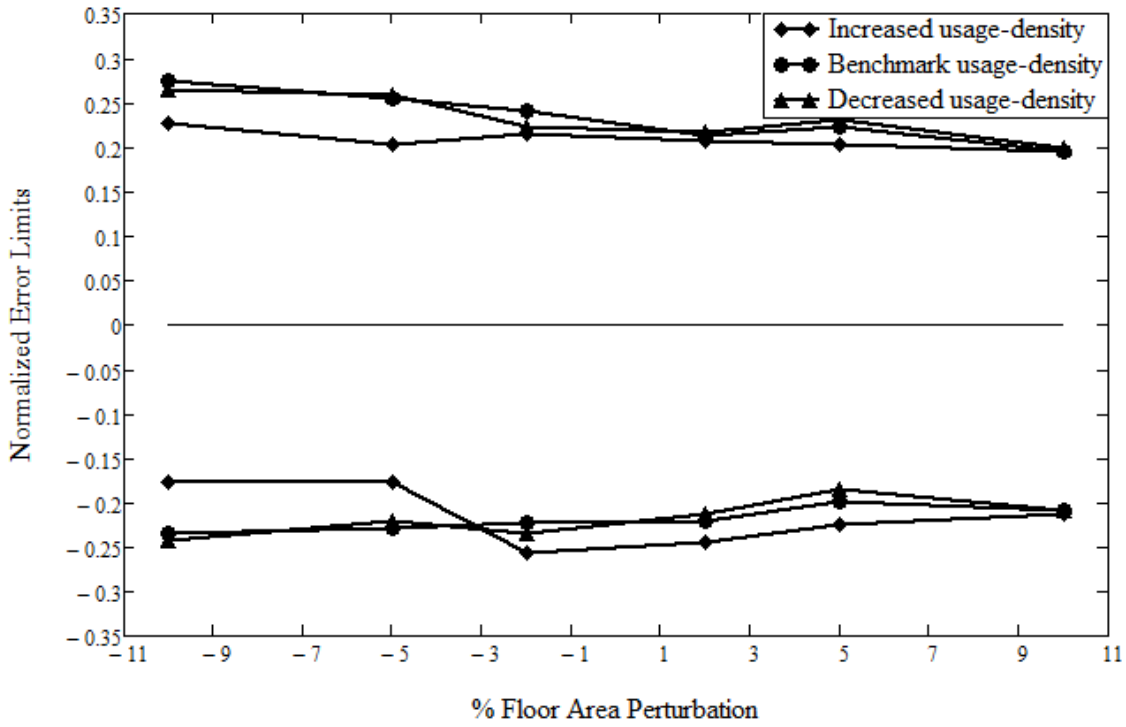

Figure 4.6 Variable Gas Error Limits for 60 Degree Rotation

The error limits found using the coefficient methodology can be compared to the error limits that result from using the reference profile to represent each test building directly. The normalized error for using the reference model directly is defined as

$$Eb_i = \frac{Sim_i - Bench_i}{\sqrt{\frac{1}{N} * \left(\sum_{j=1}^{N} Sim_j^{\,2} \right)}} \tag{4.15}$$

where Sim_i represents the hourly energy load for the test building model simulated by EnergyPlus, $Bench_i$ represents the hourly energy load for the reference model simulated using EnergyPlus, and N represents the number of hours in the corresponding month. Once the normalized error is calculated for each hour the limits which contain 95% of the

errors can be determined in the same way as described for using the coefficient methodology.

In most cases the coefficient methodology merited a reduction in the 95% error limits as compared to using the reference profile as a direct representation of the test building. Table 4.2 gives a comparison of the two methods. In Table 4.2 each rotation group is further divided according to usage-density. Each usage-density group includes 6 tests buildings (one for each floor area) each having an upper and a lower error limit. For example, the first column Table 4.2 summarizes the results for all of the configurations at 0 degrees rotation and increased usage-density. The first and second rows give the number of test points that were decreased and increased, respectively, when using the coefficient model as compared to using the reference model directly. The term "test point" denotes an upper or lower error limit for a given test building configuration. The third and fourth rows give largest decrease and increase in error limits, respectively, when using the coefficient model as compared to using the reference model directly. The same comparison is given for the 30, 60 and 90 degree rotation groups. These results reveal that the coefficient methodology decreases the error limits in almost all of the test points for the 0 degree rotation group, and that the methodology never increases the error limits by more than 0.02. While some test points yielded substantial reduction in error limits, the average change for the 0 degree group shows only a modest reduction in the 95% error limits. In general, as the rotation of the building is increased, there are more test points where the coefficient method either increased the error limits or provided no benefit. On the average, however, the coefficient method always provided a reduction in the error limits.

Table 4.2 Comparison between error limits found using coefficient methodology versus that found using the reference directly

0 Degree Group	Increased Usage	Reference Usage	Decreased Usage
Test Points Decreased	30	36	34
Test Points Increased	6	0	2
Largest Decrease	-0.114	-0.096	-0.13
Largest Increase	0.019	N/A	0.005
Average Change	-0.026	-0.033	-0.046

30 Degree Group	Increased Usage	Reference Usage	Decreased Usage
Test Points Decreased	28	22	16
Test Points Increased	8	14	20
Largest Decrease	-0.176	-0.119	-0.206
Largest Increase	0.059	0.05	0.038
Average Change	-0.053	-0.031	-0.017

60 Degree Group	Increased Usage	Reference Usage	Decreased Usage
Test Points Decreased	31	26	19
Test Points Increased	5	10	17
Largest Decrease	-0.173	-0.131	-0.177
Largest Increase	0.033	0.06	0.077
Average Change	-0.067	-0.038	-0.017

90 Degree Group	Increased Usage	Reference Usage	Decreased Usage
Test Points Decreased	32	26	19
Test Points Increased	4	10	17
Largest Decrease	-0.197	-0.171	-0.176
Largest Increase	0.056	0.062	0.082
Average Change	-0.079	-0.047	-0.01

A significant source of the error in the coefficient methodology results from lack of knowledge of the monthly loading fractions. Therefore, the coefficient methodology was also tested assuming that the monthly fractions were known. This was accomplished

by using the monthly sums from the test buildings directly. An example how the energy was calculated using this method is given in the following equation

$$(ECV_e)_i = VE_m \cdot \left[\left(V_{e,coef}\right)_i\right]_m \tag{4.16}$$

where VE_m represents the monthly sums of variable electricity.

When the monthly fractions are know the coefficient methodology shows much more consistent improvement over using the reference directly with regard to the 95% error limits. Only 31 of the 432 test points showed an increase from the error limits found when using the bench, and the largest increase was only 0.02. Additionally, the average improvement was slightly better for each test point when the monthly fractions were known. In addition to the reduction in error limits, the error distribution provides a good point of comparison. In many cases, the error distribution for the coefficient methodology was more densely packed around zero error than that for the reference model even though the error limits were equivalent. Figures 4.7 and 4.8 reveal some typical comparisons between the error distributions from using the coefficient methodology versus from using the reference profile. For example, 4.7a shows a comparison between the error distributions for variable electricity found by using the coefficient methodology (top), the reference profile (middle), and the coefficient methodology with known monthly fractions (bottom) for a test building oriented at 0 degrees rotation with +5% usage-density and +10% floor. Figure 4.7a reveals that the coefficient methodology yielded a much narrower distribution than the reference profile, but the distributions were asymmetric. At the 0 degree rotation group approximately 2/3 of the cooling and variable electricity error distributions showed a similar improvement when using the coefficient methodology. The other 2/3 of the cases showed little or no

benefit in the shape of the distributions. Notice that knowing the monthly fractions (e.g. see bottom Figure in 4.7a) shifted the distribution to be symmetric about zero. These results illustrates that using the coefficient methodology with known monthly load fractions reduces the absolute value of the error by shifting the reference energy profile to be centered on the test building energy profile. When the fractions are known the error distributions are symmetric about zero without exception, and show improvement over the reference profile for all of the configurations tested at 0 degrees rotation. Figure 4.7b shows a similar comparison for the variable gas error distribution for the 0 degree rotation group. However, frequently the reference profile gave a symmetric distribution for NG. Therefore, the shape of the distribution was improved very little by using the coefficient methodology with or without the fractions known.

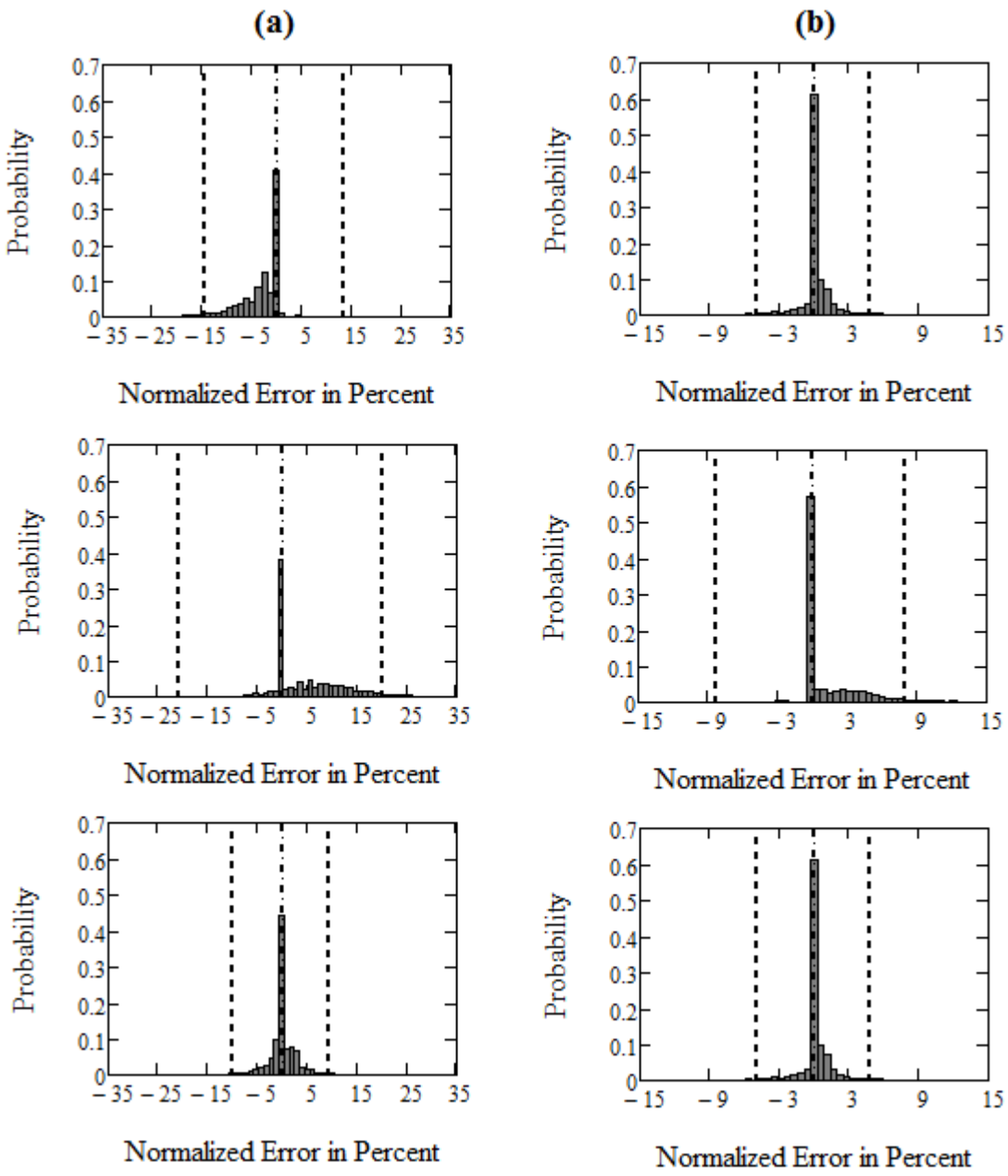

Figure 4.7 Histograms of errors for 0 degrees rotation for: (a) variable electricity at+5% usage-density, +10% floor area (b) variable gas at -5% usage-density, +5% floor area.

The rows correspond respectively to coefficient methodology, reference profile, and coefficient methodology with known monthly fractions.

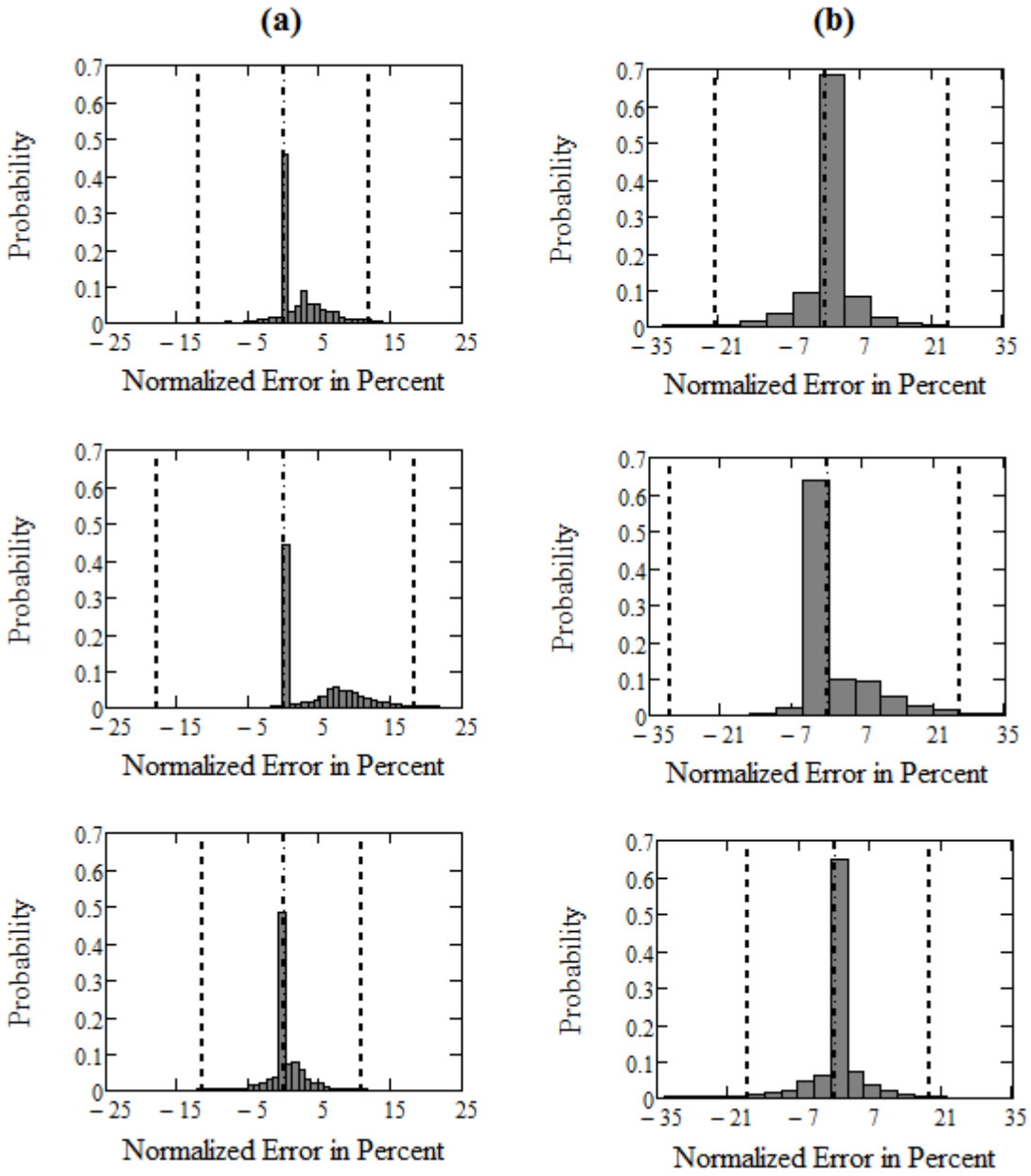

Figure 4.8 Histograms of errors for 30 degrees rotation for: (a) cooling at reference usage-density, +5% floor area (b) variable gas at -5% usage-density, +2% floor area.

The rows correspond respectively to coefficient methodology, reference profile, and coefficient methodology with known monthly fractions.

In general, the coefficient method with unknown fractions provided much less benefit in the error distribution shape when the building was rotated. For example, for the

60 degree and 90 degree rotation group, the error distribution shape showed negligible improvement in 75% of the configurations tested for variable electricity, cooling and, and variable gas. However, when the monthly fractions were known, the coefficient methodology often provided drastic improvement in the shape of the error distribution. The coefficient methodology with known monthly fractions provided significantly narrower and more symmetric error distributions as compared to using the reference profile directly in 83% of the configurations tested for variable electricity, cooling and, and variable gas. The results for the 30 degree rotation group were approximately in between those at the 0 degree rotation group and the 60/90 degree rotation groups.

4.5 Discussion of Results

The error limits for the 72 building configurations tested provide an adequate estimate of the errors that can be expected when using the coefficient method to estimate the energy profile for small perturbations from the reference building. Notice that for each of the energy types in Figures 4.5 and 4.6 the error limits roughly follow a linear pattern for the range of floor area test cases. This indicates that test buildings with floor areas in between the test points can be expected to follow the linear relationship approximately. This logic can be extended to the 30 and 90 degree test orientations since their error limits showed similar trends but with slightly reduced magnitudes. In the 0 degree orientation test buildings the trend is slightly different but similar conclusions can be drawn, and the errors are lower in magnitude compared to those found at 60 degrees. Additionally, any rotation beyond 90 degrees would yield similar results because of the symmetry of the problem. Lastly, the usage-density perturbation range of +5% is

expected to be a more than adequate representation of the expected perturbations from the reference building.

An estimate of the error that results when using the coefficient model for a given building is easily deduced from the results presented in this study. As discussed above, the results at 60 degrees rotation yielded the worst error limits of all of the configurations tested. The errors at all other orientations showed similar trends but with reduced magnitudes. Therefore, an appropriate way to use these results would be to assume that the error limits will be less than or equal to the worst case error limits presented in Figures 4.5 and 4.6 regardless of the building orientation and usage-density. For example, when using the coefficient method for a building at any orientation and with a floor area between 0 and -10% of the reference building, 95% of the normalized error should be less than +/- 0.36, +/- 0.30, +/- 0.28 for Cooling, Variable Electricity, and Variable Gas, respectively. Also, when using the coefficient method for a building of any orientation and with a floor area between 0 and +10 % of the reference, 95% of the normalized error should always be less than +/- 0.20, +/- 0.18, +/- 0.21 for Cooling, Variable Electricity, and Variable Gas, respectively.

Additionally, when using this methodology the shape of the error distributions should give confidence in using the method in general. Figures 4.4 and 4.7-4.9 illustrate that the error distributions that result from using the coefficient methodology are quite narrow with 40% or more of the errors approximately equal to zero. This means that the error limits are reduced substantially with reduction in the number of hours included. For example, when only 80 % of the 8760 errors (i.e. 80% of the errors that occur in a year) the worst case error limits for the 0 to -10% floor area case are only +/- 0.12, +/-0.10, and

+/-0.10 for Cooling, Variable Electricity, and Variable Gas, respectively. Also, note that the effect of rotation on the error should be greatly reduced for buildings that are more symmetric. For buildings less symmetric than the reference building should be expected to have more error as the building is rotated. Therefore, the results presented act only as a rough estimate.

CHAPTER V

OPTIMAL SIZING OF CHP SYSTEMS

An optimal sizing method is developed in this chapter based on an analytical scheme developed by Yun et al. [2012] for determining optimal operation decisions. Using the analytic optimal operation scheme allows for a more thorough optimal sizing method because of the minimal computational effort required as compared to mixed integer programming approaches. For example, an optimal sizing method based on this approach can more feasibly consider several years of weather data and the range of likely fuel/electricity costs for the term of operation of the PGU. The optimal sizing method presented takes advantage of this efficient optimal operation scheme and provides a robust optimal solution with respect to weather and fuel/electricity cost uncertainty. A case study of a medium sized office building is carried out by testing the algorithm for a range of 20 commercially available, engine based, power generation units (PGUs).

5.1 Analysis

In this section the optimal sizing method will be developed. In section 5.1.1 the CHP system model will be developed, and in section 5.1.2 the optimal operation scheme will be derived and summarized. Finally, in section 5.1.3 the optimal sizing method will be developed based on the CHP system model and optimal operation scheme.

5.1.1 CHP Model

The PGU model used in this work is based on a study of several industrial PGUs of varying sizes by Cho et al. [2010] that revealed a linear relationship between the power output and the rate of fuel energy input. Based on these results, the relationship between power output and fuel input is given as

$$F_{PGU} = m * E_{PGU} + b \tag{5.1}$$

where *m* and *b* are the slope and intercept of the line describing the linear relationship between power output and the rate of fuel energy input. The maximum heat energy that can be recovered from the engine is the fuel energy not converted into electric energy. The actual heat recovered, however, is limited by the efficiency of the heat recovery system, η_{hrs}, and many other factors such as incomplete combustion and heat loss to the atmosphere, which have previously been quantified in a single factor, ζ [Hueffed and Mago, 2010]. Therefore, the heat recovered from the engine by a heat recovery system is given as

$$Q_{REC} = (F_{PGU} - E_{PGU}) * \eta_{QNET} \tag{5.2}$$

where η_{QNET} represents the net heat recovery efficiency which can be defined as the product of η_{hrs} and ζ.

A simple heat storage model for the heat stored in a given time step is defined as

$$Q_{stor_{k+1}} = Q_{stor_k} + Q_{REC_k} - Q_{REQ_k} \tag{5.3}$$

where Q_{REQ} is the heat energy required to satisfy the heating demand of the building. Heat storage occurs if excess heat is generated when the CHP system operates by

following the electric load (FEL), i.e., when the PGU generates the exact amount of electricity required by the building. The (FEL) mode of operation can sometimes yield economical savings even when excess heat is generated. The purpose of the heat storage tank is to save the excess heat for future use instead of rejecting it. Notice that if the Q_{rec} is greater than Q_{REQ}, then the storage is increased, and if Q_{REC} is less than Q_{REQ}, the storage is decreased. The required heat energy from the CHP system is defined as

$$Q_{REQ} = \frac{Q_h}{\eta_{hc}} \tag{5.4}$$

where Q_h is the heating demand of the building, and η_{hc} is the efficiency of the CHP system heating coil.

A gas-fired boiler is used to supply additional heat energy when necessary. The fuel energy consumed by the boiler can be modeled as

$$F_{boiler} = \frac{Q_{REQ} - Q_{stor} - Q_{REC}}{\eta_b} \tag{5.5}$$

where η_b is the efficiency of the boiler. Additionally, the fuel required to meet the heating demand when a CHP system is not used (i.e. when a conventional system is used) is given as

$$F_{ref} = \frac{Q_h}{\eta_{ref}} \tag{5.6}$$

where Q_h is the heating demand of the building, and η_{ref} is the efficiency of the reference or conventional heating system.

5.1.2 Operation Modes that Yield Savings

A simple analytical method for determining the operation modes that generate savings is developed in this section based on the work of Yun et al. [2012]. The approach of this method is to define the operation modes that give savings for the current time step given the heating demand, electric demand, and storage energy at that time step. Savings generated by the CHP system with respect to the conventional system can be defined as

$$Savings = Cost_{ref} - Cost_{CHP} \tag{5.7}$$

where $Cost_{ref}$ is the cost of the reference system and is defined as

$$Cost_{ref} = E_{load} * C_e + F_{ref} * C_f \tag{5.8}$$

E_{load} is the electric demand of the building, C_e is the cost of electricity, and C_f is the cost of fuel. $Cost_{CHP}$ is the cost of meeting the building demands using a combination of a CHP system and the electric grid.

5.1.2.1 Case 1: Boiler Required

When the boiler is required to supply supplementary heat energy, $Cost_{CHP}$ is defined as

$$Cost_{CHP} = (E_{load} - E_{PGU}) * C_e + (F_{PGU} + F_b) * C_f \tag{5.9}$$

We will define this set of operation modes as case 1. There are three constraints on the operation modes that yield savings in case 1. First, it is assumed in Equation (5.9) that $E_{PGU} \leq E_{load}$. It has been shown in Yun et al. [2012] that operating the PGU to provide more electrical power than required by the building always diminishes savings when assuming no sale or storage of electricity. Next, Equation (5.9) is only applicable when

the boiler is needed. Therefore, an additional constraint on the operation modes that yield savings in case 1 is given by

$$Q_{REC} + Q_{stor} < Q_{REQ} \tag{5.10}$$

Using Equations (5.1), (5.2), and (5.4), Equation (5.10) can be expanded and solved for E_{PGU} as

$$E_{PGU} < \left[\frac{Q_h}{\eta_{hc}} - Q_{stor} - b * \eta_{QNET} \right] * \frac{1}{(m-1) * \eta_{QNET}} \tag{5.11}$$

The boundary of Equation (5.11) corresponds to the engine operation mode for which the heat recovered from the engine is equal to the heat energy required in addition to the energy available in storage. For convenience, the electricity provided by the engine at this boundary is defined as

$$E_{fil} = \left[\frac{Q_h}{\eta_{hc}} - Q_{stor} - b * \eta_{QNET} \right] * \frac{1}{(m-1) * \eta_{QNET}} \tag{5.12}$$

At this point, additional insight can be gained by expanding Equation (5.7) in terms of Equations (5.8) and (5.9) as

$$\begin{aligned} Savings1 = &\left(E_{load} * C_e + F_{ref} * C_f\right) - \\ &\left[\left(E_{load} - E_{PGU}\right) * C_e + \left(F_{PGU} + F_b\right) * C_f\right] \end{aligned} \tag{5.13}$$

Next, Equation (5.13) can be expanded using Equations (5.1), (5.2), and (5.4)-(5.6) as

$$\begin{aligned} \frac{Savings1}{C_f} = &E_{PGU} * \left(R_{cost} - R_{CHP}\right) + \\ &Q_h * \left(\frac{1}{\eta_{ref}} - \frac{1}{\eta_{hc} * \eta_b} \right) + \frac{Q_{stor} + \eta_{QNET} * b}{\eta_b} - b \end{aligned} \tag{5.14}$$

where R_{cost} is the ratio of the cost of electricity to the cost of fuel and R_{CHP} is defined for convenience as

$$R_{CHP} = m * \left(1 - \frac{\eta_{QNET}}{\eta_b} \right) + \frac{\eta_{QNET}}{\eta_b} \tag{5.15}$$

Note the non-dimensional factor R_{CHP} is defined to simplify the notation in Equation (5.14). This factor accounts for the efficiencies of the components of the CHP system, and, as will be demonstrated below, it provides a threshold value for the economical operation of the CHP system.

Notice in Equation (5.14) the savings for case 1 could be negative depending on the value of the parameters. Therefore, another constraint must be added to ensure that the Savings is always greater than zero. Because Equation (5.14) is linear with respect to the independent variables, it is straight forward to define an additional boundary on the operation modes that yield savings in case 1. This additional boundary can be defined by settings Savings1 equal to zero in Equation (5.14) and solving for E_{PGU} as

$$\begin{aligned} E_2 = E_{PGU} = & \frac{Q_h}{\left(R_{cost} - R_{CHP}\right)} * \left(\frac{1}{\eta_{hc} * \eta_b} - \frac{1}{\eta_{ref}} \right) \\ & \frac{-Q_{stor} - \eta_{QNET} * b}{\left(R_{cost} - R_{CHP}\right) * \eta_b} + \frac{b}{\left(R_{cost} - R_{CHP}\right)} \end{aligned} \tag{5.16}$$

where this electric load is defined as E_2 for convenience. Clearly, Equation (5.14) reveals that savings increases with E_{PGU} when $R_{cost} > R_{CHP}$ and decreases with increasing E_{PGU} when $R_{cost} < R_{CHP}$. Also, since Equation (5.14) is linear in the independent variables, E_2 is a lower bound on the operation modes that yield savings when $R_{cost} > R_{CHP}$ and an upper

bound when $R_{cost}<R_{CHP}$. A summary of the operation modes that yield savings for the case when the boiler is needed (case 1) is provided in Figure 5.1.

Case 1 (Boiler needed) Savings Regions:

IF $E_{pgu} \leq \min(E_{demand}, E_{ftl})$

IF $R_{cost} < R_{CHP}$

$E_{pgu} < E_2$

IF $R_{cost} > R_{CHP}$

$E_{pgu} > E_2$

Figure 5.1 Savings regions for case 1

5.1.2.2 Case 2: Boiler not required

A similar process can be followed to determine the savings regions for the case when the sum of the stored and recovered heat energy is greater than that required to meet the heating demand so that the boiler is not required. This will be defined as case 2. In case 2, $Cost_{CHP}$ is defined as

$$Cost_{CHP} = (E_{ref} - E_{PGU}) * C_e + (F_{PGU}) * C_f \tag{5.17}$$

As in case 1, Equation (5.17) assumes that $E_{PGU} \leq E_{load}$. Since Equation (5.17) is only applicable when the boiler is not needed, an additional constraint on the operation modes for case 2 is given as

$$E_{PGU} \geq E_{ftl} \tag{5.18}$$

where, as stated above, E_{ftl} is defined as the electric power production that corresponds to the exact heat recovery needed to meet the heating demand after all of the stored heat energy is used.

Again, expanding the savings equation, (5.7), in terms of Equations (5.8) and (5.17) yields additional insight and is given as

$$\begin{aligned} Savings2 &= \left(E_{load} * C_e + F_{ref} * C_f\right) \\ &- \left[\left(E_{load} - E_{PGU}\right) * C_e + \left(F_{PGU}\right) * C_f\right] \end{aligned} \tag{5.19}$$

In this case Equation (5.19) can be expanded using Equations (5.1), (5.2), and (5.6) as

$$\frac{Savings2}{C_f} = E_{PGU} * \left(R_{cost} - m\right) + \frac{Q_h}{\eta_{ref}} - b \tag{5.20}$$

As in case 1 a third constraint must be defined because the savings in case 2 could be negative according to Equation (5.20). The third and final constraint for the operation modes that yield savings for case 2 can be defined by setting Savings2 equal to zero and solving for E_{pgu} as

$$E_3 = E_{PGU} = \frac{-1}{\left(R_{cost} - m\right)}\left[\frac{Q_h}{\eta_{ref}} - b\right] \tag{5.21}$$

where this electric load is defined as E_3 for convenience. Equation (5.20) reveals that savings increases with E_{PGU} when $R_{cost} > m$ and decreases with increasing E_{PGU} when $R_{cost} < m$. Also, since Equation (5.20) is linear in the independent variables, E_3 is a lower bound on the operation modes that yield savings when $R_{cost} > m$ and an upper bound when $R_{cost} < m$. A summary of the operation modes that yield savings for the case when the boiler is not needed (case 2) is provided in Figure 5.2.

Case 2 (Boiler not needed) Savings Regions:

IF $E_{ftl} \leq E_{pgu} \leq E_{demand}$

IF $R_{cost} < m$

$E_{pgu} < E_3$

IF $R_{cost} > m$

$E_{pgu} > E_3$

Figure 5.2 Savings regions for case 2

5.1.3 Sizing Method

In this section a methodology is developed for selecting the PGU that, when implemented in a CHP system, will meet the building energy demands with the least cost over the total period of operation. Because the optimal sizing task seeks to minimize the total cost for several years, the success of the methodology is highly dependent on an adequate approximation of the future heating and electric demands and of the future cost of electricity and fuel. In addition, an optimal sizing methodology is of no use unless the solution represents a PGU that can actually be purchased. Therefore, a practical optimal sizing method must be based on models of commercially available PGUs. The optimal PGU sizing methodology developed in this section is based on applying the optimal operation method discussed in section 5.1.2 in such a way that adequately addresses each of these issues.

To ensure that the most cost effective PGU is selected, the optimal sizing method must consider many or all of the PGUs available on the market that are within a power output range that is appropriate for the given building. For example, in the case study that will be presented in section 5.2, manufacturer data was collected and studied for 20 PGUs

ranging in rated power output from 10 kW to 315 kW [Cummings, 2011]. The manufacturer data specified the fuel input at 25%, 50%, 75% and 100% load conditions. From this data a linear least squares fit was used to find the slope, m, and intercept, b, as defined in Equation (5.1) for each PGU. Figure 5.3 shows the normalized linear relationship for several of the 20 PGUs used in this case study.

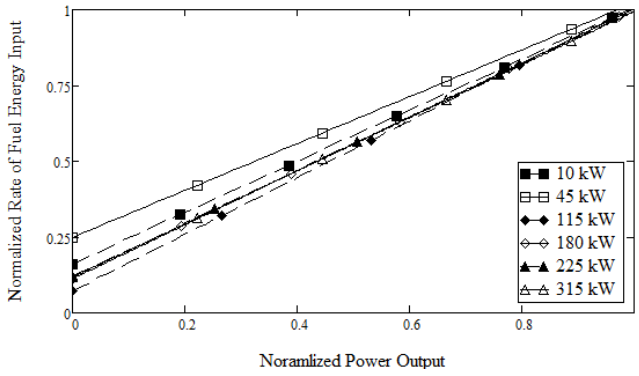

Figure 5.3 Normalized power output to fuel relationship for several PGU sizes

Previous works have used the Typical Meteorological Weather (TMY) data in simulations to calculate the hourly heating demand for a building. While most of the researchers have used typical days [Beihong and Weiding, 2006; Li et al., 2008] or weeks [Azit and Nor, 2009], an optimal sizing method based on an entire year of hourly heating and electric loads could easily be defined. Following this approach the optimal PGU size should be selected by comparing the total savings generated by operating the CHP system for an entire year with each PGU. If the methodology in section 5.1.2 is used, the total yearly operational savings for a given PGU can be defined as

$$YS = \sum_{j=1}^{H} Savings_j - \frac{CC}{N_{OY}} \tag{5.22}$$

where H is the total number of hours in a year, CC is the capital cost, N_{OY} is the number of operation years expected for the PGU, and $Savings_j$ is the operational savings generated by using the operation scheme presented in Section 5.1.2. However, consideration of historical weather conditions reveals that weather patterns often vary significantly from year to year in a given area, and, therefore, TMY data for a single year may not be the best approximation of the weather conditions that will occur during the term of operation of the CHP system. A better approximation would be to determine the heating demand for many years of historical weather data and to incorporate each year into the optimal sizing algorithm. For example, recent TMY data is based on 15 to 30 years of historical weather data. Therefore, a better approach to the optimal sizing problem is to apply the optimal operation algorithm in Section 5.1.2 for each hour and for each year of the historical weather data, and to compare the overall savings for each PGU. Then, the average yearly operational savings for each PGU can be defined as

$$YS_{MY\_AVG} = \frac{\sum_{i=1}^{N}\sum_{j=1}^{H} Savings_{j,i} - CC}{N_{OY}} \tag{5.23}$$

where N is the number of years of historical weather data that are used in the algorithm. The PGU that yields the highest YS_{MY_AVG} is more likely to be the PGU that will actually provide maximum yearly operational savings. This is because the solution will be more robust to variation in the weather conditions.

In addition, an optimal sizing method that does not consider the potential for large variation in the cost of electricity and fuel is likely to choose a PGU that is far from the optimal choice. This is clearly shown by the fact that the optimal operation mode is

dependent on the relationship between the parameters R_{cost}, R_{CHP}, and m. Therefore, if the cost ratio changes, then the operation modes that yield savings may change for some PGUs and highly affect the cost savings. Forecasting the cost of electricity and fuel for several years in advance can be quite difficult. A reasonable approach to this problem is to study the effect of the expected upper and lower limits on the cost of electricity and fuel on the optimal PGU choice. Therefore an upper limit for R_{Cost} is defined as

$$R_{costU} = \frac{C_e * (1.1)}{C_f * (0.9)} \tag{5.24}$$

and a lower limit for R_{cost} is defined as

$$R_{costL} = \frac{C_e * (0.9)}{C_f * (1.1)} \tag{5.25}$$

Figure 5.4 reveals a plot of each cost ratio, with the parameters m and R_{CHP} for each PGU. When either the current cost ratio or the upper limit cost ratio is used, $R_{CHP} < m < R_{Cost}$ for all PGUs considered. However, when R_{costL} is used, $R_{CHP} < R_{costL} < m$ for some PGUs, and this means a change in the PGU operation modes that yield savings. As shown in Figure 5.4, the operation modes that yield savings for each engine do not change much for this case. It is likely, however, that R_{cost} would be lower for other cities.

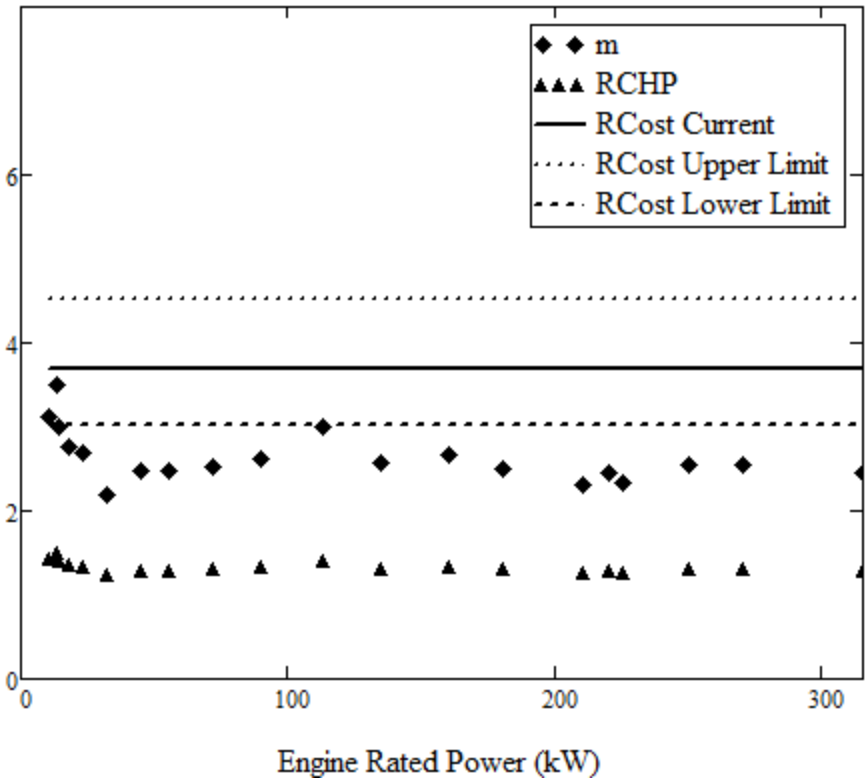

Figure 5.4 Parameters R_{cost}, m and R_{CHP} versus PGU size

To address this consideration, the operational saving should be considered for each cost ratio and for each year of weather. Therefore, the average yearly operational savings for each PGU can be defined as

$$YS_{T\_AVG} = \frac{\sum_{k}^{3}\sum_{i=1}^{N}\sum_{j=1}^{H} Savings_{j,i,k} - 3 * CC}{N_{OY}} \tag{5.26}$$

where the variable savings is summed for each of the three cost ratios defined above. The capital cost is multiplied by three because forty-five years are included in this average, and this is three times the expected lifetime of the PGU. The PGU that yields the maximum YS_{T_AVG} should be selected as the PGU that is most likely to maximize the

operational savings over the full term of use of the system. An optimal sizing decision based on the PGU that gives the maximum YS_{T_AVG} is expected to be robust with respect to weather and fuel/electricity cost uncertainty.

5.2 Case Study

The optimal sizing method presented in section 5.1.3 was tested for a medium size office DOE reference building [Torcellini, 2008]. EnergyPlus software was used to determine the building heating and electric demands. Simulations were completed for 15 years (1991 to 2004) of historical weather data for the city of Philadelphia, PA. Once the heating and electric demands were determined from EnergyPlus, the algorithm in section 5.1.3 was implemented for 20 PGUs with power outputs ranging from 10 kW to 315 kW as discussed above. To illustrate the effect of the approximation of the future cost of electricity and fuel, Figure 5.5 give plots of the YS_{MY_AVG} variable versus PGU size for different cost ratios. For display purposes, the YS_{MY_AVG} variable is normalized by the mean value of each curve. When using the YS_{MY_AVG} metric, the PGU that yields the largest YS_{MY_AVG} is the optimal choice. In Figure 5.5, all three cost ratios give a 210 kW PGU as the optimal choice. However, the difference in the shapes of the graphs reveals that the different cost ratios may significantly change the optimal choice for other cases.

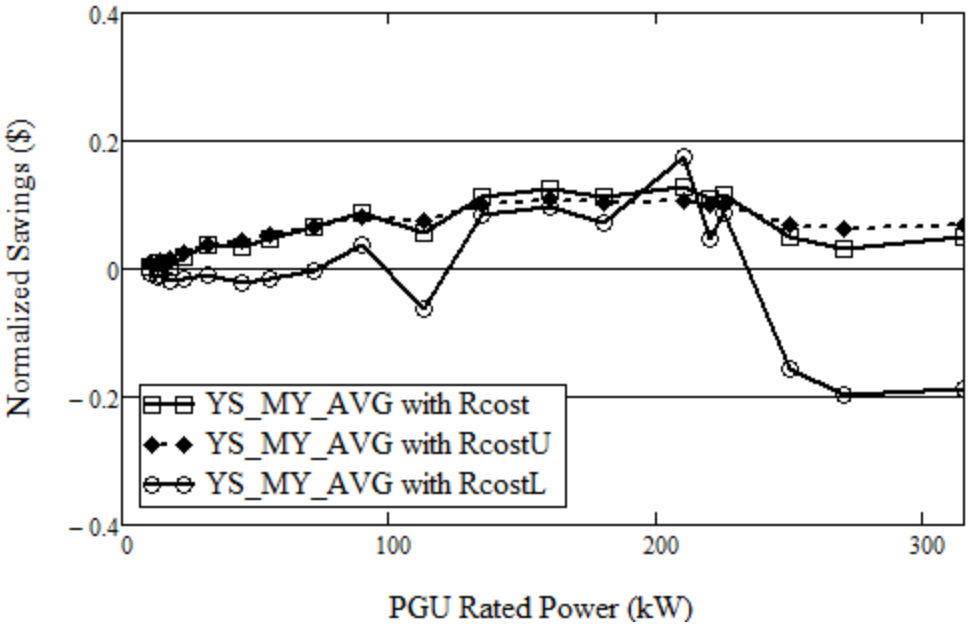

Figure 5.5 Comparison of YS_{MY_AVG} when using different R_{cost} values

The YS_{T_AVG} variable is plotted in Figure 5.6 along with the YS variable using the typical meteorological year (TMY) weather data for comparison. In this case study, the 210 kW PGU is selected as the optimal choice using either the YS_{MY_AVG} or YS with the TMY data with the current cost ratio. Therefore, in this case the effects of weather and cost variation are not significant enough to change the optimal size. However, this may not be true for other cases.

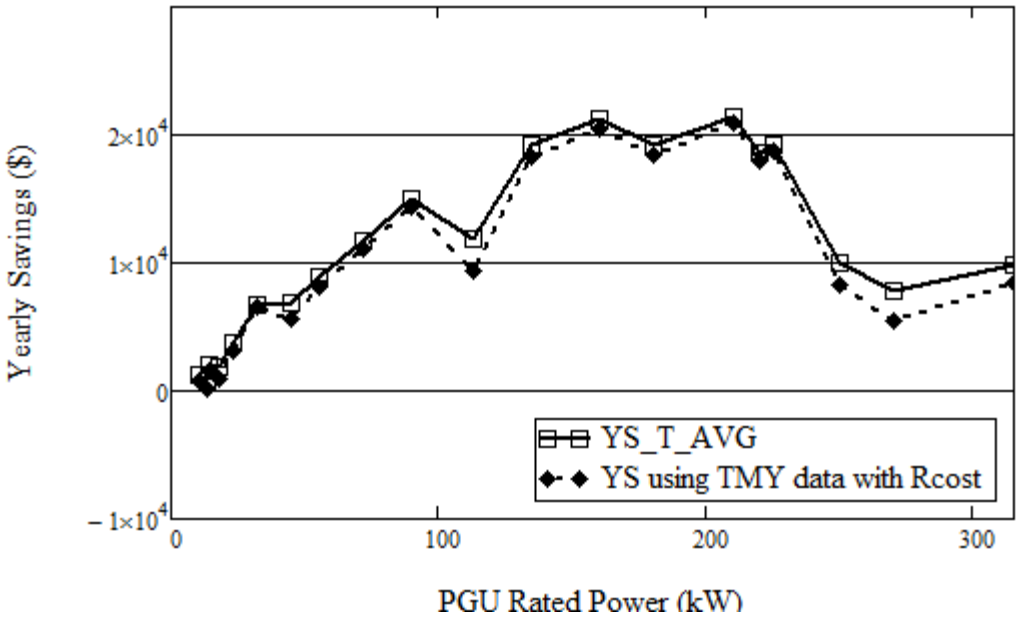

Figure 5.6 YS_{T_AVG} and YS using TMY data with the current cost ratio

Figure 5.8 gives a plot of the hourly storage over a year for the optimal PGU selected in this case study. The storage was limited to 200 kWh and the tank was assumed to lose 5% of the stored energy for each hour of storage. For this PGU and for other cases when the cost ratio is greater than both m and R_{CHP}, thermal storage was used quite frequently. In these cases the ability to store thermal energy significantly increased the operational savings. On the other hand, thermal energy was never stored in the cases when $R_{CHP} < R_{cost} < m$. This is because it is never cost efficient to produce extra thermal energy in this condition.

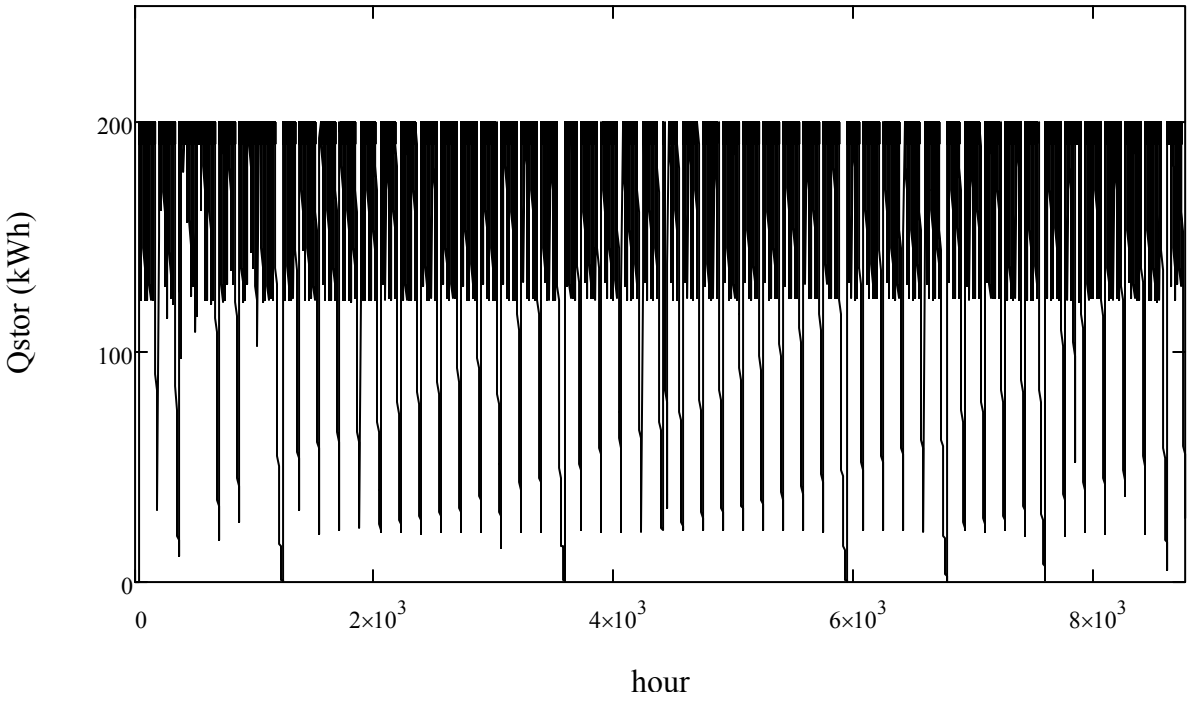

Figure 5.7 Hourly Q_{stor} for the 210 kW PGU with R_{costU} for weather data from 1997

CHAPTER VI

INTEGRATED PARAMETER ESTIMATION OF THERMAL SYSTEM MODELS

In support of predictive CHP control algorithms such as that presented by Cho et al. [2010] and Yun et al. [2011], this chapter presents a model for prediction of the temperatures at the inlet and outlet of each component of a topping-cycle, CHP system that provides heat and electricity to an experimental facility. In experimental models of multi-component thermal systems, small errors in each sub-model can propagate detrimentally through the overall model resulting in large prediction errors as the prediction time increases. These errors can be problematic when using open loop or feed-forward control schemes. This chapter demonstrates the advantages of a whole-system or integrated parameter estimation approach as opposed to the component-by-component parameter estimation approach that is widespread in the literature. This method achieves greater accuracy by requiring that the parameters for each component model are consistent with all of the measurements in the entire system. The approach is demonstrated on an experimentally based CHP system model and the resulting model is used to predict the system temperatures up to 20 minutes in advance. A comparison between the model predictions and the experimental data reveals that the parameter estimation approach employed in this work can significantly improve the prediction accuracy versus a model based on the classic, single component, input-output parameter estimation approach.

6.1 Test Facility CHP equipment

The CHP test facility used in this investigation provides heating and electricity to a small office space and shop area. A schematic of the CHP equipment set-up at the facility is shown in Figure 6.1. The system consists of five major components: a power generation unit (PGU)/exhaust heat exchanger combination, coolant-to-water heat exchanger, water tank, building heating coil, and boiler. The PGU supplies the electrical energy required by the building. During power generation, heat energy is transferred to the exhaust gas and the engine coolant. The energy in the exhaust flow is transferred to the coolant in the exhaust heat exchanger. Then, heat energy in the coolant is transferred to the water in the heat recovery loop through the recovery heat exchanger. In the heat recovery loop, water enters the recovery heat exchanger from the thermal storage tank. Once the water has been heated in the recovery heat exchanger, the stream is mixed with water from the tank, and the mixture feeds into the main water loop. The next component in the system is the building heating coil. When the room temperature is above the set point temperature, all of the flow in the main water loop bypasses the heating coil. However, when the room temperature is below the set point temperature, a portion of the flow passes through the heating coil and transfers heat to the room air that is flowing through the heating coil. Next, the boiler adds thermal energy to the main water loop when necessary. Finally, the main water loop terminates at the thermal storage tank. Details for each component will be given in the next section of this chapter. The numbered points in Figure 6.1 indicate the locations of the seven temperatures that are predicted by the model. Temperatures are measured using RTD sensors, natural gas flow rates are measured using differential pressure sensors, and all other flow rates are

measured using turbine flow meters. Standard uncertainty values for each sensor are given in Table 6.1. Only the system temperatures are predicted in this work. In future investigations, the flow rates should be modeled at each point as well, but measured flow rates are used in the model presented in this chapter.

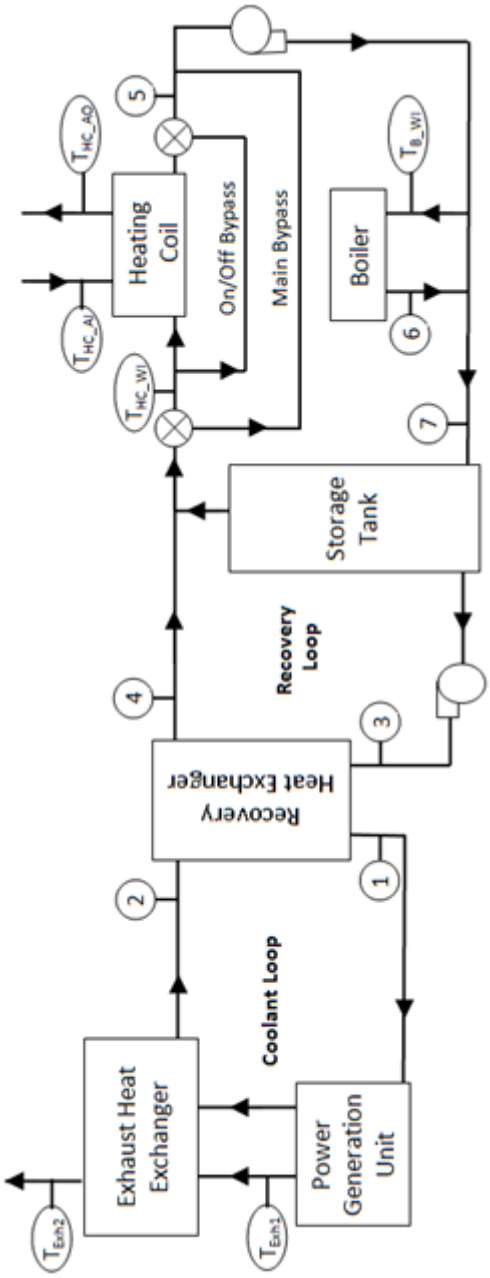

Figure 6.1 CHP System Schematic

Table 6.1 Sensor Uncertainty

Sensor	Systematic	Random
Water and Coolant RTDs (°C)	± 1.5	± 0.056
Water/Coolant Flow Meters (gal/min)	± 0.032	± 0.003
Engine Natural Gas Flow (ft^3/min)	± 1	± 0.5
Boiler Natural Gas Flow (ft^3/min)	± 2.5	± 1.25
Ambient Temperature (°C)	± 0.4	± 0.04
Heating Coil Air Temperature (°C)	± 0.03	± 0.03

6.2 CHP Model

This section presents the CHP system model developed for the test facility. The model could be used with the components connected (i.e. the input temperature to one component is the predicted output of another) or with the components separated (i.e. input temperature for each component model is a measured value). However, the models must be connected for predicting the future states of the system where measured values are not available.

6.2.1 Engine and Exhaust Heat Exchanger model

The first model incorporates both the PGU and the first stage of heat recovery. The experimental facility uses a four-cylinder, natural gas, combustion engine-generator set with a rated electrical power output of 15 kW. The hot exhaust gas leaving the engine is used to give additional heat to the coolant leaving the engine by means of a shell and tube heat exchanger. Temperature measurement of the exhaust gas is difficult to obtain with reasonable accuracy because of high temperatures that occur in the exhaust gas at the engine exit (650°C or greater), and an adequate sensor for this condition has not been installed at the facility. Therefore, to avoid the necessity of measuring the exhaust gas

temperature, the PGU and exhaust heat exchanger have been combined into a single model. The PGU/exhaust heat exchanger model is used to predict the outlet coolant temperature from the exhaust heat exchanger. A detailed model of the heat transfer in the engine requires extensive analysis and is not necessary for the purposes of this model. Instead, a simple model can be developed based on energy conservation. In general, the thermal energy delivered to the coolant should be equal to the thermal energy generated by the fuel combustion minus the thermal energy lost to the ambient at the engine exterior wall as

$$\dot{V}_{cool}\rho_{cool}c_{p\_c}(T_2 - T_1) = \dot{V}_{E\_F}c_0 - c_1(T_{amb} - T_1) \tag{6.1}$$

where c_0 is a coefficient related to the lower heating value (LHV) of the fuel, c_1 is a coefficient related to the heat transfer coefficient between the engine wall and the ambient; T_1 and T_{amb} are the temperature of the coolant at the inlet to the PGU and the ambient temperature, respectively. $\dot{V}_{E\_F}$ and $\dot{V}_{cool}$ are the natural gas flow rate and the coolant flow rate, respectively. c_{p_c} is the specific heat of the coolant. Both coefficients c_1 and c_0 are determined through a parameter estimation technique. Solving Equation (6.1) for T_2 yields the following model for the outlet coolant temperature.

$$T_2 = \frac{\dot{V}_{E\_F}c_0 - c_1(T_{amb} - T_1)}{\dot{V}_{cool}\rho_{cool}c_{p\_c}} + T_1 \tag{6.2}$$

6.2.2 Coolant/Water Heat Exchanger model

After the coolant leaves the exhaust heat exchanger it enters a flat plate heat exchanger that uses water from the heat recovery loop as the cold inlet fluid. The model

for this component must predict the outlet water and coolant temperatures based on the inlet temperatures (T_2 and T_3) and the fluid flow rates. Based on the commonly used effectiveness-NTU method the models for these outlet temperatures are defined as

$$T_1 = T_2 - \varepsilon \frac{C_W}{C_C}(T_2 - T_3) \tag{6.3}$$

$$T_4 = T_3 + \varepsilon(T_2 - T_3) \tag{6.4}$$

where C_c and C_w are the heat capacity rates of the coolant and water flows, respectively. The effectiveness, ε, is defined as an empirical function of the inlet temperatures based on a second order Taylor series model as

$$\varepsilon = c_2 T_2 + c_3 T_3 + c_4 T_2 T_3 + c_5 (T_3)^2 \tag{6.5}$$

where all of the temperature locations are defined in Figure 6.1 and again the coefficients, c, are parameters that must be estimated.

6.2.3 Water Tank Model

The heat recovery loop is combined with water stored in a 100 gallon tank to generate the main water loop. Because the tank is assumed to be well mixed, a single zone model is developed for the tank based on energy conservation as

$$c_6 \frac{dT_3}{dt} = \dot{V}_{M\_W} \rho_W c_{P\_W} (T_7 - T_3) \tag{6.6}$$

where c_6 represents the thermal capacitance of the tank, $\dot{V}_{M\_W}$, ρ_W, and c_{P_W} are the volumetric flow rate, density and specific heat of the water flowing through the main water loop (i.e. through the tank). Approximating the time derivative with a forward

difference and solving for T_3 at the future time step gives the model for the outlet temperature of the tank as

$$(T_3)_i = \frac{\dot{V}_{M\_W}\rho_W c_{P\_W}\Delta t}{c_6}\left[(T_7)_{i-1} - (T_3)_{i-1}\right] + (T_3)_{i-1} \tag{6.7}$$

6.2.4 Heating Coil Model

The building heating coil is a four pipe, cross-flow, heat exchanger that is designed to transfer heat to the return air using a portion of the flow in the main water loop. The rest of the hot water in the main water loop bypasses the coil. This bypassed flow can be used for heating an adjacent shop facility, but only the office facility was used in this study. A fan draws air into the coil from the room at a constant rate. When the room temperature falls below a set point, the hot water is directed through the coil for heating. However, when the room temperature is above the set point the hot water bypasses the coil and no heat is transferred to the air. It is observed from the experimental data that the coil has significant thermal capacitance, taking 3 to 5 minutes to cool down after mode transitions. Therefore, energy conservation for the heating coil can be written using a single thermal capacitance for the heating coil as

$$c_7 \frac{dT_{HC}}{dt} = \dot{V}_{HC\_W}\rho_W c_{P\_W}\left(T_{HC\_WI} - T_5\right)\Phi_{HC} + \dot{V}_{HC\_A}\rho_A c_{P\_A}\left(T_{HC\_AI} - T_{HC\_AO}\right) \tag{6.8}$$

where c_7 is a parameter representing the thermal capacitance of the coil which must be estimated. $\dot{V}_{HC\_W}$ and $\dot{V}_{HC\_A}$ are the volumetric flow rates of the water and air through the heating coil. Φ_{HC} is a step function that equals one if water is flowing through the coil and zero otherwise. T_{HC_AI} and T_{HC_WI} represent the inlet temperatures of the air and

water, respectively. T_{HC_AO} represents the outlet temperature of the air. The heat transfer to the water can be modeled as a function of the difference between the heating coil temperature and the inlet water temperature as

$$\dot{V}_{HC\_W}\rho_W c_{P\_W}\left(T_{HC\_WI}-T_5\right)=c_8\left(T_{HC\_WI}-T_{HC}\right) \tag{6.9}$$

where c_8 is a parameter that must be estimated. Using a forward difference to approximate the derivative in Equation (6.8) and combining with Equation (6.9) gives an equation for the outlet water flow as

$$T_{5i}=\frac{c_8}{\dot{V}_{HC\_W}\rho_W c_{P\_W}}\left[\frac{1}{c_7}\begin{pmatrix}\dot{V}_{HC\_W}\rho_W c_{P\_W}\left(T_{HC\_WI_{i-1}}-T_{5_{i-1}}\right)\Phi_{HC}\\+\dot{V}_{HC\_A}\rho_A c_{P\_A}\left(T_{HC\_AI_{i-1}}-T_{HC\_AO_{i-1}}\right)\end{pmatrix}+T_{HC_{i-1}}-T_{HC\_WI_i}\right]+T_{HC\_WI_i} \tag{6.10}$$

T_{HC_WI} is found by assuming an adiabatic mixture of the outlet from the recovery heat exchanger and the outlet from the water tank as

$$T_{HC\_WI}=\frac{T_3\left(\dot{V}_{M\_W}-\dot{V}_{HR\_W}\right)+T_4\left(\dot{V}_{HR\_W}\right)}{\dot{V}_{M\_W}} \tag{6.11}$$

where T_3 and T_4 were defined in Equations (6.7) and (6.4), and $\dot{V}_{M\_W}$ and $\dot{V}_{HR\_W}$ are the flow rates for the main water loop and the heat recovery loop.

6.2.5 Boiler Model

A natural gas boiler is the next component in the main water loop. Water flows through the boiler at rate of 20 gal/min. The boiler is set to provide heat to the main water loop when the inlet water temperature falls below a certain set point (75°C). This set point has been decided to maintain the design inlet temperature to the heating coil. Water

leaving the boiler is then mixed back with the main water loop and this mixture returns to the storage tank. It is observed from the data that significant capacitance is stored in the boiler structure. Therefore, energy conservation can be defined using a single thermal capacitance for the boiler structure as

$$c_9 * \frac{dT_B}{dt} = \dot{V}_{B\_W} * \rho_W * c_{P\_W} * \left(T_{B\_WI} - T_6\right) + c_{10} * \dot{V}_{B\_F} \tag{6.12}$$

where c_9 is a parameter representing the thermal capacitance of the boiler structure which must be estimated; T_B is the average temperature of the boiler structure; $\dot{V}_{B\_W}$ and $\dot{V}_{B\_F}$ are the volumetric flow rates of the water and fuel through the boiler, respectively; and T_{B_WI} and T_6 represent the inlet and outlet temperatures of the water, respectively. The heat transfer to the water can be modeled as a function of the difference between the boiler structure temperature and the inlet water temperature as

$$\dot{V}_{B\_W} * \rho_W * c_{P\_W} * \left(T_{B\_WI} - T_6\right) = c_{11} * \left(T_B - T_{B\_WI}\right) \tag{6.13}$$

where c_{11} is a parameter that must be estimated. Using a forward difference to approximate the derivative in Equation (6.12) and combining with Equation (6.13) gives an equation for the outlet water flow as

$$T_{6i} = \frac{c_{11}}{\dot{V}_{HC\_W}\rho_W c_{P\_W}} \left[\begin{array}{l} \frac{1}{c_9}\left(\dot{V}_{B\_W}\rho_W c_{P\_W}\left(T_{B\_WI_{i-1}} - T_{6_{i-1}}\right) + c_{10}\dot{V}_{B\_F_{i-1}}\right) \\ + T_{HC_{i-1}} - T_{HC\_WI_i} \end{array} \right] + T_{HC\_WI_i} \tag{6.14}$$

T_{B_WI} is the temperature of inlet water to the boiler and is defined as

$$\left(T_{B\_WI}\right) = \frac{T_{HC\_WI} * \left(\dot{V}_{M\_W} - \dot{V}_{HC\_W}\right) + T_5 * \left(\dot{V}_{HC\_W}\right)}{\dot{V}_{M\_W}} \tag{6.15}$$

where $\dot{V}_{M\_W}$ is the flow rate of the main water loop, V_{HC_W} is the water flow rate through the heating coil and T_{HC_WI} and T_5 were defined in Equations (6.11) and (6.10). Finally, the water flowing out of the boiler is mixed with the main system flow to give the conditions at the inlet of the tank as

$$(T_7) = \frac{T_{B\_WI} * \left(\dot{V}_{M\_W} - V_{B\_W}\right) + T_6 * \left(V_{B\_W}\right)}{\dot{V}_{M\_W}} \tag{6.16}$$

where T_{B_WI} was defined in Equation (6.15), V_{B_W} is the boiler flow rate, and T_6 was defined in Equation (6.14).

6.2.6 Model Propagation

The model developed in Sections 6.2.1-6.2.5 could be used with the components connected (i.e. the input temperature to one component is the predicted output of another) or with the components separated (i.e. input temperature for each component model is a measured value). However, the models must be connected for predicting the future states of the system where measured values are not available. As an example, Equation (6.3) can be rewritten for the separate case as

$$T_{4\_S} = T_{3\_m} + \varepsilon * \left(T_{2\_m} - T_{3\_m}\right) \tag{6.17}$$

or for the connected case as

$$T_{4\_C} = T_{3\_p} + \varepsilon * \left(T_{2\_p} - T_{3\_p}\right) \tag{6.18}$$

where variables with subscript _m indicate a measured value and variables with subscript _p, indicate a model predicted or calculated value. Time propagation is achieved using the dynamic elements (i.e. the elements that have thermal capacitance) such as the water

tank, heating coil, and boiler. Each of these elements are modeled with a time derivative term based on the energy stored in the thermal capacitance. These derivatives are modeled with a forward difference, which makes the model predictions dependent on previous time steps. These dynamic equations are used to propagate from one time step to the next.

6.3 Parameter Estimation

The most common errors that occur in modeling based on experimental measurements are from errors in measurements, incorrect choice of parameters, and incorrect choice of basis functions [Crassidis and Junkins, 2004]. The errors from incorrect choice of basis functions are the main drawback in using black-box models as mentioned in the introduction. The basis functions developed in section 6.2, however, should be adequate since they are defined based on physical laws. There can also be significant errors in the measurements, and, therefore, a detailed uncertainty analysis should be performed to analyze the accuracy of the system measurements and to correct sensor bias errors. Uncertainty analysis methods for interconnected systems have been and time varying systems have been presented by in the literature [Weathers et al., 2010; Weathers and Luck, 2012]. The study presented in this chapter did not include a detailed uncertainty analysis; instead, sensor bias errors were minimized by calibrating the system of sensors to ensure consistency according to energy conservation during steady state operation. Finally, the errors in the model coefficients can be minimized using the well-known least squares method. This method selects the coefficients that minimize the sum of the squares of the residual error for each component. As an example, the sum of the

squares of the residual errors for the temperature at location 3 (see Figure 6.1) is defined as

$$e_3 = \sum_{i=0}^{N} \left(T_{3\_p_i} - T_{3\_m_i}\right)^2 \tag{6.19}$$

where N is the total number of measured/predicted data points used in the estimation and T_{3_p} and T_{3_m} are the predicted and measured temperatures at location 3 in Figure 6.1. For the model developed in Section 6.2, the predicted values of interest are T_1 through T_7 (see locations in Figure 6.1) as defined Equations (6.2-6.4), (6.7), (6.10), (6.14), and (6.16). A sum for residual errors was calculated for each of these predictions for the case when the individual component models were separated and for the case when they were connected. All of these residual errors were summed into a cost function that was minimized in the least-squares procedure to estimate the best parameters. The cost function for the separate case is defined as

$$J_{sep} = \sum_{L=1}^{7} e_{L\_sep} \tag{6.20}$$

where e_{L_sep} is the residual error for a given location, L, in Figure 6.1 and for the case when the model predicted values are calculated using the separated models (i.e. the inputs to the component models are measured values). Similarly, the cost function for the connected case is defined as

$$J_{conn} = \sum_{L=1}^{7} e_{L\_conn} \tag{6.21}$$

where e_{L_conn} is the residual error for a given location, L, in Figure 6.1 and for the case when the model predicted values are calculated using the connected model (i.e. the inputs to the component models are model predicted values).

As discussed above, the typical approach is to estimate the parameters for each component model separately, requiring each component model to be consistent with the input and output measurements of that component. This method works quite well for steady conditions and predictions of the current output based on a measured input. However, component models developed using this method produce results that diverge severely when using them to predict values several time steps ahead. For several time steps-ahead prediction, the individual components must be connected, with the output from one component used as input to other components. In the connected model, small errors in any one component model propagate through each model and can cause large errors. One way to reduce the magnitude of these errors is to estimate the parameters of the model with the components already connected. This method requires each component to be consistent with all of the system sensors. There is correlation between sensors due to their interconnected nature. Accounting for this correlation helps minimize the effect of the errors in the model.

Selecting the parameters to minimize J_{conn} as defined in Equation (6.21) requires a nonlinear least squares minimization. This task is computationally difficult when estimating a large number of parameters simultaneously. However, given a good set of initial guess values for the coefficients the minimization algorithm converges faster. Therefore, the coefficients were first selected by performing an input output least squares estimation using the cost function J_{sep}, and, then, these coefficients were used as the initial guess in a nonlinear conjugate-gradient minimization algorithm to perform a parameter estimation using J_{conn} as the cost function. The coefficients are modified only slightly, but the difference is enough to greatly improve the prediction accuracy in the

connected model. In the case tested with the 12 parameters to be estimated and 3500 of data points in the training set (500 for each measurement location) the parameter estimation procedure was quite feasible computationally, taking only two or three minutes to run on a standard laptop computer. As long as a good initial guess is provided for the parameters as mentioned above, the method should work efficiently for modeling efforts of similar or even larger scale.

6.4 Results

Model parameters were estimated using data taken on two separate days at the CHP test facility. A variety of electrical and thermal demands were imposed on the system to ensure the robustness of the model. Based on this data, the model parameters were estimated using the two approaches (i.e. separate and connected) defined in Section 6.3. Plotting all of the temperatures for each case would be impractical, so only the outlet temperature from recovery heat exchanger (i.e. T_4) will be used to display the trends in the data. The other temperatures follow similar trends. First, the parameters were estimated for each component separately (i.e. minimization of J_{sep}) using measured temperatures at the inlet and outlet of each component. Figure 6.2 reveals a comparison of the measured recovery heat exchanger water outlet temperature versus that found when the separated component model was used. At each time step the predicted temperature is always based on a measured input temperature. As expected, the predicted temperatures match the measured temperatures quite well for this case. Note that data from two different days were used in this plot. The first 20 minutes of data are from one day and the second 30 minutes of data are from another day. The sharp jump in the data is due to a change in test conditions from the first day to the second.

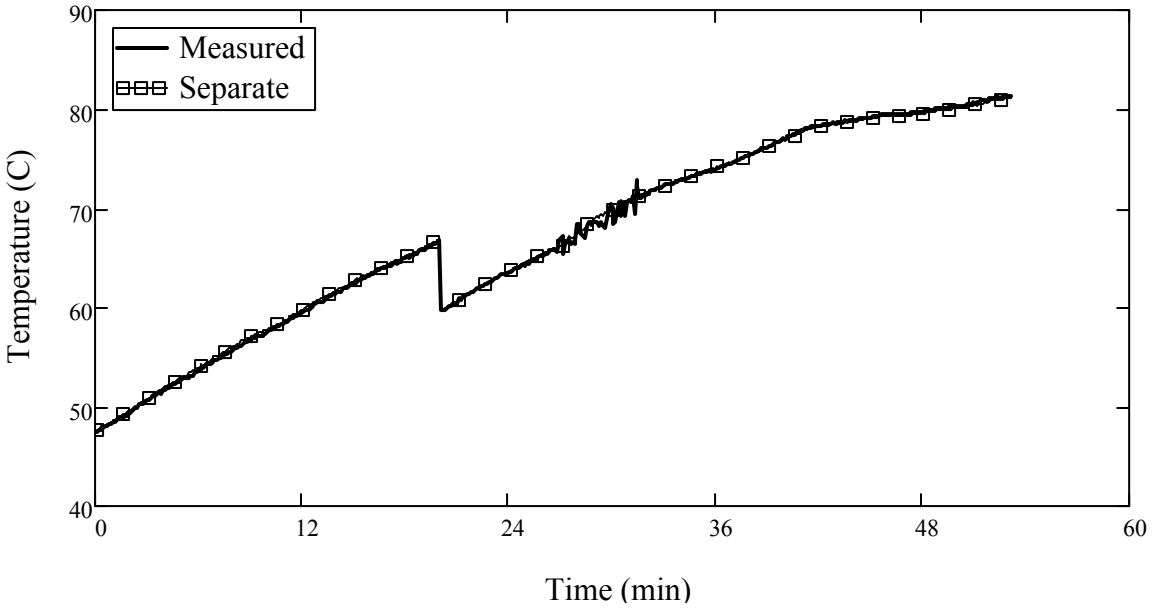

Figure 6.2 Single time step predition where the parameters were estimated separately (Recovery heat exchanger water outlet temperature, T_4)

Next, the components were connected so that the predicted output temperature from one component was the input to another. Figure 6.3 shows that, when the separately identified models are connected, the predictions tend to drift away from the measured values as the prediction time increases yielding much less accurate results. Also, Figure 6.3 reveals that using the parameters selected to minimize J_{conn} removes the drift in the prediction and provides much more accurate results.

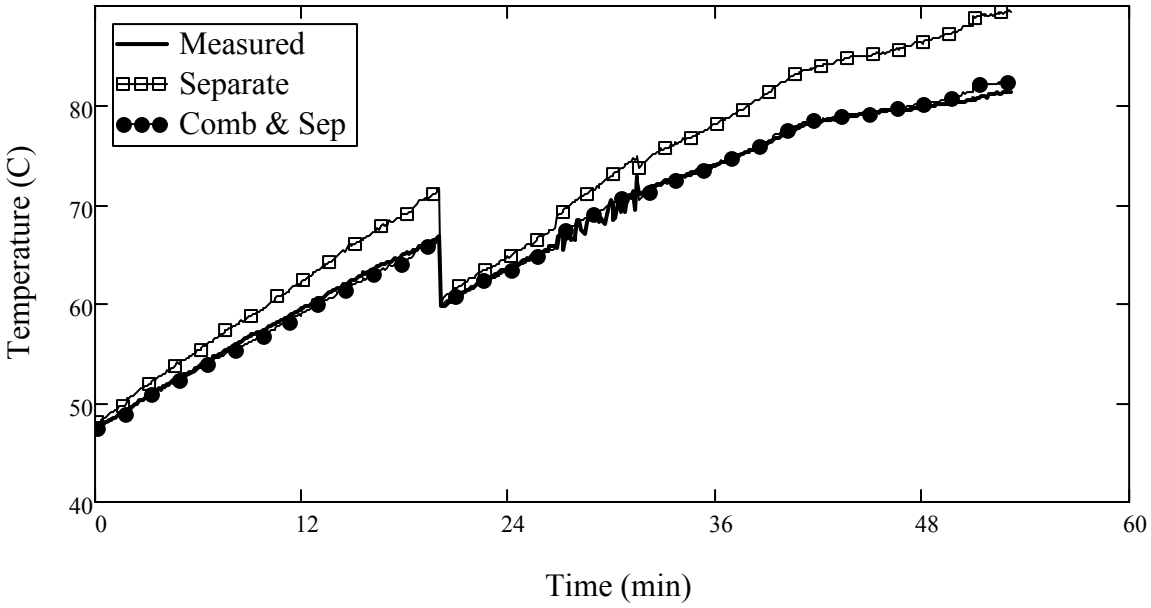

Figure 6.3 Connected model using coefficients from each of the parameter estimation methods (Recovery heat exchanger water outlet temperature, T_4)

After the model coefficients were selected according to the two methods (i.e. minimizing J_{sep} and minimizing J_{conn}), the models were used to predict the temperature for a new set of data. Even with a new set of data outside the training data, the coefficients estimated using J_{sep} still provide accurate results for current or single time step predictions as shown in Figure 6.4. Again, however predictions using the coefficients from the separate parameter estimation are much less accurate when the components are connected for prediction of several time steps ahead. Two cases were tested for comparison. In the first case the models were used to predict the system temperatures for 10 minutes in advance (100 time steps), and in the second for 20 minutes. Figures 6.5 and 6.6 show a comparison between the measured data and model predictions using the coefficients from the two parameter estimation methods. In both

cases, the model is much more accurate when using the coefficients from the combined parameter estimation method.

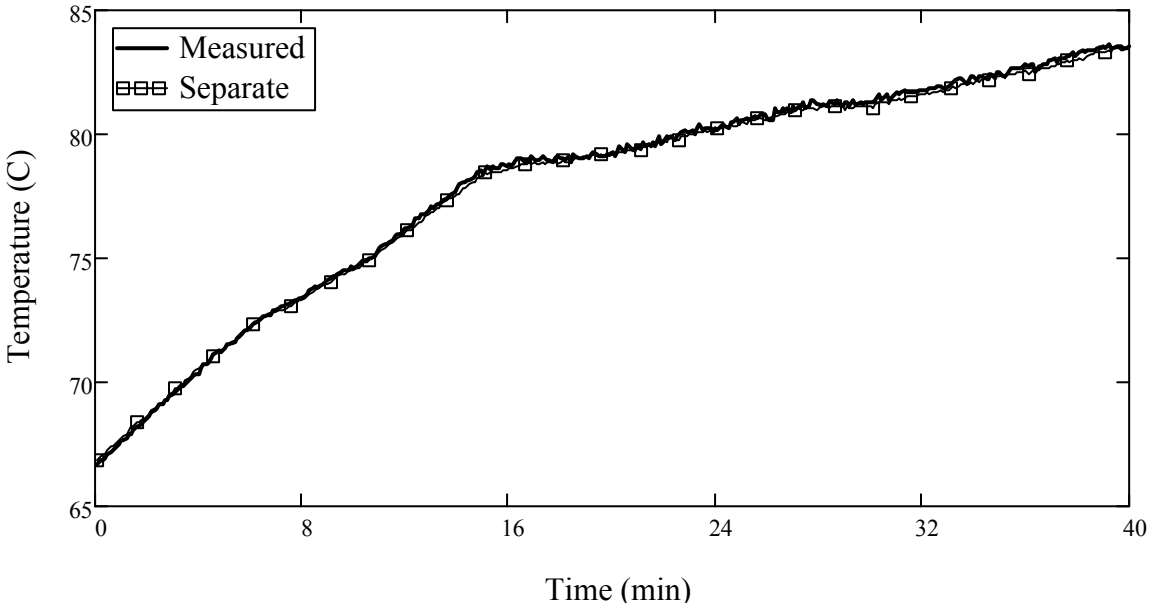

Figure 6.4 Single time step predition where the parameters were estimated separately (Recovery heat exchanger water outlet temperature, T_4)

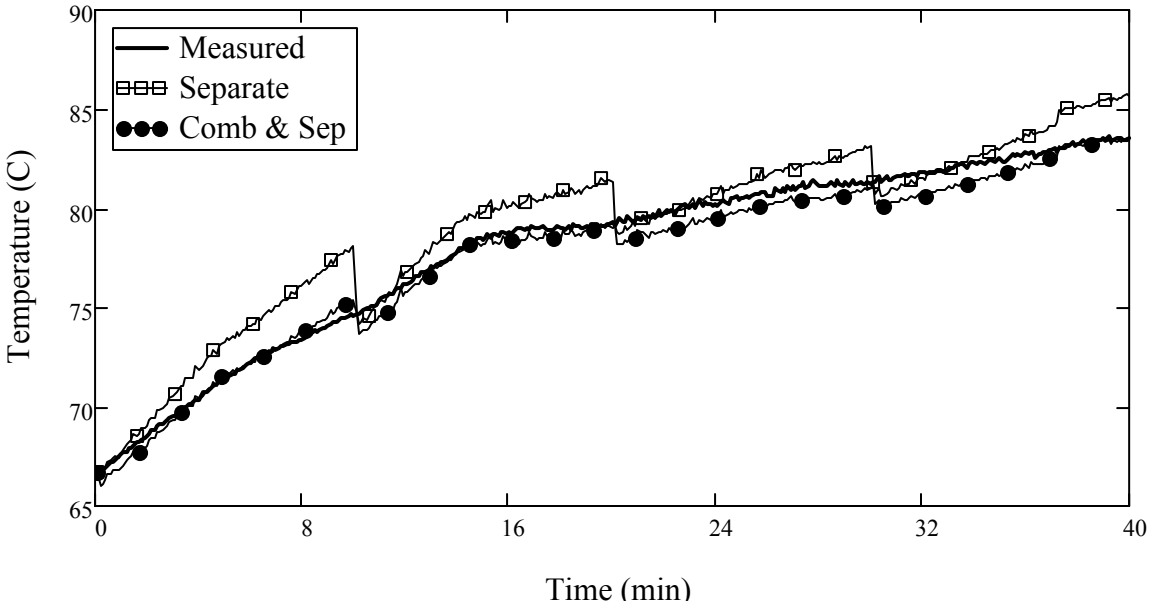

Figure 6.5 Example comparison of the methods for 10 minute prediction (Recovery heat exchanger water outlet temperature, T_4)

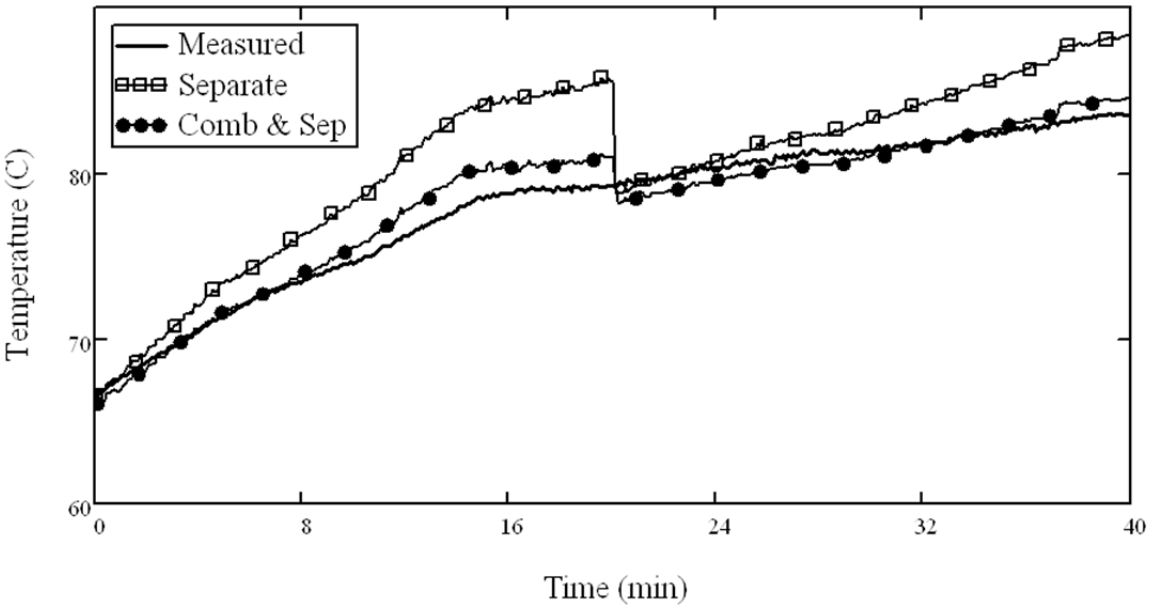

Figure 6.6 Example comparison of the methods for 20 minute prediction (Recovery heat exchanger water outlet temperature, T_4)

As in the recovery heat exchanger outlet water temperature prediction, the model obtained using the connected method provided a large improvement for all of the system predictions. The total sum of the squared residual error was reduced extensively for the 10 and 20 minute predictions using data outside of the training data as shown in Table 6.2. Table 6.2 also illustrates the improvement for the case where the connected model is used for the training data set. Additionally, the combined case was more accurate in predicting the temperature at the output for each of the component models as shown in Figures 6.7 and 6.8. These figures give the total squared error for each component. This total error is normalized by the number of time steps in the simulation. As can be seen in Figures 6.7 and 6.8 the estimation procedure gave more improvement for some component models than others. However, for each component model the error was reduced. This builds confidence in the overall effectiveness of the parameter estimation method.

Table 6.2 Total Squared Error for Prediction Using Both Parameter Estimation Methods

Cost function used in estimating model parameters	J_{conn} for10 minute prediction	J_{conn} for 20 minute prediction	J_{conn} for training data set
J_{sep}	5354	27949	55809
J_{conn}	2592	6441	2048

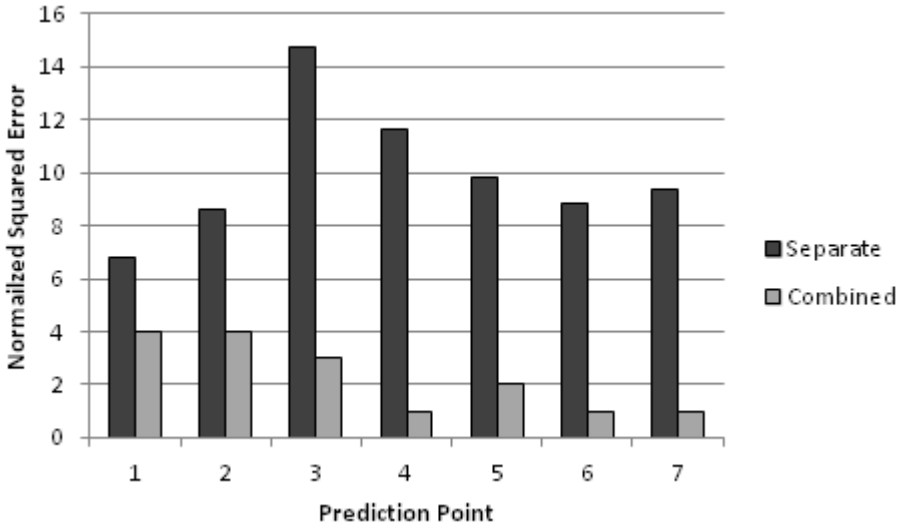

Figure 6.7 Normalized squared error for each prediction point for 10 minute prediction

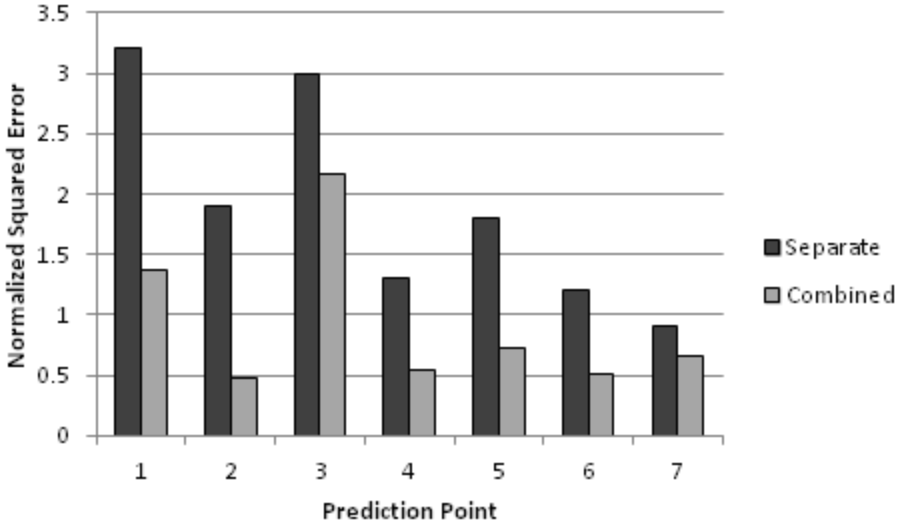

Figure 6.8 Normalized squared error for each prediction point for 20 minute prediction

CHAPTER VII

Summary, Conclusions and Future Work

7.1 Summary and Conclusions

This dissertation began, in Chapter I, by showing how improvement in the energy efficiency of building energy systems can have a significant impact on overall US energy usage. The main area of improvement addressed in Chapter 1, was the large amount of wasted energy in traditional power generation. CCHP systems were shown to have much higher efficiencies because of their ability to use waste heat for heating and cooling the building where the electricity is used. Chapter I then introduced several obstacles to the effective implementation of CCHP systems in the areas of uncertainty analysis, building load prediction, optimal component sizing, and predictive modeling of CCHP systems. The objectives of this dissertation were then defined to partially address each of these obstacles. To give context to the work presented in this dissertation, Chapter II presented a literature review on the current research trends in the areas of uncertainty analysis, building load prediction, optimal CCHP component sizing, and predictive modeling of thermal systems.

Chapter III presented an uncertainty analysis of a representative steady-state model of a CCHP system operating under FEL and FTL strategies. The analysis was performed on a medium sized office building in Atlanta, GA. The main goal of chapter III was to find the uncertainty in the model predictions of primary energy consumption,

cost of operation, and carbon dioxide emissions. As an integral part of this uncertainty analysis, this study presented practical approaches to obtain the uncertainty in input parameters such as the thermal load, natural gas and electricity prices, and engine performance.

The total uncertainties and the uncertainty percentage contributions (UPC's) were presented for each performance metric. The total uncertainties showed that the model can be used to make legitimate comparisons between FEL and FTL operation strategies and that the uncertainty in PEC and CDE are minimal in comparison to the uncertainty in operational cost. The UPC charts showed that the uncertainty in the weather, energy prices, and engine operation were the most significant contributors to the overall uncertainty. This fact revealed that the model can be significantly improved by taking into account the variation in weather and energy prices.

Chapter IV gave an analysis of a methodology for using existing EnergyPlus reference building energy profiles to estimate the energy profiles of buildings with similar characteristics to a given reference model. By extending the reference models to estimate the profiles of similar buildings, the methodology can eliminate the need for creating highly sophisticated building models in some cases. The error in using the methodology was examined for 72 distinct test buildings. A sensitivity analysis was performed for moderate changes in building size, orientation, and usage. While using the coefficient methodology to estimate the building load does not always provide large improvement over using the reference profile, it does consistently provide improve the estimate by using the energy bill. In most cases, the level of similarity between the real building and the reference building may not be known. Therefore, the coefficient

methodology provides the advantage of using information that is known to be true about the building with minimal effort. The 72 test buildings provide an adequate assessment of the error expected in using the method. Based on this error assessment, users can easily decide whether the method is suitable for their applications.

Chapter V presented an optimal sizing method that is robust to variation in fuel/electricity cost and weather. The sizing method used an analytical optimal operation algorithm, thus making the method computationally efficient. This efficiency was exploited, incorporating simulations from multiple years of weather data and energy prices. Also, performance curves from commercially available PGU's were incorporated. For the case study presented, the method of characterizing fuel/electricity cost variation gave the same optimal solution as using found using only the current cost ratio and typical meteorological year (TMY) weather data. Therefore, this work establishes that using the TMY weather data and the current fuel/electricity cost can give accurate results for some cases. This may not be true for all cases, however.

Finally, Chapter VI demonstrated the advantages of a whole-system or integrated parameter estimation approach for a predictive CHP system model. The model was tested for temperature predictions up to 20 minutes in advance from a set of initial conditions. The model obtained by estimating the parameters for each component separately exhibited large drifts from the measured data when attempting to make predictions several time steps in advance (Figures 6.5 and 6.6). The integrated parameter estimation approach reduced drift by requiring each component model to be consistent with all of the system temperature measurements (Figures 6.5 and 6.6). The results also showed that

this integrated parameter estimation approach can significantly improve the accuracy for the overall system as illustrated in Table 6.2 and Figures 6.7 and 6.8.

7.2 Future Work

The topics covered in this dissertation are broad, and, therefore, there are many possible applications and improvements. For example, the method developed in Chapter III can easily be applied to other building energy system simulations. The uncertainty in the thermal load and fuel prices would have a large impact on many building energy system types. Also, in the future, the model should be modified to address different time scales as needed for other building simulation objectives.

The building load estimation methodology discussed in chapter IV is accurate enough for some objectives, but more accurate estimation methods should be developed in other cases. Future work should be directed at finding a reasonable means to estimate the monthly energy load fractions of the building. The fractions could likely be corrected with minimal energy usage measurement required, and the results reveal that the consumption profiles can be greatly improved with better estimates of the monthly fractions.

For the case studied, the optimal sizing method presented in Chapter V gave the same solution as a method that does not consider yearly weather and energy cost variation. In future work, more case studies should be carried out to determine if these factors ever affect the optimal solution. Additionally, future work should include a more accurate estimate of future cost of electricity and fuel. Perhaps the method should be modified to incorporate a probabilistic definition of the future cost of electricity and fuel.

Chapter VI demonstrated an integrated parameter estimation approach on a CCHP system. In future work the model should be extended to include the building so that the building energy loads can be predicted. Additionally, the integrated parameter estimation method demonstrated is applicable for a variety of applications that contain a system of connected components. In similar system models, this method can be applied to significantly improve the prediction accuracy.

REFERENCES

Anderson, M. Buehner, M., Young, P., Hittle, D., Anderson, C., Tu, J., and Hodgson, D., 2007, "An experimental system for advanced heating, ventilating and air conditioning (HVAC) control," *Energy and Buildings*, 39 (2), pp. 136-147.

Azit, A.H. and Nor, K.M., 2009, "Optimal sizing for a gas-fired grid-connected cogeneration system planning," *IEEE Transactions on Energy Conversion*, 24 (4), pp. 950-958.

Balan, R., Cooper, J., Chao, K., Stan, S., and Donca, R., 2011, "Parameter identification and model based predictive control of temperature inside a house," *Energy and Buildings*, 43 (2-3), pp. 748-758.

Beihong, Z. and Weiding, L., 2006, "An optimal sizing method for cogeneration plants," *Energy and Buildings*, 38 (3), pp. 189-195.

Braun, J. E., Montgomery, K. W., and Chaturvedi, N., 2001, "Evaluating the Performance of Building Thermal Mass Control Strategies," *HVAC & R Research*, 7 (4), pp. 403-428.

Bruno, J.C., Miquel, J., and Castells, F., 2000, "Optimization of energy plants including water/lithium bromide absorption chillers," *International Journal of Energy Research*, 24 (8), pp. 695-717.

Canyurta, O.E., Ozturka, H.K., Hepbaslib,A., and Utlu, Z., 2005, "Estimating the Turkish residential–commercial energy output based on genetic algorithm (GA) approaches," *Energy Policy*, 33 (8), pp. 1011-1019.

Catalina T., Virgone J., and Blanco E., 2008, "Development and validation of regression models to predict monthly heating demand for residential buildings," *Energy and Buildings,* 40 (10), pp. 1825–1832.

Coleman, H.W., Steele. W.G., 2009, Experimentation and Uncertainty Analysis for Engineers, John Wiley & Sons, New York, USA.

Corrado, V. and Mechri, H.E., 2009, "Uncertainty and sensitivity analysis for building energy rating," *Journal of Building Physics*, 33 (2), pp. 125-156.

Chen, T. Y. and Athienitis, A. K., 2003, “Investigation of practical issues in building thermal parameter estimation,” *Building and Environment*, 38 (8), pp. 1027-1038.

Chen, T. Y., 2002, “Application of adaptive predictive control to a floor heating system with a large thermal lag,” *Energy and Buildings*, 34 (1), pp. 45-51.

Cho, H., Luck, R., and Chamra, L.M., 2010, "Supervisory Feed-Forward Control for Real-Time Topping Cycle CHP Operation," *ASME Journal of Energy Resources Technology*, 132 (1), pp. 0124011-01240112.

Cho, H. J, 2009a, “Dynamic Simulation and Optimal Real-Time Operation of CHP Systems for Buildings,” Dissertation, Mississippi State University.

Cho, H.J., Mago P.J., Luck, R., and Chamra, L.M., 2009b, “Evaluation of CCHP systems performance based on operational cost, primary energy consumption, and carbon dioxide emission by utilizing an optimal operation scheme,” *Applied Energy*, 86 (12), pp. 2540-2549.

Crassidis, J. and Junkins, J., 2004, Optimal Estimation of Dynamic Systems, Chapman & Hall/CRC, Boca Raton, Florida, USA.

Cummins industrial generator data. February 2011. Available from: http://generatorjoe.com/SubCat.aspx?categoryId=532

Deru, M., Griffith, B., and Torcellini, P., 2006, “Establishing benchmarks for DOE Commercial Building R&D and Program Evaluation,” National Renewable Energy Laboratory. Available at: http://www.nrel.gov/docs/fy06osti/39834.pdf

Dominguez-Munoz, F., Cejudo-Lopez, J.M., and Carrillo-Andres, A., 2010, “Uncertainty in peak cooling load calculations,” *Energy and Buildings*, 42, pp. 1010-1018.

Energy Information Administration, 2007, Independent Statistics and Analysis, Electric Power Annual 2007 – State Data Tables, U.S. Department of Energy. Available from: http://www.eia.doe.gov/cneaf/electricity/epa/epa_sprdshts.html.

Energy Information Administration (EIA), 2011, “Annual Energy Review 2010,” US, Department of Energy (DOE), DOE/EIA-0384(2010), Available at: http://www.eia.gov/totalenergy/data/annual/index.cfm.

Energy Information Administration (EIA), 2012, “Annual Energy Outlook 2012 Early Release,” US, Department of Energy (DOE), DOE/EIA-0383ER(2012), Available at: http://www.eia.gov/forecasts/aeo/er/.

Environmental Protection Agency, Energy Star Program, U.S. Department of Energy, 2008. Available from: http://energystar.gov/.

Frey, H.C., 1992, "Quantitative analysis of uncertainty and variability in environmental policy making," Available from: Directorate for Science and Policy Programs, American Association for the Advancement of Science, 1333 H Street, NW, Washington, DC.

Fumo, N., Mago, P., and Luck, R., 2010 "Methodology estimate building energy consumption using EnergyPlus benchmark models," *Energy and Buildings*, 42 (12), pp. 2331-2337.

Gamou, S., Yokoyama, R., and Ito, K., 2002, "Optimal unit sizing of cogeneration systems in consideration of uncertain energy demands as continuous random variables," *Energy Conversion and Management,* 43 (9-12), pp. 1349-1361.

Georgia Public Service Commission, 2009, Natural Gas, Georgia Gas Marketers' Price. Available from: http://www.psc.state.ga.us/gas/marketerpricing/pricecard-09.asp.

Gugliermetti, F., Passerini, G., and Bisegna, F., 2004, "Climate models for the assessment of office buildings energy performance," *Building and Environment*, 39 (1), pp. 39-50.

Haeseldonckx, D., Peeters, L., Helsen, L., and D'haeseleer, W., 2007, "The impact of thermal storage on the operational behavior of residential CHP facilities and the overall CO2 emissions" *Renewable and Sustainable Energy Reviews*, 11 (6), pp. 1227-1243.

Houwing, M., Ajah, A.N., Heihnen, P.W., Bouwmans, I., and Herder, P.M., 2008, "Uncertainties in the design and operation of distributed energy resources: The case of micro-CHP systems," *Energy*, 33 (10), pp. 1518-1536.

Hueffed, A. and Mago, P.J., 2010, "Influence of prime mover size and operational strategy on the performance of CCHP systems under different cost structures," *IMechE Journal of Power and Energy*, 224 (5), pp. 591-605.

International Energy Agency (IEA), 2008, "Combined Heat and Power: Evaluating the benefits of greater global investment," OECD/IEA, Paris, France.

Kawashima, M., Dorgan, C. E., and Mitchell, J. W., 1996, "Optimizing system control with load prediction by neural networks for an ice-storage system," *ASHRAE Transactions*, 102 (1), pp. 1169-1178.

Li, C.Z., Shi Y.M., and Huang, X.H., 2008, "Sensitivity analysis of energy demands on performance of CCHP system," *Energy Conversion and Management*, 49 (12), pp. 3491-3497.

Longo, G., Gasparella, A., and Zilio, C. 2005, "Analysis of an absorption machine driven by the heat recovery on an I.C. reciprocating engine," *International Journal of Energy Research, 29 (8)*, pp. 711-722.

MacDonald, I. and Strachan, P., 2001 "Practical application of uncertainty analysis," *Energy and Buildings*, 33 (3), pp. 219-227.

Mago, P.J., Fumo, N., and Chamra, L.M., 2009, "Performance analysis of CCHP and CHP systems following the thermal and electric load," *International Journal of Energy Research*, 33 (9), pp. 852-864.

Malico, I., Carvalhinho, A.P., and Tenreiro, J., 2009, "Design of a trigeneration system using a high-temperature fuel cell," International Journal of Energy Research, 33 (2), pp. 144-151.

Moran, A., Mago, P.J., and Chamra, L.M., 2008, "Thermoeconomic Modeling of Micro-CHP (Micro-Cooling, Heating, and Power) for Small Commercial Applications," *International Journal of Energy Research*, 32 (9), pp. 808-823.

Mustafaraj, G., Chen, J., and Lowry, G., 2010, "Development of room temperature and relative humidity linear parametric models for an open office using BMS data," *Energy and Buildings*, 42 (3), pp. 348-356.

Nassif, N., Moujaes, S., and Zaheeruddin, M., 2008, "Self-tuning dynamic models of HVAC system components," *Energy and Buildings*, 40 (9), pp. 1709-1720.

Neto, A.H. and Fiorelli, F.A.S., 2007, "Use of simulation tools for managing buildings energy demand," *Proceedings: Building Simulation*, International Building Performance and Simulation Association, Available at: http://simulationresearch.lbl.gov/EP/ep_main.html

Pedrini, A., Westphal, F.S., and Lamberts, R., 2002, "A methodology for building energy modeling and calibration in warm climates," *Building and Environment*, 37 (8-9), pp. 903-912.

Piacentino, A. and Cardona, F., 2008, "An original multi-objective criterion for the design of small-scale polygeneration systems based on realistic operating conditions," *Applied Thermal Energy*, 28 (17-18), pp. 2391-2404.

Ren, H., Gao, W., and Ruan, Y., 2008, "Optimal sizing for residential CHP system," *Applied Thermal Engineering*, 28 (5-6), pp. 514-523.

Torcellini, P., Deru, M., Griffith, B., Benne, K., Halverson, M., Winiarski, D., and Crawley, D.B., 2008, “DOE Commercial Building Benchmark Models.” ACEEE 2008 summer study on energy efficiency in buildings, NREL Conference Paper NREL/CP-550-43291, http://www.nrel.gov/docs/fy08osti/43291.pdf

Stadler M., Firestone R., Curtil, D., and Marnay, C., 2006, “On-site generation simulation with EnergyPlus for commercial buildings,” in *Proceedings of ACEEE 2006 Summer Study on Energy Efficiency in Buildings*, Asilomar, CA.

Sun, Z.G., and Guo, K.H., 2006, “Cooling performance and energy saving of a compression-absorption refrigeration system driven by a gas engine,” *International Journal of Energy Research*. 30 (13), pp. 1109-1116.

Voorspools, K.R. and D’haeseleer, W.D., 2006, “Reinventing hot water? Towards optimal sizing and management of cogeneration: A case study for Belgium,” *Applied Thermal Energy*, 26 (16), pp. 1972-1981.

Wang, L., Mathew, P., and Pang, X., 2012, “Uncertainties in energy consumption introduced by building operations and weather for a medium-size office building,” *Energy and Buildings*, 53, pp. 152-158.

Wang, S., and Xu, X., 2006, “Simplified building model for transient thermal performance estimation using GA-based parameter identification,” *International Journal of Thermal Sciences*, 45 (4), pp. 419-432.

Weathers, J.B. and Luck, R., 2012, “Time-varying uncertainty in shock and vibration applications using the impulse response,” *Shock and Vibration*, 19 (3), pp. 433-446.

Weathers, J.B., Luck, R., Weathers, J.W., 2010, "A modular approach to uncertainty analysis," *ISA Transactions*, 49 (1), pp. 19-26.

Wilcox, S. and Marion, W., 2008, “Users Manual for TMY3 Data Sets,” National Renewable Energy Laboratory, Golden, CO, NREL/TP-581-43156.

Yang, J., Rivard, H., and Zmeureanu, R., 2005, “On-line building energy prediction using adaptive artificial neural networks,” *Energy and Buildings*, 37 (12), pp. 1250-1259.

Yao, Y, Lian, Z., Liu, S., and Hou, Z., 2004, “Hourly cooling load prediction by a combined forecasting model based on analytic hierarchy process,” *International Journal of Thermal Sciences*, 43 (11), pp. 1107-1118.

Yik , F.W.H., Burnett, J., and Prescott, I., 2001, “Predicting air-conditioning energy consumption of a group of buildings using different heat rejection methods,” *Energy and Buildings*, 33 (2), pp. 151-166.

Yokoyama, R., Wakui, T., and Satake, R., 2009, “Prediction of energy demands using neural network with model identification by global optimization,” *Energy Conversion and Management*, 50 (2), pp. 319–327.

Yun, K.T, Cho, H., Luck, R., and Mago, P.J., 2011, "Real-time combined heat and power operational strategy using a hierarchical optimization algorithm," *Journal of Power and Energy*, 225 (4), pp. 403-412.

Yun, K., Luck, R., Mago, P. J. and Smith, A., 2012, “Analytic solutions for optimal power generation unit operation in combined heating and power systems,” *ASME Journal of Energy Resource Technology*, 134 (1), pp. 011301-1-011301-8.

Zhou, Q., Wang, S., Xu, X., and Xiao, F., 2008, “A grey-box model of next-day building thermal load prediction for energy-efficient control,” *International Journal of Energy Research*, 32 (15), pp. 1418-1431.

Zhu., Y., 2006. “Applying computer-based simulation to energy auditing: A case study,” *Energy and Buildings*, 38 (5), pp. 421-428.

APPENDIX A

THERMAL LOAD FACTORS FOR UNCERTAINTY ANALYSIS

The thermal load factors are defined explicitly as

$$T1_j = \sum_{i=0}^{hours_j} Q_{c_i} \qquad T2_j = \sum_{i=0}^{hours_j} Q_{h_i} \qquad T3_j = \sum_{i=0}^{hours_j} Q_{c_i}\Phi_{3e_i}\Phi_{1e_i}$$

$$T4_j = \sum_{i=0}^{hours_j} Q_{h_i}\Phi_{3e_i}\Phi_{1e_i} \qquad T5_j = \sum_{i=0}^{hours_j} E_{load_i}\Phi_{3e_i}\Phi_{1e_i} \qquad T6_j = \sum_{i=0}^{hours_j} \Phi_{3e_i}\Phi_{1e_i}$$

$$T7_j = \sum_{i=0}^{hours_j} Q_{c_i}\Phi_{4e_i}\Phi_{2e_i} \qquad T8_j = \sum_{i=0}^{hours_j} Q_{h_i}\Phi_{4e_i}\Phi_{2e_i} \qquad T9_j = \sum_{i=0}^{hours_j} \Phi_{4e_i}\Phi_{2e_i}$$

$$T10_j = \sum_{i=0}^{hours_j} Q_{c_i}\Phi_{3e_i}\Phi_{2e_i} \qquad T11_j = \sum_{i=0}^{hours_j} Q_{h_i}\Phi_{3e_i}\Phi_{2e_i} \qquad T12_j = \sum_{i=0}^{hours_j} \Phi_{3e_i}\Phi_{2e_i}$$

$$T13_j = \sum_{i=0}^{hours_j} E_{load_i}\Phi_{3e_i}\Phi_{2e_i} \qquad T14_j = \sum_{i=0}^{hours_j} Q_{c_i}\Phi_{1e_i} \qquad T15_j = \sum_{i=0}^{hours_j} Q_{h_i}\Phi_{1e_i}$$

and $hours_j$ represent the number of hours in the j-th month. $E1$, $E2$, E3, E4, and E5 represent variables that are only dependent on the electric load and are defined as follows

$$E1_j = \sum_{i=0}^{hours_j} E_{load_i}\Phi_{1e_i} \qquad E2_j = \sum_{i=0}^{hours_j} \Phi_{1e_i} \qquad E3_j = \sum_{i=0}^{hours_j} \Phi_{2e_i} \qquad E4_j = \sum_{i=0}^{hours_j} E_{load_i}\Phi_{2e_i} \qquad E5_j = \sum_{i=0}^{hours_j} E_{load_i}$$

$C1$, C2 and $C3$ are constants defined as

$$C1 = \frac{\eta_{rec}}{\eta_B}\left(1 - \frac{1}{m}\right) \qquad C2 = \frac{b}{m}\left(\frac{\eta_{rec}}{\eta_B}\right) \qquad C3 = \frac{\eta_{rec}}{\eta_B}\left(\frac{b - E_{PGU\_nom}}{m} - E_{PGU\_nom}\right)$$

A physical description of some of the thermal load factors would be helpful at this point. For example, T1 and T2 indicate the monthly sum of the cooling and heating loads, respectively. T3 and T4 indicate the monthly sum of the cooling and heating loads for the hours when the boiler is used to supplement the heat recovered by the engine. T5 indicates the monthly sum of the electrical load for the hours when the boiler is used to supplement the heat recovered by the engine and the engine is providing for the entire electric load of the building. T6 indicates the total number of hours per month that the system is operating in this mode. T11 indicates the monthly sum of the heating load for

the case when the boiler has to supplement the heat recovered by the engine and the electric load is greater than the nominal rating of the engine.